

**E/I ratio is maintained constant in the cultured neocortical networks  
despite variation in the proportion of GABAergic interneurons**

Thesis  
for the degree of

**Doctor rerum naturalium (Dr. rer. nat.)**  
approved by the Faculty of Natural Sciences of Otto von Guericke  
University Magdeburg

by M.Sc, Wenxi Xing

born on 04. Aug. 1987

in Ying Kou, P.R. China

Examiner: Prof. Dr. Thomas Vogt

Prof. Dr. Eckhard Friauf

submitted on:

27. Oct. 2022

defend on:

06. Nov. 2023

---

## Table content

<b>TABLE CONTENT</b> .....	<b>II</b>
<b>FIGURE AND TABLE INDEX</b> .....	<b>IV</b>
<b>ABBREVIATIONS</b> .....	<b>V</b>
<b>1. ABSTRACT</b> .....	<b>1</b>
1.1 ABSTRACT.....	1
1.2 ZUSAMMENFASSUNG.....	3
<b>2. INTRODUCTION</b> .....	<b>5</b>
2.1 INs .....	5
2.1.1 The generation of cortical INs .....	5
2.1.2 The migration of cortical INs .....	6
2.1.3 Subclasses of Neocortical INs .....	7
2.1.4 Neurotransmitters .....	8
2.1.5 The development of neural circuits .....	9
2.1.6 Function role of GABA signaling in neural circuit development.....	9
2.1.6.1 Depolarizing GABA signaling .....	9
2.1.6.2 GABA signaling in spontaneous network activity .....	10
2.1.6.3 The balance of excitation and inhibition is regulated by GABA signaling during neural circuit formation .....	11
2.1.7 Cortical INs in culture .....	12
2.1.8 Regulation of the number of cortical INs .....	13
2.2 DISEASES AND TREATMENT .....	14
2.3 THE AIMS OF MY STUDY .....	15
<b>3. MATERIALS AND METHODS</b> .....	<b>17</b>
3.1 LAB-HOUSED ANIMALS.....	17
3.2 MATERIALS .....	17
3.2.1 BUFFER .....	17
3.2.2 CELL CULTURE MEDIUM .....	18
3.2.2 MEDIAM FOR CELL CULTURE .....	18
3.3 CELL CULTURE .....	19
3.3.1 Petri dishes for cell culture .....	19
3.3.2 Primary rat astroglial cell cultures .....	19
3.3.3 Neocortical neurons in culture.....	19
3.3.4 Cortical networks.....	20
3.3.5 Preparation of dissociated MGE.....	21
3.3.6 PN/IN ratio generation.....	22
3.4 IMMUNOCYTOCHEMISTRY .....	22
3.4.1 Cell density analysis .....	24
3.4.2 Immunostaining to determine GABA and Venus co-expression.....	24
3.4.3 Caspase immunocytochemistry .....	25
3.4.4 BrdU immunocytochemistry .....	25
3.4.5 Measurement of soma size by immunostaining.....	26
3.5 ELECTROPHYSIOLOGY .....	26
3.5.1 Whole-cell voltage-clamp recordings.....	26
3.5.2 Application of water-soluble drugs in our cultures .....	27
3.5.3 Quantitative analysis of single cell voltage-clamp recordings .....	27

---

3.6 IN VITRO CALCIUM IMAGING EXPERIMENTS .....	28
3.6.1 Calcium imaging of single-cell spontaneous neuronal activity in cortical cultures ..	28
3.6.2 Burst analysis .....	29
3.7 DATE ANALYSIS .....	29
<b>4. RESULTS.....</b>	<b>30</b>
4.1 GABA/NEUN/DAPI CO-LOCALIZATION AND EGPF/NEUN/DAPI CO-LOCALIZATION .....	30
4.2 MGE-DERIVED CELLS DISPLAY MOLECULAR PROPERTIES OF CORTICAL INs .....	32
4.3 EARLY DEVELOPMENT OF MGE-dCTX NETWORKS .....	33
4.3.1 Defined PN/IN ratios .....	33
4.3.2 Network-specific apoptosis rates .....	36
4.3.3 INs influence PNs proliferation in a density-dependent manner .....	37
4.3.4 Regulation of IN proliferation rates .....	38
4.4 ANALYSIS OF THE DEVELOPMENT OF CELL DENSITY IN NETWORKS WITH DIFFERENT PN/IN RATIOS .....	39
4.4.1 Developmental dynamics and estimating the long-term changes in MGE-dCtx networks .....	39
4.4.2 Developmental dynamics and estimating the long-term changes in MGE-wCtx networks .....	41
4.5 MEASUREMENT OF PN AND IN SOMA SIZE .....	42
4.6 IN DENSITY DETERMINES CORTICAL NETWORK ACTIVITY .....	43
4.7 WHOLE-CELL PATCH-CLAMP RECORDINGS .....	46
4.7.1 Physiological impact of IN ratio variation on synaptic transmission .....	46
4.7.2 Characterization of sPSC bursts .....	49
4.7.3 Characterizations of post-synaptic currents in our cultures .....	52
4.7.3.1 sEPSC events .....	52
4.7.3.2 sIPSC events .....	54
4.7.4 Charge transfer balance between sEPSCs and sIPSCs .....	55
<b>5. DISCUSSION.....</b>	<b>58</b>
5.1 IN CLASSIFICATION .....	58
5.2 INs IMPACT ON THE SURVIVAL OF PNs .....	59
5.3 dCTX NETWORKS VS. wCTX NETWORKS .....	60
5.4 INTRINSICALLY DETERMINED CELL DEATH OF DEVELOPING CORTICAL INs .....	61
5.5 CONTRIBUTION OF INs IN SPONTANEOUS NETWORK ACTIVITY .....	62
5.6 MORPHOLOGY CHANGES ARE CORRELATED WITH SYNAPTIC NETWORK ACTIVITY .....	63
<b>6 REFERENCE LIST .....</b>	<b>67</b>
<b>7. DECLARATION OF HONOUR .....</b>	<b>85</b>

---

## Figure and table index

Figure 1: Immunolabeling of cells in the T00 networks or T25 networks.....	31
Figure 2: Double-immunolabeling with antibodies against CR, PV, and SOM in rat cortical cultures.....	33
Figure 3: The development of PN densities in networks with different IN content during seven days of cultivation <i>in vitro</i> .....	34
Figure 4: MGE-derived INs regulate PN density at the developmental stage of 1 <sup>st</sup> week in culture. ....	36
Figure 5: Caspase-3-immunoreactive cells in T25 networks. ....	37
Figure 6: IN density influence on PN cell proliferation rates. ....	38
Figure 7: Population dynamics in different types of networks.....	40
Figure 8: Developmental changes of normalized neuronal densities in different network types. ....	41
Figure 9: Analysis of the structure differences in dCtx and wCtx networks during network development.....	42
Figure 10: Soma size analysis. ....	43
Figure 11: Analysis of calcium imaging data in T05, T25, T30 networks.....	45
Figure 12: Influence of GABAergic inputs on sEPSC parameters in PNs. ....	47
Figure 13: Analysis of spontaneous post-synaptic currents in the intracellular voltage-clamp recordings. ....	48
Figure 14: Spontaneous PSC Bursts.....	51
Figure 15: Developmental changes in sEPSCs in neurons of T05 and T45 networks. ....	53
Figure 16: Developmental changes in sIPSCs in neurons of T05 and T45 networks. ....	55
Figure 17: Charge transfer and charge transfer ratios for single sPSCs.....	57
Table 1: A summary of analysis of the number of cells in network burst. ....	49
Table 2: Summary of sEPSC and sIPSC parameters in PNs and INs of T05 and T45 networks. ....	65

---

## Abbreviations

[Ca <sup>2+</sup> ] <sub>i</sub>	intracellular calcium concentration
aCSF	artificial cerebrospinal fluid
AMPA	$\alpha$ -amino-3-hydroxy-5-methyl-4-isoxazole propionic acid
Ara-C	1- $\beta$ -D-Arabinofurano-sylcytosine
BDNF	brain-derived neurotrophic factor
BMI	( - )-bicuculline methiodide
BrdU	5-Bromo-2'-deoxyuridine
BSA	bovine serum albumin
CDF	cumulative distribution frequency
CGE	caudal ganglionic eminence
CNQX	6-cyano-7-nitroquinoxaline-2,3-dione disodium salt
CNS	central nervous system
CP	cortical plate
CR	Calretinin
DAPI	fluorescence dye-labeled DNA
dCtx	dorsal cortex
DIC	different interference contrast
DIV	days <i>in vitro</i>
DMEM	Dulbecco's modified Eagle's medium
DNA	deoxyribonucleic acid
E	embryonic day
E/I	excitation/inhibition
EDTA	ethylenediaminetetraacetic acid
EPSC	excitatory post-synaptic current
GABA	$\gamma$ -aminobutyric acid
GABA <sub>A</sub> R	GABA type A receptor
GFP	green fluorescence protein

IN	GABAergic interneuron
IPSC	inhibitory post-synaptic current
KCC2	potassium-chloride co-transporter
KW-ANOVA	Kruskal-Wallis one-way analysis of variance on ranks
MGE	medial ganglionic eminence
MW-RST	Mann-Whitney rank sum test
MZ	marginal zone
N2	serum-free culture medium
NeuN	neuron-specific nuclear protein
NKCC	Na <sup>+</sup> -k <sup>+</sup> -Cl <sup>-</sup> -cotransporter
NMDA	N-methyl-D-aspartate
P	postnatal day
PBS	phosphate-buffered saline
PCR	polymerase chain reaction
PDL	Poly-D-Lysine
PN	projection neuron
PV	Parvalbumin
ROIs	position regions of interest
SEM	standard error of the mean
SOM	Somatostatin
SVZ	subventricular zone
T00	0% GABAergic interneurons
T05	transplant 5% GABAergic interneurons
T45	transplant 80% GABAergic interneurons
Tris	tris (hydroxymethyl) aminomethane
VGAT	vesicular GABA uptake transporter
VIP	vasoactive intestinal peptide
wCtx	whole cortex

# 1. Abstract

## 1.1 Abstract

The stable neocortical networks are generated by the number of glutamatergic projection neurons (PNs), and GABAergic interneurons (INs) maintained at a constant ratio. Since the PN/IN ratio deviations are often associated with the development of neuron pathologies, however, there are limited studies performed on how the altered PN/IN ratios may impact neuronal development and synaptic function.

Therefore, during my Ph.D. study, I used cell culture techniques to generate neuronal networks with defined PN/IN ratios to address the question whether the manipulated PN/IN ratios vary over time and what impacts they may have on PNs and INs survival, proliferation, and the development of network activity, as well as how they influence the excitation/inhibition (E/I) balance of the individual cell.

Networks with different PN/IN content were generated by plating PNs that were obtained from the dorsal cortex of wild-type animals at a density of 1500 cells/mm<sup>2</sup>. After 24 hours, 5% (low GABA, T05), 30% (medium GABA, T25), and 80% (high GABA, T45) of dissociated MGE precursor cells from VGAT-Venus transgenic rats were added, respectively.

During the first week *in vitro*, the initial proportion of transplant INs in cultures was not altered, but the IN content modulated PN numbers, suggesting an increased proliferation in the presence of INs. In the following weeks (7-28 DIV), PNs and INs showed similar cell elimination dynamics. The fraction of INs increased or remained the same in the investigated cultures. The cellular PN/IN ratios remained constant, reflecting the initial plating. When the entire dorsolateral cortex (wCtx, a slightly more mature network containing more interneurons and post-mitotic projection neurons) was applied, the results differed. As there was a greater reduction in IN density in the wCtx networks, the proportion of INs decreased in all network types. Interestingly, the profile of rapid decline in IN fraction in the wCtx was not observed if the cultures were grown in gabazine (a GABA<sub>A</sub> receptor antagonist). Cultures developed spontaneous synchronous network activity at the end of the first week. This synchronous network activity can be examined by Fluo-3 fluorescence imaging of Ca<sup>2+</sup> transients. A burst was defined as more than 10% of all active neurons activated simultaneously in a given field. The analysis of calcium imaging data showed an increase in burst frequency combined with a decrease in the number of neurons participating in a burst and desynchronization in the network with higher IN content (T45 networks). Network activity patterns varied between a stereotypically fully synchronized bursting activity and a more desynchronized bursting pattern

with periodic excitability changes. To access the E/I balance of the individual cell, spontaneous glutamate-mediated currents (sEPSCs) and GABA<sub>A</sub>-mediated post-synaptic currents (sIPSCs) were recorded in 10-minute-long spontaneous voltage-clamp recordings in T05 and T45 networks in a total of 167 PNs and 229 INs between 6-30 DIV. Charge transfer of isolated sPSCs and sPSC burst charge transfer were calculated in each cell. With the help of Mini Analysis, we calculated the mean charge transfer of isolated sPSCs based on integral area values (pAms). An analysis of the mean charge transfer of sPSC bursts was conducted in MATLAB by computing the integral area values above the baseline. The results showed that no matter what the PN/IN proportions in the network, for both transplant types and both cell types, the sIPSC charge transfer/(sEPSC charge transfer + sIPSC charge transfer) ratio (cellular E/I balance) in isolated sPSC was mostly constant (except for a small change in INs of T05 networks). In contrast, when the sPSC bursts were considered, significant differences in the sIPSC burst charge transfer/(sEPSC burst charge transfer + sIPSC burst charge transfer) ratio (network bursts E/I balance) were detected between networks with different PN/IN proportions.

In summary, the results of this study suggest that the cellular E/I balance may maintain constant, regardless of cell numbers. In contrast, the network bursts E/I balance and the maturation of spontaneous network activity are critically dependent on the structural PN/IN ratio.

## 1.2 Zusammenfassung

Neokortikale Netzwerke weisen ein charakteristisches, konstantes Verhältnis zwischen der Anzahl der glutamatergen Projektionsneuronen (PN) und der GABAergen Interneuronen (IN) auf. Da Abweichungen in diesem Verhältnis häufig mit der Entwicklung von Neuronenpathologien in Verbindung gebracht werden, gibt es jedoch nur wenige Studien darüber, wie sich ein verändertes PN/IN-Verhältnis auf die neuronale Entwicklung und synaptische Funktion auswirken kann.

In meiner Doktorarbeit habe ich Zellkulturtechniken verwendet, um neuronale Netzwerke mit definierten PN/IN-Verhältnissen zu erzeugen. In diesen definierten Netzwerken habe ich untersucht, ob sich die manipulierten PN/IN-Verhältnisse im Laufe der Zeit verändern und welche Auswirkungen die experimentell erzeugten PN/IN-Verhältnisse auf das Überleben und die zelluläre Proliferation von PNs und INs haben. Mit bildgebenden und elektrophysiologischen Methoden habe ich die Netzwerkaktivität, sowie das Erregungs-/Hemmungsgleichgewicht (E/I) einzelner Zelle in diesen Netzwerken analysiert.

Netzwerke mit unterschiedlichem PN/IN-Gehalt wurden durch Ausplattieren von PNs, die aus dem dorsalen Kortex von Wildtyp-Tieren gewonnen wurden, in einer Dichte von 1500 Zellen/mm<sup>2</sup> erzeugt. Nach 24 Stunden wurden 5% (niedriges GABA, T05), 30% (mittleres GABA, T25) bzw. 80% (hohes GABA, T45) der dissoziierten MGE-Vorläuferzellen von VGAT-Venus-transgenen Ratten hinzugefügt.

Während der ersten Woche *in vitro* veränderte sich der ursprüngliche Anteil der Transplantat-INs in den Kulturen nicht, aber der IN-Gehalt modulierte die PN-Zahlen, was auf eine verstärkte Proliferation in Gegenwart von INs hindeutet. In den folgenden Wochen (7-28 DIV) zeigten PNs und INs eine ähnliche Dynamik der Zellelimination. Der Anteil der INs nahm in den untersuchten Kulturen zu oder blieb gleich. Die zellulären PN/IN-Verhältnisse blieben konstant, was die anfängliche Auspflanzung widerspiegelt. Wenn der gesamte dorsolaterale Kortex (wCtx, ein etwas reiferes Netzwerk mit mehr Interneuronen und post-mitotischen Projektionsneuronen) verwendet wurde, waren die Ergebnisse unterschiedlich. Da die IN-Dichte in den wCtx-Netzwerken stärker abnahm, sank der Anteil der INs in allen Netzwerktypen. Interessanterweise wurde das Profil des schnellen Rückgangs des IN-Anteils in den wCtx nicht beobachtet, wenn die Kulturen in Gabazin (einem GABA<sub>A</sub>-Rezeptor-Antagonisten) gezüchtet wurden. Die Kulturen entwickelten am Ende der ersten Woche spontane synchrone Netzwerkaktivität. Diese synchrone Netzwerkaktivität kann durch Fluo-3-Fluoreszenzbildgebung von Ca<sup>2+</sup>-Transienten untersucht werden. Als ein Burst wurde Netzwerkaktivität definiert, bei der mehr als 10% aller aktiven Neuronen innerhalb eines bestimmten Feldes gleichzeitig aktiv sind. Die Analyse der

Kalzium-Bildgebungsdaten zeigte eine Zunahme der Burst-Häufigkeit in Verbindung mit einer Abnahme der Burst-Teilnahme und einer Desynchronisation in dem Netzwerk mit höherem IN-Gehalt (T45-Netzwerke). Die Aktivitätsmuster des Netzwerks variierten zwischen einer stereotyp voll synchronisierten Burst-Aktivität und einem eher desynchronisierten Burst-Muster mit periodischen Erregbarkeitsänderungen. Um das E/I-Gleichgewicht der einzelnen Zellen zu ermitteln, wurden spontane Glutamat-vermittelte Ströme (sEPSCs) und GABA<sub>A</sub>-vermittelte postsynaptische Ströme (sIPSCs) in 10-minütigen spontanen Spannungsklemmenaufzeichnungen in T05- und T45-Netzwerken in insgesamt 167 PNs und 229 INs zwischen 6-30 DIV aufgezeichnet. Der Ladungstransfer von isolierten sPSCs und der sPSC-Burst-Ladungstransfer wurden in jeder Zelle berechnet. Der mittlere Ladungstransfer von isolierten sPSCs wurde aus den integralen Flächenwerten (pAms) in MiniAnalysis ermittelt. Der mittlere Ladungstransfer von sPSC-Bursts wurde in MATLAB durch Berechnung der integralen Flächenwerte über der Basislinie analysiert. Die Ergebnisse zeigten, dass unabhängig von den PN/IN-Verhältnissen im Netzwerk für beide Transplantattypen und beide Zelltypen das Verhältnis von sIPSC-Ladungstransfer/(sEPSC-Ladungstransfer + sIPSC-Ladungstransfer) (zelluläres-E/I-Gleichgewicht) in isolierten sPSC weitgehend konstant war (mit Ausnahme einer kleinen Änderung in INs von T05-Netzwerken). Im Gegensatz dazu wurden bei Betrachtung der sPSC-Bursts signifikante Unterschiede im Verhältnis sIPSC-Burst-Ladungstransfer/(sEPSC-Burst-Ladungstransfer + sIPSC-Burst-Ladungstransfer) (Netzwerk-Bursts E/I- Gleichgewicht) zwischen Netzwerken mit unterschiedlichen PN/IN-Anteilen festgestellt.

Zusammenfassend deuten die Ergebnisse dieser Studie darauf hin, dass das zelluläre E/I-Gleichgewicht unabhängig von der Anzahl der Zellen konstant bleibt. Im Gegensatz dazu sind das E/I-Gleichgewicht der Netzwerkbursts und die Reifung der spontanen Netzwerkaktivität kritisch vom strukturellen PN/IN-Verhältnis abhängig.

## 2. Introduction

### 2.1 INs

#### 2.1.1 The generation of cortical INs

Neuronal structures, including the cerebral cortex, consist of various neurons. These neurons can be distinguished in their generated position, unique morphology, connectivity, and input/output function. In general, there are two major types of cortical neurons, glutamatergic projection neurons (PNs) and GABAergic interneurons (INs) (Beaulieu 1993; Meyer et al., 2011). In contrast to other neuronal structures of the brain, however, these two main classes of cortical neurons are generated in different brain regions. PNs, including pyramidal cells, using glutamate as their neurotransmitters, are born from progenitor cells located in the pallium, whereas INs originate in the embryonic sub-pallium and they distribute through the striatum, amygdala, and cerebral cortex [for review, see (Parnavelas 2002; Wonders and Anderson 2006)]. The sub-pallium of rodents and primates, including human beings, can be divided into several progenitor domains.

Lineage analyses in rodents have shown that cortical INs arise predominantly from these regions, including the medial ganglionic eminence (MGE), the caudal ganglionic eminence (CGE) (Tamamaki et al., 1997; Wichterle et al., 1999; Nery et al., 2002; Xu et al., 2004), the preoptic region, which includes the preoptic area (POA), and the adjacent preoptic-hypothalamic (POH) border domain and the septum (Gelman et al., 2009; Gelman and Marin 2010). Each domain is featured by the expression of a specific combination of transcription factors. These transcription factors, including *distal-less homeobox 1 (Dlx1)*, *distal-less homeobox 2 (Dlx2)*, *achaete-scute family bHLH transcription factor 1 (Ascl1)*, *GS homeobox 1 (Gsx1)* and *GS homeobox 2 (Gsx2)*, *aristaless-related homeobox (Arx)*, *LIM homeobox 6 (Lhx6)*, are required for the specification of all INs and restrict the generation of INs into a certain class (Lim et al., 2018). For example, Lhx6-expressing cortical INs originate from the MGE and primarily differentiate into parvalbumin-positive subpopulations (Cobos et al., 2005; Cobos et al., 2006; Liodis et al., 2007; Zhao et al., 2008). The generation of MGE-derived INs in mice commences around E9.5 (embryotic days) with a peak at E13.5 (Miyoshi et al., 2007), and INs start to be generated in the caudal ganglionic eminence (CGE) at E12.5 (Miyoshi et al., 2010). At prenatal stages (E14-E19), GABA-positive cells can be observed mainly in the subplate (SP), marginal zone (MZ), and subventricular zone (SVZ). They get progressively drained from these regions between P0 (postnatal day) and P8. GABA immunoreactivity is present at E14 in the cortical plate (CP) but exhibits its mature pattern only on postnatal days. By P16-P21, the pattern of GABA immunoreactivity reaches similar levels to that of the adult brain (Del Rio et al., 1992).

### 2.1.2 The migration of cortical INs

The adult mammalian cortex is characterized by a 6-layered structure. This structure is formed mainly through the radial migration of pyramidal neurons, which colonize cortical layers following an inside-out integration sequence (Angevine and Sidman 1961; Rakic 1974; Caviness Jr 1982; Fairén et al., 1986). The post-mitotic pyramidal neurons (early-born cells) move from the VZ/SVZ to the pial surface, forming the pre-plate layer. Subsequently, late-born cells split the pre-plate layer into the superficial MZ (layer I) and deeper SP layer, establishing CP in between. Eventually, cells sort out within the CP to form layer VI first and migrate past their predecessors to form the more superficial V-II layers.

INs from their birth-place migrate first tangentially to the proper cortical regions and then radially through the CP to reach their final locations (Anderson et al., 1997; Nery et al., 2002). The tangential migration of these cells follows three distinct migratory streams [for review, see (Yanagida et al., 2012)]. The migrating INs into MZ or SVZ are the routines for the majority ones. Migrating into SP is for a smaller group. Remarkably, INs avoid migrating through the CP during tangential migration, whereas pyramidal cells begin forming cortical layers in this location (Wichterle et al., 2001). When INs invade the CP, they switch their direction radially, migrating to their destinations (Polleux et al., 2002; Luhmann et al., 2015). Finally, in the final phase of migration INs migrate into the specific layers of the cortex where they eventually allocate, likely by responding to chemical signals that are produced by the pyramidal cells (Lodato et al., 2011; Miyoshi and Fishell 2011; Marin 2013).

It has long been recognized that, as a whole, INs colonize cortical layers following an inside-out sequence of integration similar to that followed by pyramidal cells, with early-born cells occupying deeper layers and late-born cells occupying superficial layers (Cavanagh and Parnavelas 1989; Anderson et al., 2002). However, there are exceptions to this rule as it has been observed that early-born neurons occupy around 2 locations, layer V (a large peak) and layers II/III (a minor peak) (Yozu et al., 2004). Further studies in rats have shown that MGE-derived INs indeed follow the inside-out laying pattern. However, CGE-derived INs seem to allocate superficial layers following an outside-in pattern, with early-born cells settling in layers II/III and late-born in layers V-VI (Rymar and Sadikot 2007). These results indicate that the final allocation of INs in the CP is not only dependent on the time when they generate but is also determined by their birth-place.

### 2.1.3 Subclasses of Neocortical INs

The cortical INs are comprised of highly heterogeneous various subpopulations, which can be defined by: (1) their morphology (soma, axonal, and dendritic arbors); (2) molecular markers including but not restricted to calcium-binding proteins (parvalbumin, calretinin, calbindin), neuropeptides [e.g., vasoactive intestinal peptide (VIP), neuropeptide Y (NPY), reelin, somatostatin], and receptors (e.g., 5-hydroxytryptamine receptor 3A (5HT3R), Metabotropic glutamate receptor 1 (mGluR1), Cannabinoid receptor type 1 (CB1); (3) their post-synaptic target cells/their subcellular compartments; (4) area of origins and transcription factors involved in subtype fate determination; (5) intrinsic physiological properties; and (6) function in the adult brain (Kubota et al., 1994; Gonchar and Burkhalter 1997; Petilla Interneuron Nomenclature et al., 2008). Researchers have identified at least 20 different cortical subtypes and 21 hippocampal subtypes (Klausberger and Somogyi 2008; Fishell and Rudy 2011). According to their neurochemical content, INs in the postnatal neocortex can be divided into three major subclasses: parvalbumin (PV)-, somatostatin (SOM)-, and calretinin (CR)-expressing cells (Kubota et al., 1994; Gonchar and Burkhalter 1997). Several lines of evidence in mice have shown that early-born (E11.5-E14.5) INs originate from the MGE and mainly produce the parvalbumin (PV)- and somatostatin (SOM)-expressing subtypes, which contribute primarily to deep cortical layers, and late-born (E14.5-E16.5) INs derive predominantly from the CGE and generate CR- and/or VIP-expressing interneurons, and preferentially occupy the superficial cortical layers (Nery et al., 2002; Xu et al., 2004; Butt et al., 2005; Fogarty et al., 2005; Cobos et al., 2006; Miyoshi et al., 2007; Miyoshi et al., 2010). PV<sup>+</sup> interneurons are the largest class of cortical INs, which can be further divided into three major subclasses: chandelier cells, basket cells, and translaminal interneurons. All of these cells exhibit the feature of fast-spiking properties. Chandelier cells or axo-axonic cells selectively form synapses onto the axon initial segments of pyramidal cells (Szentagothai and Arbib 1974; Jones 1975; Somogyi 1977) and are particularly enriched at the border between layers 1, 2, and 6 (Taniguchi et al., 2013). PV<sup>+</sup> basket cells innervate somata (Wang et al., 2002) and form synapses on proximal dendrites on pyramidal cells or other cortical INs (Hu et al., 2014). They are distributed through 2 to 6 layers in the neocortex and across cortical regions. PV<sup>+</sup> translaminal interneurons constitute a relatively rare type than PV<sup>+</sup> chandelier neurons and PV<sup>+</sup> basket cells. They are mainly rich in 5 and 6 layers (Buchanan et al., 2012; Bortone et al., 2014). SOM-expressing interneurons are the second largest class of INs, which can be divided into two main subclasses: Martinotti and non-Martinotti cells (Tremblay et al., 2016; Riedemann 2019). Martinotti cells are well beyond 50% in layer 2/3 (Ma et al., 2006; Xu et al., 2013). Usually, they have spindle or ovoid-shaped somata with diverse somatodendritic morphologies (Marin-Padilla 1990; Riedemann 2019). They are characterized by a long translaminal ascending axon that arborized profusely in layer 1 (Ma et

al., 2006; Xu et al., 2013; Hilscher et al., 2017). Non-Martinotti cells lack axons in layer 1 and are found throughout layers 2 to 6. The larger fraction of non-Martinotti cells with a basket-cell-like morphology is in layer 4, where they primarily target PV<sup>+</sup> basket cells (Halabisky et al., 2006; Ma et al., 2006; Xu et al., 2013). One of the subpopulations of cortical non-Martinotti SOM<sup>+</sup> interneurons is the so-called long-range INs, whose axons can project to the remote brain areas and mostly co-express neuronal nitric oxide synthase (NOS), chondrolectin (Chodl), and NPY (He et al., 2016) and are mainly found in layer six as well as the white matter (Tamamaki and Tomioka 2010; Tomioka et al., 2015). The function of long-range INs is thought to generate rhythmic oscillations in the hippocampus (Ben-Ari et al., 1989). These neurons in the white matter receive the excitation from the cortical inputs but lack the thalamic inputs. However, how the long-range INs regulate the neocortical circuits is still unknown.

#### 2.1.4 Neurotransmitters

##### Glutamate

Glutamate, a dicarboxylic amino acid, is the principal excitatory neurotransmitter in the mammalian cerebral cortex and generally acts on two types of ionotropic receptors: AMPA receptors and NMDA receptors (R) (N-methyl-D-aspartate) (Bekkers and Stevens 1989). AMPA receptors mediate fast excitatory synaptic transmission and induce depolarization in post-synaptic neurons, whereas NMPA receptors initiate synaptic plasticity [for review, see (Traynelis et al., 2010)].

##### GABA

On the other hand,  $\gamma$ -aminobutyric acid (GABA) is the main inhibitory neurotransmitter in the mature CNS, which is released by INs. It acts on GABA<sub>A</sub>, GABA<sub>B</sub>, and GABA<sub>C</sub> receptors (Sivilotti and Nistri 1991). Whereas the GABA<sub>B</sub> receptors are G-protein-coupled metabotropic receptors (G-protein coupled receptors and not dependent on the electrochemical equilibrium of chloride ions for their function), both GABA<sub>A</sub> and GABA<sub>C</sub> receptors are Cl<sup>-</sup>-permeable receptors (Bortone and Polleux 2009). Even if GABA can depolarize the immature cell membrane during the early development (LoTurco et al., 1995), in general, GABA<sub>A</sub> receptors hyperpolarize cells to avoid neuronal overexcitability (Kahle et al., 2008). Thus, many interesting reviews address the idea that GABAergic signaling regulates neuronal activity precisely (Cline 2005; Akerman and Cline 2006; Berg et al., 2007; Dornn et al., 2010; Sun et al., 2010; Yizhar et al., 2011).

### 2.1.5 The development of neural circuits

It is thought that the development of neural circuits in a brain can be divided into three separate phases (Katz and Shatz 1996).

The first phase of the development of neural circuits is named the early activity-independent phase. During this phase, neurons migrate to their destined positions and establish initial crude connectivity (Katz and Shatz 1996). During the phase of spontaneous activity, spontaneous activity has been observed to occur transiently in many organs (Milner and Landmesser 1999; Crépel et al., 2007; Tritsch et al., 2007; Watt et al., 2009; Martini et al., 2021) and influence the developing neuronal circuits. In the later activity-dependent phase, when the sense organs gradually mature, the final refinement of the developing circuits relies more on sensory-evoked activity and less on spontaneous activity (Katz and Shatz 1996; Kilb et al., 2011; Martini et al., 2021; Redolfi and Lodovichi 2021).

### 2.1.6 Function role of GABA signaling in neural circuit development

#### 2.1.6.1 Depolarizing GABA signaling

GABA acts through GABA<sub>A</sub> receptors, permeable to Cl<sup>-</sup> (Kahle et al., 2008). The direction of current flow in response to GABA is determined by the Cl<sup>-</sup> gradient across the cell membrane (LoTurco et al., 1995)

The intracellular levels of Cl<sup>-</sup> in a neuron are controlled by the relative expression of two proteins. One protein is the potassium-chloride cotransporter 2 (KCC2), which transports Cl<sup>-</sup> out of a cell. The other one is the sodium-potassium-chloride cotransporter 1 (NKCC1), which leads to the uptake of the concentration of the Cl<sup>-</sup> ([Cl<sup>-</sup>]<sub>i</sub>) in a cell (Russell 2000). During the early stages of neuronal development in the immature neocortical neurons, the expression of KCC2 is relatively low. In contrast, the expression of NKCC1 is relatively high. The down-regulation of KCC2 and up-regulation of NKCC1 cause a developmental increase in [Cl<sup>-</sup>]<sub>i</sub>. The cell membrane is depolarized. As neurons mature, neurons change their complement of chloride transporters. The developmental up-regulation of KCC2 and down-regulation of NKCC1 lead to a decrease in [Cl<sup>-</sup>]<sub>i</sub>. The cell membrane is hyperpolarized.

In many brain regions, neurons receive GABAergic inputs before glutamatergic inputs during early stages (Sin et al., 2002; Akerman and Cline 2006); thus, for a long time, GABA has been known as the excitatory transmitter (Obata et al., 1978; Mueller et al., 1984; Ben-Ari et al., 1989). For instance, in the immature hippocampus, the developing networks generate primitive

patterns of network activity, notably the giant depolarizing potentials (GDPs) (Ben-Ari et al., 1989). GDPs disappear when the GABA<sub>A</sub> receptor-mediated depolarization switch to hyperpolarization (Leinekugel et al., 1997). Or ionotropic glutamate or GABA<sub>A</sub> receptor antagonists can block this spontaneous activity (Hanson and Landmesser 2003; Hanson and Landmesser 2004). Thus, the depolarizing GABA is crucial for generating GDPs in the developing hippocampus. The discovery that the depolarizing action of GABA shifts to hyperpolarizing was also observed in the neurons of the cortex (Martina et al., 2001; Gullledge and Stuart 2003), including in cultured embryonic rat cortex (Voigt et al., 2001; Opitz et al., 2002). This shift is regarded as a conserved mechanism [for review, see (Batista-Brito and Fishell 2009)].

#### 2.1.6.2 GABA signaling in spontaneous network activity

During early development, neural structures, such as the spinal cord, hippocampus, cochlea, cerebellum, thalamus, etc., show spontaneous activities (Milner and Landmesser 1999; Crépel et al., 2007; Tritsch et al., 2007; Watt et al., 2009; Martini et al., 2021). Although the architectures of these neural structures differ, the mechanisms that generate and propagate spontaneous network activity are similar (Blankenship and Feller 2010).

It has been found that the developing neural structure is affected by spontaneous activity in many aspects. For example, spontaneous activity controls the proliferation of GFAP-positive precursors in the postnatal SVZ (GFAP, glial fibrillary acidic protein) (Liu et al., 2005). In addition, Mennerick and Zorumski (2000), as well as Zheng and Poo (2007) review studies on the effects of spontaneous activity at the early stage of neuronal development on neuronal migration and survival, respectively. Furthermore, the specifications of neurotransmitters (Spitzer 2012) and the growth of axons and dendritic trees (Uesaka et al., 2006) are required for the generation of spontaneous activity.

During early development, neurons via glutamate receptors drive the spontaneous activity, but the excitatory action of GABA also contributes. Thus, the rate of spontaneous activity can be blocked or slowed by glutamate and GABA<sub>A</sub> receptors antagonist (Hanson and Landmesser 2003; Hanson and Landmesser 2004). In the cultured rat cortex, the spontaneous activity occurs as early as 7 DIV (days *in vitro*). In the cultured rat hippocampus, it occurs at 3–7 DIV (Cohen et al., 2008). Due to it is characterized by simultaneous transients of  $[Ca^{2+}]_i$ , a network calcium transient can be recorded by  $Ca^{2+}$  imaging (Opitz et al., 2002). At the initial neural development stage, the rate of synchronized activity is low. Only a small proportion of neurons in cultures synchronously participate. The functional GABA<sub>A</sub> receptor has been shown to play a vital role

in driving this synchronous spontaneous activity during the first half of the second week, during which GABA acts in an excitatory manner (Voigt et al., 2005). After 12 days in cultures, this recurrent activity becomes not required for depolarizing GABA. As neurons mature, nearly all of them participate in this synchronous oscillatory activity, and the rate of it increases (Opitz et al., 2002). Consistent with the MEA (Micro Electrode Arrays) analyses (Baltz et al., 2010), the study in my research also revealed the density of GABA in a network determines spontaneous activity patterns (Xing et al., 2021).

Previous research revealed the observations of the features of developing spontaneous network activity in the cerebral cortex *in vitro* and *in vivo* are comparable (Adelsberger et al., 2005).

### 2.1.6.3 The balance of excitation and inhibition is regulated by GABA signaling during neural circuit formation

Maintaining the balance of excitation and inhibition (E/I balance) in a neuron and neuronal networks is essential for normal brain development. As mentioned in chapter “2.1.6.1”, the direction of  $\text{Cl}^-$  ions flow through  $\text{GABA}_A$  receptors depends on the intracellular levels of  $\text{Cl}^-$ , the levels of which are regulated by the  $\text{Cl}^-$  transporters. Previous work has shown that immature brains are susceptible to epilepsy due to the altered  $\text{Cl}^-$  transporter function (Dzhala et al., 2005). Thus,  $\text{Cl}^-$  is crucial for adjusting the E/I balance during neuronal development. During early development, hyperpolarizing GABAergic inhibition and glutamatergic excitation are both relatively weak. As development progresses, both increase (Hollrigel and Soltesz 1997; Dunning et al., 1999). Evidence *in vitro* has shown that neuronal activity modulates the E/I balance in an activity-dependent manner. (Kilman et al., 2002; Liu 2004). One hypothesis assumes that inhibition is regulated by matching the excitation level during the circuit development. That is, rather than acting as a controller of circuit development, the development of increased hyperpolarization GABA transmission could respond to the changes in the glutamatergic excitatory drive. In studies, it has been proposed the coordination of subsequent levels of excitatory and inhibitory inputs is required for early depolarizing GABA. Multiple lines of evidence have confirmed that an increase in the ratio of inhibitory to excitatory input is caused by a premature hyperpolarizing shift in  $\text{Cl}^-$  reversal potential (Chudotvorova et al., 2005; Akerman and Cline 2006; Ge et al., 2006). For instance, in the *Xenopus* visual system *in vivo*, reducing the levels of  $\text{Cl}^-$  in tectal neurons by increasing the expression of the  $\text{K}^+$ - $\text{Cl}^-$  co-transporter KCC2 results in the activation of the  $\text{GABA}_A$  receptor from depolarizing to hyperpolarizing. As a consequence, the inhibitory of GABAergic inputs to the tectal neurons is increased. This is in agreement with the general idea. The inhibitory GABA inputs are regulated

by glutamatergic synapses, while the establishment of glutamatergic synapses is required for the depolarizing GABA [for review, see (Chudotvorova et al., 2005)]. Thus, it may be at the beginning of synaptogenesis, when different types of homeostatic mechanisms are in place, depolarizing GABA plays a crucial role in driving neuronal circuits. With neuronal maturation, the shift in the action of GABA from excitatory to inhibitory, which is mediated by activity-dependent control of  $K^+$ - $Cl^-$  co-transporter KCC2 (Fiumelli and Woodin 2007), could also be part of the mechanisms that adjust to E/I balance.

### 2.1.7 Cortical INs in culture

As genetic factors determine the identity of cortical INs (Huang 2009; Cossart 2011), dissociated INs grown *in vitro* develop similar morpho-physiological properties to those observed *in vivo* (de Lima and Voigt 1997; Voigt et al., 2001; Kawaguchi and Kondo 2002; de Lima et al., 2004). Thus, evidence has been largely accumulated on the properties of developing cortical INs in cultured embryonic rat neocortex (de Lima and Voigt 1997; Voigt et al., 2001; de Lima et al., 2004; Wu et al., 2006; Oenarto et al., 2014).

In cultured embryonic rat neocortex, two IN subpopulations, Large INs, and Small INs, were identified (de Lima and Voigt 1997). The first subclass of cortical INs is Large INs. They are found in 4 hours after plating. The second main type of cortical INs is Small INs. They are generated in the culture between 4 DIV-12 DIV. During the second week of the intro, Large INs possess apparent large soma. Their thick axons are densely interconnected, forming long-range connections (Voigt et al., 2001). In mature cultures, a large number of Large INs are PV-positive cells (de Lima et al., 2004). The majority of PV<sup>+</sup> Large INs are fast-spiking cells (Itami et al., 2007). In Small INs, the soma of cells is small bipolar, or multipolar. Their axons are thin (de Lima and Voigt 1997; de Lima et al., 2004). Both CR and VIP are expressed in them (Kawaguchi and Kubota 1997). Compared with physiological differences between Large INs and Small INs, it has been reported that Large INs play a vital role in generating early spontaneous activity during network formation (Voigt et al., 2001). In the early postnatal stages, Large INs, which have high connectivity and GABA-driven depolarization, can drive synchronous activity without glutamatergic transmission. In contrast, Small INs have been demonstrated strongly rely on synchronous activity during 4 DIV to 12 DIV (de Lima et al., 2004). Thus, we can distinguish these two types of INs from their morphologies or their role in the networks.

### 2.1.8 Regulation of the number of cortical INs

For the brain to function properly, neural networks should maintain stable levels of activity, although they are sculpted by experience (Tatti et al., 2017).

In the neocortex, the preservation of balanced excitatory and inhibitory synaptic drive into cortical INs is thought to be crucial for maintaining neural network function (Gogolla et al., 2009). The mean proportions of INs in the neocortex of rodents [15-16%, (Beaulieu 1993; Gabbott et al., 1997)], and primates [20-25%, (Hendry et al., 1987; Gabbott and Bacon 1996; Mao et al., 2001; Froemke 2015)] may be structural correlates of the E/I balance. Considering the distant origin of PNs and INs, it is interesting how the number of cortical INs is ultimately determined. One possibility is that cortical INs are overproduced, and then after their migration into the cortex, the excess INs are eliminated through programmed cell death. Studies *in vitro* have shown that even without external factor-induced, cortical INs death is intrinsically programmed (Xu et al., 2004). In Southwell et al.'s studies (2012), roughly 12 days after INs are born in the sub-pallium, they undergo apoptosis. It seems to be that when they reach a predetermined cellular age, they die. Inconsistent with the observations *in vivo* that early-born infragranular layer INs disappeared before late-born supra-granular layer INs (Wong et al., 2018). It seems that INs are programmed to die when they reach a particular maturation stage. Therefore, it is intriguing to wonder why not all INs die during normal development. Several lines of evidence suggest that the process of programmed cell death is linked to the integration of INs into nascent cortical circuits. First, it is suggested that the fate of INs is determined by their own activity levels at the beginning of the cell death period (Wong et al., 2018). If INs are activated before cell death occurs, they are more likely to survive. Second, cell-autonomous manipulation of the excitability of cortical INs affects their survival. For instance, increasing the excitability of INs using DREADDs (interneurons expressing designer receptors exclusively activated by designer drugs) or NaChBac (bacterial voltage-gated sodium channel) cell-autonomously enhances their survival (Denaxa et al., 2012; Priya et al., 2018) while decreasing the excitability of INs through over-expressing of Kir2.1 (inward-rectifying potassium channel) cell-autonomously diminishes their survival (Close et al., 2012; Priya et al., 2018).

However, research examining the molecular mechanisms regulating programmed cell death in cortical INs is limited. One factor PTEN (phosphatase and tensin homolog), seems to be a critical protein in regulating programmed cell death. This protein antagonizes the activity of the serine-threonine kinase AKT (Stambolic et al., 1998), which is a pivotal mediator of neuronal survival (Datta et al., 1997; Dudek et al., 1997). Interestingly, during the period of programmed cell death, the rising the levels of PTEN in cortical INs result in INs in the infragranular layer

increasing first, followed by superficial layer INs (Wong et al., 2018). Studies have shown that this process is controlled by the protein PTEN (Wong et al., 2018). First, when deleting the gene *Pten* from postmitotic MGE-derived INs can decrease apoptosis in these neurons (Wong et al., 2018). Second, the expression of PTEN in INs is non-cell autonomously repressed by experimentally increasing the activation of pyramidal cells (Wong et al., 2018), and thus, the survival of INs is increased. In sum, the PTEN signaling pathway is likely to be required for IN apoptosis during the period of programmed cell death.

## 2.2 Diseases and treatment

Perturbations of the E/I balance have often been identified as deficits of GABAergic signaling, and a plethora of neuropathologies associated with E/I disbalance (e.g., schizophrenia, epilepsy) show IN deficits (Sloviter 1996; Cossart et al., 2005; Avramescu et al., 2009; Jin et al., 2011). Moreover, genetic disturbances of IN development, especially those resulting in decreased numbers of some types of INs, are associated with cortical network hyperexcitability and seizures (Powell et al., 2003; Cossart et al., 2005; Mohler 2006; Azim et al., 2009; Friocourt and Parnavelas 2010; Deidda et al., 2014). Interestingly, INs' subtypes show differential vulnerability to insults and are differentially affected in diseased conditions (Zhang and Poo 2001; de Lima et al., 2004; Gill et al., 2010). In recent years, transplanting precursor neurons or stem cells into a diseased or injured brain may allow the reconstitution of neural circuits in the recipient animal (Bjorklund and Lindvall 2000; Emsley et al., 2004; Winkler et al., 2005).

To ensure success, the transplanted cells should have the capacity for dispersing and differentiating appropriately into mature neurons with correct neurotransmitters or neuropeptides. Ideally, these cells should functionally integrate into the affected areas, replace lost neurons, restore function and promote brain self-repair. Publications have revealed that MGE cells dissected from the embryos and transplanted into an adult brain can migrate, differentiate into INs, and functionally integrate into the host brain (Alvarez-Dolado et al., 2006; Hunt et al., 2013; Howard and Baraban 2016). In addition, studies on the transplantation of GABAergic precursors in animal models have shown that INs played a vital role in decreasing the susceptibility of seizures during seizure induction (Zipancic et al., 2010; Hunt et al., 2013; Hammad et al., 2015). Thus, to develop cell-transplanted therapies in the postnatal brain, it is essential to demonstrate that transplanted neuronal precursors can migrate, differentiate, and form functional synapses.

### 2.3 The aims of my study

Multiple mechanisms have been proposed in chapter “2.1.8” to explain how the PN/IN ratio is achieved during development. However, it is still unclear which regulatory processes are involved in establishing the excitation/inhibition (E/I) ratio or PN/IN ratio and how these INs affect the global inhibition circuits during the development. Thus, in this study, we used cell culture techniques to generate neuronal networks with defined PN/IN ratios to address the question whether the manipulated PN/IN ratios change over time and how individual nerve cell regulates their spontaneous excitatory (sEPSCs) and inhibitory (sIPSCs) post-synaptic currents to stay functional.

To answer these questions, we prepared cultured neurons from the dorsal portion of E16 rat cortices. At this early stage, the first PNs destination for layers 6 and 5 are generated from dorsal cortex neuroblasts (dCtx) [see book review by (Bayer and Altman 1991)]. For some experiments, we used the whole cortex as neuronal donor tissue, which was obtained from the entire cortical wall, including the dorsal and lateral parts. Due to the developmental gradients of the rat cortex (Bellion et al., 2003; Bellion and Metin 2005), the lower lateral portion of the rat cortical anlage, at E16, was invaded by MGE-derived INs, whereas the higher dorsal part is free of INs (Batista-Brito and Fishell 2009; Chu and Anderson 2015). Consequently, an E16 whole cortex contained a few early-born INs. In contrast, dissociated neurons from the E16 rat dorsal cortex formed IN-depleted neuronal cultures (T00 networks) that consisted predominantly of cortical PNs. To these T00 networks, we added 5%, 30%, and 80% of dissociated Venus-expressing INs to generate T05, T25, and T45 networks, respectively. These Venus-expressing INs were obtained from the dissociated MGE of VGAT-Venus transgenic rat embryos at E14.

Neuronal networks with different predefined PN/IN ratios (T05, T25, and T45 networks) were characterized using immunocytochemistry,  $Ca^{2+}$ -imaging methods, and electrophysiology. The molecular phenotypes of transplanted-MGE precursors were analyzed using antibodies against GABA, calretinin (CR), parvalbumin (PV), and somatostatin (SOM). sEPSCs and sIPSCs were recorded from PNs and INs between 6 and 30 DIV.

The specific aims of this study are:

- First, how do INs influence the initial development of the dorsal cortical networks?
- Second, which one affects PNs' survival by total neuron density or IN density?
- Third, is there a time window in which INs can be integrated successfully into the network?

This includes the question of the most effective age and functional state of the network for interneuronal integration.

- Fourth, how do GABAergic precursor cells change the network in PN and IN morphological properties, synaptic connectivity, E/I balance, and network activity?

These results are expected to provide valuable data for using GABAergic precursor cells as the therapeutic tools in preventing chronic alteration of E/I balance associated with neurodevelopmental diseases such as autism, schizophrenia, and seizures.

### 3. Materials and Methods

#### 3.1 Lab-housed animals

In our study, the brains of Wistar rats (Charles River, Sulzfeld) and VGAT-Venus transgenic rats (Uematsu et al., 2008) were used to prepare neuronal cultures. Ear biopsies were collected by ear punch from 3.5- to 4- week-old rats for genotyping. The genotype of rats was identified by polymerase chain reaction (PCR). The animals were kept in standard laboratory cages with nesting materials, food, and water supplies. They were housed in a room with a constant room temperature ( $21 \pm 0.3^\circ\text{C}$ ), a 12 h light-dark cycle, and a humidity of  $55 \pm 10\%$ . The animal was cared for according to the European Committee Council Directive (63/10 EEC). The local animal care committee established ethical guidelines for using experimental animals in research (Landesverwaltungsamt Sachsen-Anhalt).

#### 3.2 Materials

##### 3.2.1 Buffer

<u>artificial cerebrospinal fluid (aCSF)</u> (PH 7.4)	<u>0.75 mM MgCl<sub>2</sub></u> <u>1.25 mM NaH<sub>2</sub>PO<sub>4</sub></u> <u>1.5 mM CaCl<sub>2</sub></u> <u>5 mM KCl</u> <u>15 mM HEPES/NaOH</u> <u>20 mM D-glucose</u> <u>140 mM NaCl</u> <u>Aqua dest.</u>
<u>Phosphate buffered saline (PBS)</u> (PH 7.4)	<u>1.4 mM KH<sub>2</sub>PO<sub>4</sub></u> <u>2.6 mM KCl</u> <u>8.1 mM Na<sub>2</sub>HPO<sub>4</sub></u> <u>137 mM NaCl</u> <u>Aqua dest.</u>
<u>Tris/metabisulfite solution</u>	<u>0.05 M Tris (pH 7.5)</u> <u>0.85% sodium metabisulfite</u> <u>Aqua dest.</u>

<u>Preincubation solution</u>	<u>1.2% Triton X-100</u> <u>3% bovine serum albumin</u> <u>10% normal goat serum</u> <u>Tris/metabisulfite solution</u>
-------------------------------	--

### 3.2.2 Cell culture Medium

<u>Primary antibody</u>	<u>0.6% Triton X-100</u> <u>3% bovine serum albumin</u> <u>10% normal goat serum</u> <u>Tris/metabisulfite solution</u>
<u>Secondary antibody</u>	<u>0.1 M PBS (pH 7.4)</u> <u>0.3% Triton X-100</u> <u>2% bovine serum albumine</u> <u>5% sucrose</u> <u>10% normal goat serum</u>

### 3.2.2 Mediam for cell culture

Dissociation buffer	0.5% trypsin/EDTA (Gibco, Carlsad, USA) in Hank's medium
Hank's medium ( <u>PH 7.4</u> )	20 mM HEPES (Carl Roth, Karlsruhe, Germany) Hank's balanced salt solution (Gibco, Carlsad, USA)
Medium for astrocyte	10% fetal calf serum (FCS; Gibco, Carlsad, USA) Dulbecco's modified Eagle medium (DMEM, Gibco, Carlsad, USA)
Medium for N2 neuron	25% Ham's F12 (Gibco, Carlsad, USA) 75% DMEM (Gibco, Carlsad, USA)N2 supplements (Gibco, Carlsad, USA)

### **3.3 Cell culture**

#### 3.3.1 Petri dishes for cell culture

To prepare cultured cortical neurons, a unique set-up of dishes was used to allow neurons to grow in the center free of glial cells. Every glass coverslip that had been acid-cleaned was attached to a 10-mm hole in the bottom of a 60 mm Petri dish and given an overnight treatment with poly-D-lysine (PDL, 0.1 mg/ml in borate buffer pH 8.5, 36°C). A Plexiglas ring was sealed with silicon grease around the hole and served as a temporary barrier, preventing the glial cells from spreading over the coverslip. After the neurons were attached, the plastic ring was taken off so that the media between the centrally cultivated neurons and the peripherally cultured feeder glia cells could be freely exchanged.

#### 3.3.2 Primary rat astroglial cell cultures

Astroglial cultures were prepared from the cerebral hemispheres of the newborn or P 0-2 Wistar rats, as published in detail by (de Lima and Voigt 1999). Briefly, meninges were carefully removed after hemispheres were dissected in sterile conditions. The tissue was cut into small pieces with sharp blades in Hank's medium (HBSS, Ca<sup>2+</sup> and Mg<sup>2+</sup> free, Invitrogen; 20 mM HEPES, pH 7.4), and it was then triturated through G21 and G25 syringe needles to break up the tissue's components. In tissue culture flasks (175 cm<sup>2</sup>), cells were planted at low densities in Dulbecco's modified Eagle's medium (DMEM) with 10% fetal calf serum (FCS) and then incubated at 36°C in a 5% CO<sub>2</sub>/95% air incubator. Twice per week, the medium was switched out. After two weeks, confluent cultures were shaken overnight at room temperature on a rotatory platform at 180 rpm (rotations per minute) to eliminate non-astroglial cells. For pure neuronal cultures or for conditioning freshly prepared serum-free medium, confluent astroglial cultures were employed as feeder layers. Five to eight days before the neurons plating in the central area, purified astroglial cells were seeded in the outer region of the Petri dish bottom at 300 cells/mm<sup>2</sup>.

#### 3.3.3 Neocortical neurons in culture

After 16 days of insemination (day of insemination named as E1), Wistar rats were treated with 4% chloral hydrate (1 ml/100 g body weight) for anesthesia, and embryos were isolated to a petri dish by caesarean section for neuronal cultures. 10% chloral hydrate was given to the mother rats after the removal of the embryos to trigger the death. The embryonic neocortical hemispheres were collected from the embryos in ice-cold Hank's medium. Cells were harvested

from the dorsal (dCtx) or whole (wCtx) cortex (see below). The cortex's meninges were carefully removed with scissors. The isolated cortical tissue was minced and incubated with 0.5% trypsin/EDTA (ethylenediaminetetraacetic acid; Boehringer Mannheim, Germany) in Hank's medium for 15 min at 36°C to dispute cell-to-cell contacts, and then the cortical tissue was treated with trypsin inhibitor-DNAase solution [0.52 mg/ml soybean trypsin inhibitor, 0.04 mg/ml DNAase I and 3 mg/ml bovine serum albumin (BSA) dissolved in DMEM] after removing the trypsin/EDTA solution. The cortical tissue was mechanically triturated three times using G21 and G25 syringe needles to generate the suspended cells. The suspended cells were collected by centrifugation (10 min, 1200 rpm) and resuspended in Hank's medium.

The proportion of live cells was assessed using propidium iodide. For neuronal cultures, the cells were seeded onto the PDL-coated sterile coverslips in dishes with an astrocytic feeder layer and incubated in an N2 medium in a humidified 5% CO<sub>2</sub> incubator at 36°C. The plated cell density was 1500 cells/mm<sup>2</sup>. Three times per week, one-third of the total volume of the culture media was replaced with the glia-conditioned medium. To prevent cell aggregation and reduce neuronal network detachment, between 5 and 8 DIV (days *in vitro*), freshly dissociated astrocytes were plated onto the neurons at the density of 300 cells/mm<sup>2</sup> except astrocytic feeder layer growing outside the neuronal network. Under this circumstance, neuronal networks were maintained at high quality for four weeks for further study.

The cortical neurons from E16 embryos were separated into two sets according to cellular content. We used the E16 dorsal cortex as neuronal donor tissue for dCtx cultures in one separation. In the other set, we used the entire dorso-lateral cortical wall (excluding the hippocampus and basal telencephalic anlage) as donor tissue for wCtx cultures. As Bellion et al. (2003, 2005) reported, at E16, neurons from the lateral regions are more developed than those from the dorsal regions due to the developmental gradients in the cortical anlage from lateral to medial. GABAergic precursors from the MGE invade the developing cortex from ventro-lateral to the dorso-medial region (Batista-Brito and Fishell 2009; Chu and Anderson 2015). Thus, at E16, a wCtx preparation contains early-born INs, while the dorso-medial part still lacks INs. GABAergic neuronal populations developed in the dorsal and dorso-lateral parts of the rat embryonic cortex revealed differences shown in "Result" section "4.4.2".

### 3.3.4 Cortical networks

To obtain IN-free networks (T00 networks), the cell suspension from the dorsal cortex of E16 wild-type rat embryos was plated at 1500 cells/mm<sup>2</sup> onto PDL-coated coverslips in an N2 medium. After four hours *in vitro*, two fields were selected randomly in each dish to check

whether the cells were attached to the coverslips. More than 70% of the plated cells effectively adhered to the coverslips ( $1101.0 \pm 18.3$  cells/mm<sup>2</sup>;  $n = 270$  fields). Data were collected from 105 cultures. The cell density increased by a factor of 1.47 within 24 h cell proliferation (live cell counts at 1 DIV) to around  $1614.0 \pm 30.8$  cells/mm<sup>2</sup> ( $n = 270$  fields). At 2 DIV, cultures were then given Ara-C (a mitotic inhibitor, 1- $\beta$ -D-Arabinofurano-sylcytosine; Calbiochem) at a final concentration of 5  $\mu$ M to terminate the cell proliferation, and after 24 hours, a glial-conditioned medium was switched out to remove completely Ara-C. A drop in neuronal density was observed as a result of the natural occurrence of cell death and the stop of cell proliferation by Ara-C after 2 DIV. At 7 DIV, in fifteen cultures from six independent experiments, we found the mean NeuN-(neuron-specific nuclear protein) positive cell density in T00 networks was  $1309.7 \pm 42.5$  cells/mm<sup>2</sup> (mean  $\pm$  SE,  $n = 180$  fields). In the same cultures, the number of NeuN co-expressed GABA was meager ( $0.8 \pm 0.25$  INs/mm<sup>2</sup>, mean  $\pm$  SE,  $n = 180$  fields). These GABA neurons, also known as parvalbumin-expressing Large-INs, are the first subpopulation entering the developing cortex (De Lima and Voigt, 1997; Voigt et al., 2001; De Lima et al., 2004).

### 3.3.5 Preparation of dissociated MGE

GABAergic precursor cells were prepared from the dissociated MGE obtained from the VGAT-Venus transgenic rat embryos at E14 (Uematsu et al., 2008). The gene *VGAT*, vesicular GABA transport, facilitates GABA transporting into synaptic vesicles. The gene *Venus* (a derivative of yellow fluorescent protein (YFP) can enhance fluorescence 20-fold brighter than GFP. In GABA-positive neurons can also find fluorescent Venus. Before the dissected MGE was transplanted into the dish, each embryo was examined under a fluorescent microscope to confirm Venus. We only prepared embryos that have eGFP-expressing in CNS. Due to the high density of GABA precursor neurons destined for the neocortex present in E14 MGE in rat embryos, this preparation offered greatly enriched INs. We plated MGE cells at 1500 cells/mm<sup>2</sup> and cultured them identical to all other cortical network conditions. After plating for 4 hours, we counted the cells. 84.5% of the plated cells effectively adhered to the coverslips ( $1268.1 \pm 34.7$  cells/mm<sup>2</sup>;  $n = 74$  fields). Data were from three independent experiments. In each dish, we randomly picked two fields to count the cells. The cell density increased from  $1268.1 \pm 34.7$  cells/mm<sup>2</sup> to around  $1738.0 \pm 39.8$  cells/mm<sup>2</sup> by a factor of 1.37 within 24 h cell proliferation ( $n = 74$  fields). At 7 DIV, the neuronal density of NeuN-positive cells was  $970.8 \pm 49.9$  cells/mm<sup>2</sup> (mean  $\pm$  SE,  $n = 40$  fields). In the majority of NeuN cells, GABA and Venus are co-expressed ( $90.6\% \pm 0.96$ , mean  $\pm$  SE,  $n = 40$  fields). Data were collected from four cultures in two experiments.

### 3.3.6 PN/IN ratio generation

To obtain networks with defined PN/IN ratios, live cell counts were applied to E16 dCtx network 4 hours after planting. Cells were counted under phase contrast illumination. The number of the cultures we used is mentioned in section “3.3.4”. Twenty-four hours later (live cell counts at 1 DIV), we calculated the cell density of this type of network again. To generate the intended PN/IN ratios, we added the freshly dissociated E14 MGE neurons, the desired densities of which were calculated based on 1 DIV dCtx network densities, into these dCtx networks. In our study, we designed three network types. Networks were with low MGE-derived IN content. We added every five MGE cells to every 100 cortical cells (5:100). The total cell density of MGE cells in dCtx networks is 4.8% (**T05 networks**). Networks were with medium MGE-derived IN content. **T25 networks** were generated by adding 20-40 MGE cells to every 100 cortical cells (30:100; 23.1%). Networks were with higher MGE-derived IN content (**T45 networks**). Every 80 MGE cells were diluted in every 100 neocortical cells (80:100; 44.4%). To control for intrinsic GABA content, we cultured T00 networks in all experiments.

After transplanting the MGE-derived INs into the 1 DIV dCtx networks, the networks increased within 24 h; then, the networks received Ara-C (5  $\mu$ M final concentration). After 24 h Ara-C incubation, a fresh glia-conditioned N2 medium completely replaced the older culture media that contained Ara-C. According to our experimental design, MGE-derived INs proliferated for twenty-four hours while PNs increased for forty-eight hours. As a result of the Ara-C treatment, the uncontrolled cell proliferation stopped, and the cells were synchronized to enter a post-mitotic phase. In this way, all cultures began in the same condition so that we could compare their post-mitotic developmental changes in different network types. The treatment for all network types was identical during the cultivation period of four weeks.

### **3.4 Immunocytochemistry**

To identify and analyze the different neuron populations, a combination of three to four fluorescent antibodies was applied for cell treatment.

Cultures were treated with 4% paraformaldehyde and 0.01% glutaraldehyde (in 0.1 M PBS (phosphate-buffered saline; 0.1M PS + 0.9% NaCl; PH 7.4) for 30min at 36°C to stain GABA. Cultures were then washed in 3  $\times$  0.1 M PBS and 3  $\times$  0.05M Tris [tris (hydroxymethyl) aminomethane]/metabisulfite solution (Sol. C, 0.85% sodium metabisulfite in 0.05 M Tris buffer pH 7.5). Further, cells were incubated with ethanolamine (1 M in Sol. C) for 20 min and pre-

treated with 3% BSA, 10% normal goat serum (NGS), and 1.2% Triton X-100 (in 0.05 M Sol. C) for 3h to reduce aldehyde-induced autofluorescence. Triton-X 100 as a non-ionic detergent was used to improve antibody penetration. After washing with  $3 \times 0.05$  M Sol. C, cultures were incubated with rabbit anti-GABA antibody (dilution 1:2000, Millipore, AB131-rb, polyclonal antibody) in 0.05 M Sol. C overnight at room temperature. After the primary antibody incubation, all washed were made with  $3 \times 0.1$  M PBS and  $3 \times 0.05$  M Sol. C. Primary antibodies were labeled with secondary Alexa Fluor 488 goat anti-rabbit IgG antibody (1:250, #A-11008, Molecular Probes) in 0.1 M PBS for 2 h at room temperature.

Without incubating with 0.01% glutaraldehyde, cultures were treated with 4% paraformaldehyde for 30 min at 36°C for all other immunostaining. After washing with  $3 \times 0.1$  M PBS, cultures were incubated in 0.1 M PBS for 1 hour at room temperature. Without washing steps, cultures were incubated overnight at room temperature with one of the following antibodies: monoclonal mouse anti-NeuN (1:1000, clone A60; #MAB377, Millipore), chicken anti-GFP (1:2000, #GFP-1020, Aves), rat anti-Somatostatin (1:100, #MAB354, Millipore), mouse anti-Parvalbumin (1:10000, #PV235, SWANT, LTD) or mouse Calretinin (1:2000, #6B3, SWANT). After the primary antibody incubation, cultures were washed with  $3 \times 0.1$  M PBS and were incubated for 2 h at room temperature with one of the following secondary antibodies: Alexa Fluor 488 goat anti-chicken IgG (1:250, #A-11039, Molecular Probes), Alexa Fluor 555 goat anti-mouse IgG (1:250, A-21422, Molecular Probes) or Alexa Fluor 555 goat anti-rat IgG (1:250, A214342, Molecular Probes). The number of apoptotic cells was accessed with chicken rabbit anti-caspase 3 (1:250, Asp175, # 9661, Cell signaling Technologies) followed by Cy5-Goat anti-Rabbit IgG (1:400, #111-175-144, Dianova, Hamburg, Germany), and cell proliferation was accessed by mouse anti-BrdU (1:50, #11170376001, Sigma) followed by Alexa Fluor 555 goat anti-mouse IgG (1:250, A-21422, Molecular Probes).

For all double or triple immunolabeling, antibodies were incubated separately and consecutively after the scheme: first primary antibody,  $3 \times$  PBS/ $3 \times$  PBS, and  $3 \times$  Sol. C wash, first second antibody,  $3 \times$  PBS wash, 30 min paraformaldehyde fixation, second primary antibody,  $3 \times$  PBS wash, and so forth. After the final  $3 \times 0.1$  M PBS wash, all coverslips were dehydrated in an ethanol series, cleared in two changes of xylene, and mounted over clean slides with Fluoromount. Before embedding the coverslips in Fluoromount, they were briefly treated with 1 min DAPI (fluorescence dye-labeled DNA; 500 ng/ml final concentration) to label the cell nuclei. The DAPI staining allowed identifying all non-neuronal cells and pycnotic nuclei. T00 networks were cultivated in every preparation to control IN content in the receiving cortical networks. As no MGE cells were added to the T00 networks, INs were recognized by anti-GABA and anti-NeuN antibodies and DAPI (**Fig. 1 A**).

### 3.4.1 Cell density analysis

After immunostaining, the coverslips were randomly assigned to numbers. The numbers marked on the coverslips were not revealed until the observers had done the entire analysis work. The number of cultures in each experiment was 48. Each of the four network types and four ages contained three cultures. Ten fields were randomly chosen in each dish at regularly spaced points for the photos taken, and photomicrographs were taken under a 40× objective lens with the appropriate filters. In each field, 3 to 4 micrographs were usually collected according to the number of fluoro-chromes used. With the help of Meta Morph (version v.7.8.0.0, Molecular Devices, LLC), all images were further processed to one RGB image, and the immuno-positive cells were counted manually to determine the cell density. INs were identified as eGFP( + )/NeuN( + ), or in T00 networks, INs were identified as GABA( + )/NeuN( + ). PNs were identified as eGFP( - )/NeuN( + ). All other analyses marked cells with gray values of the regions of interest (ROIs). In cell-free areas, we place an additional three ROIs for background correction. All ROI values, including three ROIs from the background, were then logged into data files. We further processed all acquired data using MATLAB (2020, MathWorks, Natick, MA, USA). In the cell density series, nine experiments were performed for dCtx (**Figs. 3, 7, 8**), five experiments were performed for high/low density (**Fig. 4**), and three experiments were conducted for wCtx (**Fig. 9**).

### 3.4.2 Immunostaining to determine GABA and Venus co-expression

As mentioned in the method section “3.3.5”, Venus and GABA can be co-expressed in transgenic rat brains (VGAT; (Uematsu et al., 2008)). Thus, to check the co-expression between the neurotransmitter GABA and Venus expression of MGE cells in our cultures, neuronal networks of T25 type at 14 DIV were immunolabelled for eGFP (red) and GABA (green) (**Fig. 1 D**). In this experiment, the GABA antibody required glutaraldehyde fixation. However, fixation with glutaraldehyde can cause background fluorescence. Thus, to reduce the glutaraldehyde-induced background fluorescence, a series of different glutaraldehyde/paraformaldehyde mixtures combined with varying antibody concentrations were tested to obtain an optimal compromise between strong specific immunofluorescence signal and low background staining.

After immunostaining, ten fields were randomly selected and photographed in each coverslip. Micrographs were analyzed with Meta Morph software. All Venus-expressing cells were marked as ROIs. To determine the background noise, three additional ROIs were placed at the

cell-free area. ROIs were then transferred to the corresponding 12-bit GABA images, and the mean gray value of each ROI was logged into a data file along with the background noises. Data files were further analyzed with MATLAB. When the mean ROI pixel intensity was more than five times the standard deviation of the mean gray values measured in background noise, we regarded a Venus-expressing cell as an IN.

### 3.4.3 Caspase immunocytochemistry

To investigate cells undergo apoptosis within the first week networks, we prepared T00 networks and T25 networks from two independent experiments, including three cultures per day and experiment, and immunostained these cultures with anti-GABA (T00 networks) or anti-eGFP (green) antibody, anti-NeuN (red) antibody, anti-Caspase (infra-red) antibody and DAPI (blue) (**Fig. 5 C**) on five sequential days (2, 3, 4, 5, and 6 DIV) to analyze day-by-day variation in the number of apoptotic cells. The preparation of T00 networks were as controls. The measured fields were randomly chosen. At each field, green, infra-red, blue, and red stains were taken as separate color micrographs, using appropriate filters on an Axiovert S100 TV microscope with a 100× oil objective. All PNs were marked as ROIs. To determine the background noise, we placed three additional ROIs on the cell-free areas. ROIs were then transferred to the corresponding caspase images, and the mean gray value of each ROI was logged into a data file along with the background noises. Data were analyzed in MATLAB with a predefined threshold. The percentage of PNs which underwent apoptosis was expressed as the apoptosis number of PNs/the total number of PNs × 100. Apoptotic PNs were defined as caspase-3( + )/eGFP( - ) cells.

### 3.4.4 BrdU immunocytochemistry

The detection of cell proliferation *in vitro* can be achieved using the immunocytochemical marker 5-Bromo-2'-deoxyuridine (BrdU), a thymidine analog that incorporates the DNA of proliferating cells during the S-phase of the cell cycle. Cells were cultured without Ara-C treatment, and BrdU (the final concentration is 2 μM, #15240, SERVA) was added to the culture medium for 12 hours or 24 hours incubation. After BrdU incubation, cells were stained with eGFP (green) antibody, BrdU (red) antibody, and DAPI (blue) (**Fig. 6 C**). Photomicrographs were taken using 40× objective with the appropriate filter settings. ROIs were drawn on the surfaces of INs and PNs in the fluorescence images. ROIs were then transferred to 12-bit grayscale of the BrdU images, and the mean gray values were logged into a data file and further

analyzed with MATLAB. The detection threshold was determined for every field by position 3 ROIs on BrdU( - ) and 3 ROIs on weakly BrdU( + ) labeled neurons. Data were acquired from four independent preparations (2 for 12 h BrdU incubation and 2 for 24 h BrdU incubation). Each preparation had three cultures per network type and age (T00, T05, T25, and T45 networks). In each network type, the number of analyzed cells was displayed as follows The number of apoptotic PNs in T00 networks is 9,388; 9,715 PNs and 1,485 INs in T05 networks; 10,320 PNs and 421 INs in T25 networks; 10,716 PNs and 736 INs in T45 networks.

### 3.4.5 Measurement of soma size by immunostaining

To examine the morphologic changes of INs and PNs, we analyzed the soma size of PNs and INs in T05, T20, and T30 networks. Cells were stained for NeuN (red), eGFP (green) (**Figs. 7 A-C**). Data were collected from four independent experiments. Images were taken using 40× objective with the appropriate filter settings to analyze the cells. Micrographs were superimposed in Meta Morph with the function of the color align command, and the outline of each cell body was drawn by hand using the region tool. Across all T05, T20, and T30 networks, the soma surfaces of 2447 PNs and 3162 INs were analyzed on collecting days of 7, 14, and 21 DIV. In each network type, the number of analyzed INs was as follows: IN T05 networks (327, 286, 300); IN T20 networks (374, 232 303, 368); IN T30 networks (415, 340, 449). The number of analyzed PNs for 21 DIV: PN T05 networks (210); PN T20 networks (175); PN T30 networks (203).

## **3.5 Electrophysiology**

### 3.5.1 Whole-cell voltage-clamp recordings

Electrophysiological recordings for single cell were performed from 6 up to 30 days (in the dish). To make a recording chamber, an acrylic insert was placed into the culture dish, where cells were fully submerged in a volume of 1-1.5 ml. The cells were constantly supplied with the heated HEPES-buffered artificial cerebrospinal fluid (aCSF, pH 7.4, 300-310 mOsmol/kg) (27-29°C) at 1-2 ml/min in a heat-controlled chamber (Inline Heater SH-27B, TC-324B, Warner Instrument Corporation). Whole-cell voltage-clamp recorded from PNs and INs were performed at 40× using ZEISS Axiovert S100 TV microscope equipped with fluorescence optic.

Patch pipettes with tip resistances of 2.5-4.5 MΩ were pulled from borosilicate glass (GC150TF-10, Harvard Apparatus LTD, London, UK). Pipette solutions for voltage-clamp recordings was [in mM]: 0.1 EGTA, 0.07 CaCl<sub>2</sub>, 0.75 Na-GTP, 1 MgCl<sub>2</sub>, 4.5 Mg-ATP, 10 HEPES, 13 CsCl,

117 D - gluconic acid, pH 7.2, 290-300 mOsmol/kg. CsOH was used to adjust the pH value of D - gluconic acid to 7.25.

Recordings were performed using a patch-clamp L/M-EPC-7 amplifier (List-Medical-Electronic) with a 1 kHz filter. Raw data were exported from the Pulse software (v.8.74 von HEKA Elektronik Dr. Schulze GmbH). Liquid junction potential was 10 mV in 27-29°C for the solution in cultures. After the whole-cell configuration in voltage-clamp mode was established, resting membrane potential could be measured. For recording 5-min inwardly-directed spontaneous glutamatergic post-synaptic currents (sEPSCs), the holding potential was set to  $-60$  mV (**Figs. 13 B, D, E, F**, black traces). In the same neuron, outwardly-directed spontaneous GABAergic post-synaptic currents (sIPSCs) were recorded at 0 mV for 5 min (**Figs. 13 A, D, E, F**, red traces). Between recordings, the polarity sequence was selected with a random change.

### 3.5.2 Application of water-soluble drugs in our cultures

All drugs were dissolved in 100-1000 $\times$  stocks and stored at  $-20^{\circ}\text{C}$ . Just before application, we diluted them to the final concentration. To confirm glutamatergic currents, cultures were perfused with normal aSCF containing 2.5  $\mu\text{M}$  6-cyano-7-nitroquinoxaline-2,3-dione disodium salt (CNQX, Tocris, Bristol, UK) and 12.5  $\mu\text{M}$  D-( - )-2-amino-5-phosphonopentanoic acid (D-APV, Tocris, Bristol, UK). sEPSCs were recorded at  $-60$  mV ( $n = 12$ ). For GABAergic current recordings, cultures were perfused with normal aCSF containing 20  $\mu\text{M}$  ( - )-bicuculline methiodide (BMI; Sigma, USA) or 25  $\mu\text{M}$  SR 95531 (gabazine; Tocris, Bristol, UK). sIPSCs were recorded at 0 mV (BMI,  $n = 21$ ; gabazine,  $n = 8$ ).

### 3.5.3 Quantitative analysis of single cell voltage-clamp recordings

Mini Analysis software (version 6.0.3, Synaptosoft, Decatur, GA), e.g., a software program that detects and measures spontaneous synaptic events, was applied for analyzing the single cell recording. As shown in **Figs. 13 A and B**, isolated sPSCs (arrows in **D**) were manually picked using this software. Since very active cells had mostly superimposed single sPSCs, sometimes it was challenging to find sufficient isolated sPSCs for quantification. The minimum criteria for isolated sPSCs analysis were 30 for both well-isolated sEPSCs and sIPSCs. A maximum of 100 sEPSCs and 100 sIPSCs per cell was confirmed. In 10 min total recording time, in IN-depleted T00 networks, a cell was considered free of GABA inputs if it had 0 sIPSCs and over 30 sEPSCs. The synaptic signals of amplitude, rise time, decay time, and area (sPSC charge transfer and

sPSC burst charge transfer) in every cell were calculated. The integral area values (pAms) obtained from Mini Analysis were used to determine the mean charge transfer of sPSCs. Analyses of the mean charge transfer of large network bursts (**Figs. 13 D-F**) were obtained from MATLAB. The integral area values above the baseline were determined manually by choosing the beginning and end of each event in MATLAB.

To access cellular and network E/I balance, the sIPSC charge transfer/(sEPSC charge transfer + sIPSC charge transfer) ratio and the sIPSC bursts charge transfer/(sEPSC burst charge transfer + sIPSC burst charge transfer) ratio were calculated, respectively.

Between 6 and 30 DIV, we recorded 51 PNs in T00 networks, 89 PNs and 113 INs in T05 networks, and 78 PNs and 116 INs in the T45 network. All data were collected from 188 cultures, which were from six independent experiments. We then separated the recordings into the following groups according to the different developmental stages of the same cell type for statistical analysis. 15 PNs and 29 INs were recorded in the First week (6-9 DIV); 61 PNs and 74 INs in the Second week (12-16 DIV); 71 PNs and 61 INs in the Third week (19-23 DIV); 71 PNs, and 65 INs in the Fourth week (26-30 DIV) (see **Table 2**).

### **3.6 *In vitro* calcium imaging experiments**

#### **3.6.1 Calcium imaging of single-cell spontaneous neuronal activity in cortical cultures**

Calcium imaging was used to measure calcium dynamics in neurons from T05, T25, and T45 networks at 14, 21, and 28 DIV to investigate the spontaneous network activity. For each network type, we prepared three cultures, and all cultures were obtained from three independent experiments. To help the dye into the cells, cultures were treated with 5  $\mu$ M Fluo-4 AM (#F14201, Molecular Probes, Thermo Fisher Scientific) for 1 hour. Cultures were then rinsed with HEPES-buffered aCSF for at least 30 min to de-esterificate Fluo-4 AM. An inverted microscope (Axiovert S100 TV, Zeiss, Oberkochen, Germany) outfitted with a charge-coupled device camera (Cool Snap ES, Visitron Systems, Puchheim, Germany) was used to record the changes in the fluorescence in neurons at room temperature. In every culture, ten randomly chosen fields were examined. In each selective field, fluorescence images were successively captured for 4 min at 1 Hz. Later, the visible cells in each field were identified using differential interference contrast (DIC) images.

### 3.6.2 Burst analysis

To identify neurons as being synchronous, data were analyzed by the program Meta Morph (version 7.8.0.0, Molecular Devices, Sunnyvale, CA, USA) as previously reported (Opitz et al., 2002). Fluorescence images were recorded at ten randomly selected fields of each dish, and in each dish active neurons were counted by DIC images. Every single active neuron was marked as ROI. To measure the background noise, we placed additional ROIs on the cell-free region. For calculating the fluorescence intensity over time, all ROIs were superimposed on the fluorescence images captured every second for 4 min. The threshold was determined to be more than five times the standard deviation of the background noise. When the absolute difference of gray values exceeded this threshold, a change in the intracellular ( $[Ca^{2+}]_i$ ) was considered significant. Based on previous findings (Opitz et al., 2002), when the synaptic transmission in a network is completely blocked, Opitz et al. pointed out 7.5% as the maximal fraction of neurons in culture simultaneously active during spontaneous activity. Thus, our study defined a burst being more than 10% of all active neurons within a given field that is simultaneously active. The minimum number of cells that were co-activated was determined to be seven. With the aid of MATLAB, we could further examine the changes in the intracellular ( $[Ca^{2+}]_i$ ) levels.

### **3.7 Data analysis**

All our data were performed with Sigma Stat (version 3.5, SPSS Inc., Chicago, IL) to analyze statistically. Initially, we tested them for normality (Kolmogorov-Smirnov test) and Equal Variance. Nevertheless, we used parametric or non-parametric statistical methods to examine the date when the  $p$ -value violated the normality assumption. The differences between experimental sets were evaluated using Student's  $t$ -test or Mann-Whitney rank sum test (MW-RST). Differences for comparison of multiple ages or culturing conditions were tested with one-way analysis of variance (ANOVA) followed by the Holm-Sidak test or Kruskal-Wallis one-way ANOVA on ranks (KW-ANOVA) followed by the Dunn's method. Two-way ANOVA was used to analyze the differences between network types, including independent of age or density variations. A Chi-square test was used to compare the proportions of BrdU-labeled INs and PNs in multiple conditions. Data are expressed as means  $\pm$  standard error (SE) or means  $\pm$  standard error of the mean (SEM) or medians, and the presentation forms were illustrated in every figure legend. A  $p$ -value less than 0.05 is considered statistically significant. Asterisks represent the degree (\*,  $p \leq 0.05$ ; \*\*,  $p \leq 0.01$ , \*\*\*,  $p \leq 0.001$ ). A  $p$ -value more than 0.05 is considered insignificant (n. s). Unless otherwise stated, the  $n$ -values in the text or figure legends indicate the analyzed field number or neuron number.

## 4. Results

### 4.1 GABA/NeuN/DAPI co-localization and eGFP/NeuN/DAPI co-localization

In this study, MGE-INs were obtained from transgenic rats. The Venus and VGAT were co-expressed in a cell. Therefore, it was tested if Venus-expressing cells are positive for GABA. The number of Venus-positive cells co-expressing GABA was quantified in T25 networks at 14 DIV. The results showed that 95.4% (352 GABA cells among 369 Venus cells) of eGFP-positive (Venus) cells were co-expressed GABA, indicating that GABA-positive and Venus-expressing cells are a high degree of neuronal overlap populations (**Fig. 1 D**). In our cultures, we also found the cell was GABA positive but not expressed Venus. **Figure 1 E** (large arrows) shows a rare eGFP-negative GABAergic cell. These eGFP-negative GABAergic cells are present in wild-type Wistar rats, not from the transgenic animals, known as L-GABA (de Lima and Voigt 1997). Because GABAergic cells were clearly identified in 95.4% of the Venus-positive cells by co-localization of fluorochrome, we were able to classify eGFP-positive/NeuN-positive neurons from transgenic Venus-expressing rats as INs and eGFP-negative/NeuN-positive neurons as PNs.

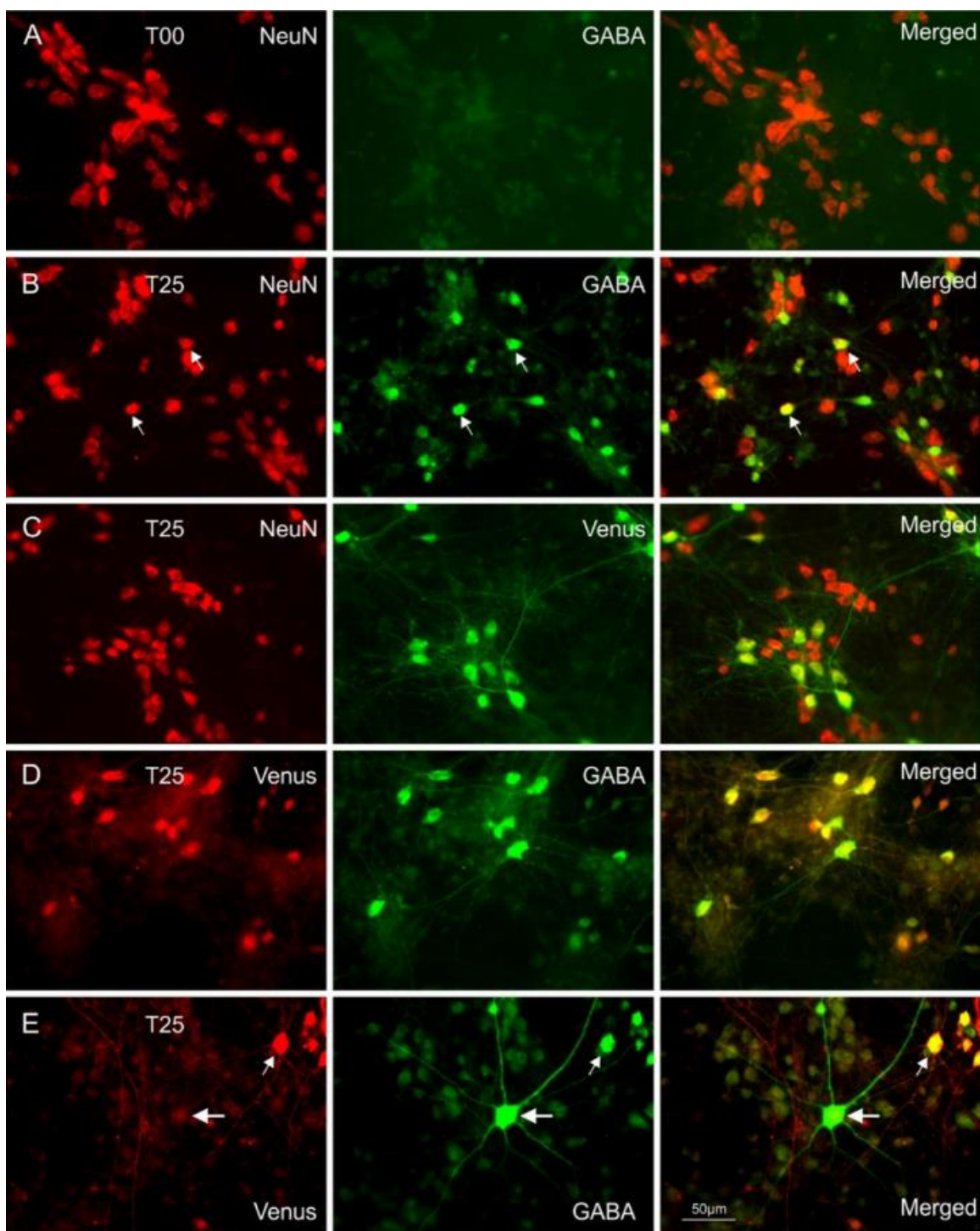


**Figure 1: Immunolabeling of cells in the T00 networks or T25 networks.**

(A) Representative photomicrographs of NeuN immunoreactivity (left) and GABA-staining cells (middle) in T00 networks. The vast majority of NeuN-immunoreactive cells did not co-localize with GABA marker, illustrating most neurons (NeuN) were PNs in this network type. (B) NeuN immunoreactivity (left) co-labeled with GABA immunoreactivity (middle) in T25 networks. To obtain T25 networks, we plated 30% dissociated MGE cells on GABA-depleted (T00) networks. The MGE cells were dissociated from transgenic VGAT-Venus expressing E14 rat embryos. Two strongly NeuN/GABA-positive neurons were marked by arrows in the right-hand column of B. (C) NeuN immunoreactivity (left) co-localized with fluorescence Venus (middle) in T25 networks. (D) Co-localization of Venus fluorescence (left) with

GABA immunoreactivity (middle) in T25 networks. **(E)** A rare Venus-negative INs was found in T25 cultures (large arrows). The cell co-expressed eGFP and GABA (small arrows) was of MGE-derived INs from transgenic VGAT-Venus expressing E14 rat embryos. Images **(A-E)** show the cultures are all from the 14-day-old collection. The right-hand column of **A-E** shows the merged images. The scale bar in **E** applies in all images.

## 4.2 MGE-derived cells display molecular properties of cortical INs

Based on their neurochemical makers, such as neuropeptides (e.g., NPY, SOM, and VIP) and calcium-binding proteins (calbindin, CR, and PV) (Kubota et al., 1994; Gonchar and Burkhalter 1997), cortical INs can be divided into several subclasses. To evaluate the neuronal phenotype and molecular features of the transplanted MGE-eGFP cells, we used immunocytochemistry in T25 cultures by preparing from dCtx/MGE-INs of E14/E16 rats to characterize 28 DIV cells. In this experiment, we confirmed three subtypes (CR, PV and SOM) of INs (**Fig. 2**) in our cultures and calculated the portion of each chemical subtype in the GABAergic (Venus-positive) populations. The proportion of CR-positive cells among cells with eGFP-fluorescence was 13.4% (389 out of 2899 eGFP<sup>+</sup> cells). The proportion of PV-positive cells among all eGFP-positive cells was 6.9% (165 out of 2383 eGFP<sup>+</sup> cells). SOM-positive cells presented 17.3% of all eGFP-positive cells (406 out of 2342 eGFP<sup>+</sup> cells). Cultures were obtained from two independent preparations. The number of cultures for CR, PV and SOM experiment is 12, 14 and 12, respectively. Taken together, CR, PV, and SOM-positive cells covered 37% of eGFP-labeled cells in 28 DIV cultures.

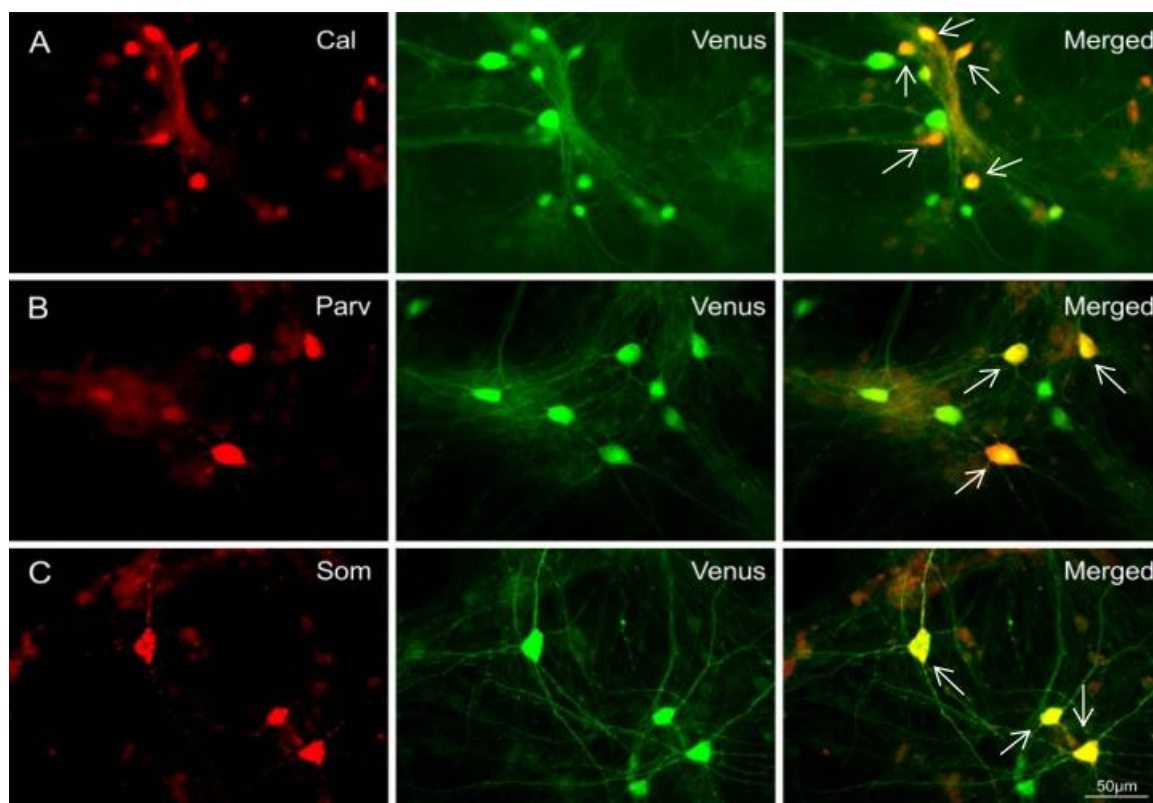


**Figure 2: Double-immunolabeling with antibodies against CR, PV, and SOM in rat cortical cultures.**

Molecular characterization of MGE-derived cells in T25 networks at 28 DIV. Immunocytochemistry co-localization of derived eGFP<sup>+</sup> cells (green, middle column) with CR (A), PV (B), and SOM (C) (red, left). Merged images are shown to the right. Arrows show double-immunolabeling cells for eGFP with specific markers. The scale bar in C applies in all images.

### 4.3 Early development of MGE-dCtx networks

#### 4.3.1 Defined PN/IN ratios

To investigate the contribution of INs to the developing neuronal networks, we conducted a series of experiments. In the first question, we asked how the number of INs affected the initial development of the network when they were added to the 1-day-old dCtx networks (**Fig. 3**). Based on our experimental design, all network types (T00, T05, T25, and T45 networks, see methods) were plated with the same density of dissociated neurons from the E16 dCtx (PNs) first (**Fig. 3 A, black bars**). After twenty-four hours, the increasing fractions of the embryonic GABAergic precursors derived from E14 MGE were then transplanted to the groups of 1-day-old PN cultures to generate the designed network types. These neuronal network sets contained four neuronal network types: T00 networks: no transplanted INs, T05 networks: 4.8% of transplanted INs, T25 networks: 23.1% of transplanted INs, T45 networks: 44.4% of

transplanted INs; (**Fig. 3 A, gray bars**). Under all these culture conditions, at 7 DIV, the differences in INs proportions were maintained close to their initial plating proportions (0.07%, 5.08%, 24.39%, 49.28% for T00 networks, T05 networks, T25 networks, T45 networks respectively,  $p < 0.001$ ; **Fig. 3 C**). At 1 DIV, the density of PNs were observed similarly for all network types ( $1614.0 \pm 30.8$  cells/mm<sup>2</sup>, mean  $\pm$  SE,  $n = 210$ ; **Fig. 3 A, black bars**). Interestingly, at 7 DIV, the data showed a detectable difference in PN density among networks with different IN content. The mean PN density at 7 DIV for each network type was as follows: [T00 networks:  $1308.9 \pm 42.5$  (mean  $\pm$  SE),  $n = 149$ ; T05 networks:  $1071.89 \pm 32.1$ ,  $n = 150$ ; T25 networks:  $718.3 \pm 21.4$ ,  $n = 240$ ; T45 networks:  $548.3 \pm 28.9$ ,  $n = 113$ ;  $p \leq 0.001$ ; **Fig. 3 B**]. Compared to the 1 DIV data, T00 networks had the lowest PN loss at 7 DIV, while T45 networks had the highest (**Fig. 3 B**).

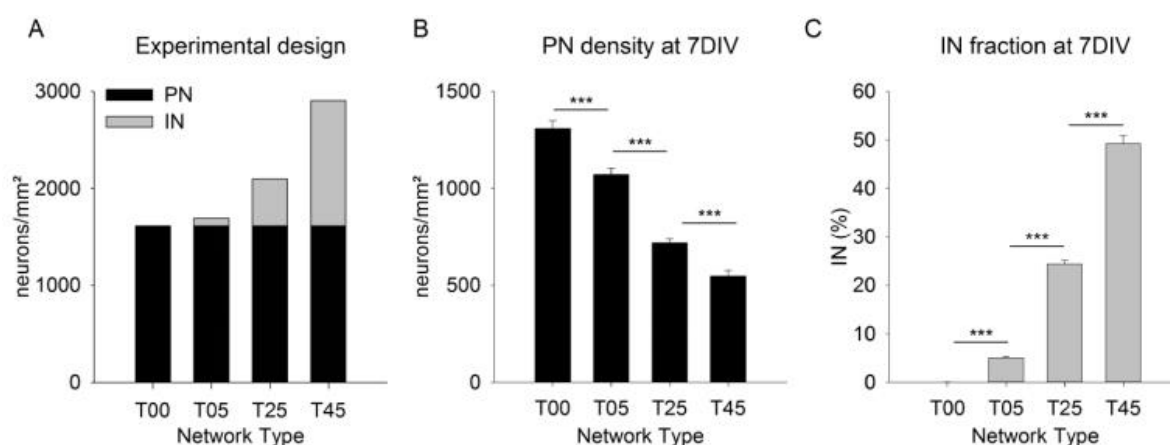


**Figure 3: The development of PN densities in networks with different IN content during seven days of cultivation *in vitro*.**

To obtain the networks with an increasing IN content (**A**, gray bars), the dissociated MGE-derived INs were added to 1 DIV networks with the same density of PNs (**A**, black bars). At 7 DIV, the density of PNs decreased with increasing GABA content (**B**). The proportion of INs in each network type was not observed to vary in the first week of cultivation in the dish (**C**). The results are presented as means  $\pm$  SE. The levels of significant differences between network types are present by asterisks (\*\*\*)  $p \leq 0.001$ .

The outcome above may be explained by two possibilities. The total neuron density was designed to increase with each neuronal network type (T00 networks, T05 networks, T25 networks, and T45 networks). T00 networks had the lowest total cell density value, and T45 networks had the highest (**Fig. 3 A**). Firstly, we assumed that the limitations of nutritional factors in the culture medium affect cell survival. If this were true, the elimination of PNs would increase with higher total cell density (**Fig. 3 B**). Alternatively, culture conditions may have always been sufficient, but PN survival was directly or indirectly affected by IN density. Accordingly, the survival of PNs observed in no MGE-INs transplanted networks (T00 networks

was highest while in highest IN content networks was worst (T45 networks), with values declining between (**Fig. 3 B**).

Thus, to test these two possibilities, network pairs with the same PN/IN ratios but different absolute plating densities were designed (**Fig. 4 A**). In the low-density planting sets (T00<sub>L</sub>/T45<sub>L</sub> networks), the T00<sub>L</sub>/T45<sub>L</sub> networks (**Fig. 4 A**) were prepared starting with the initial cell density of T00 networks (1500 cell/mm<sup>2</sup>) (**Fig. 3 A**), whereas in the high-density planting sets (T00<sub>H</sub>/T45<sub>H</sub> networks), the T00<sub>H</sub>/T45<sub>H</sub> networks (**Fig. 4 A**) were prepared with the original cell density of T45 networks (**Fig. 3 A**, i.e., 2800 cells/mm<sup>2</sup>). Before adding MGE cells, the cell densities of T00<sub>L</sub>/T45<sub>L</sub> and T00<sub>H</sub>/T45<sub>H</sub> networks were calculated (The wild-type networks T00<sub>L</sub> and T45<sub>H</sub> networks:  $1587.9 \pm 32.7$  cells/mm<sup>2</sup>, mean  $\pm$  SE; T00<sub>H</sub> networks:  $2856.3 \pm 51.8$  cells/mm<sup>2</sup>, T45<sub>L</sub> networks:  $1014.8 \pm 24.3$  cells/mm<sup>2</sup>,  $n = 150$  fields for each set; **Fig. 4 A**, black bars). Based on 1 DIV cell densities of T45<sub>L</sub> and T45<sub>H</sub> networks, MGE-INs were added to T45<sub>L</sub> and T45<sub>H</sub> networks at the required number for matching cell density with respectively T00<sub>L</sub> and T00<sub>H</sub> networks (**Fig. 4 A**, gray bars). According to our assumption, if total neuron density influences cell survival, we would find a significantly higher cell loss rate in both T00<sub>H</sub> and T45<sub>H</sub> networks. Alternatively, PN survival was regulated by IN content. The results would be shown both T45<sub>L</sub> networks and T45<sub>H</sub> networks have a higher cell death rate compared to their T00 counterparts. At 7 DIV, the density of PNs in each cultured networks exhibited as follows: T00<sub>L</sub> networks:  $1482.7 \pm 37.0$  cells/mm<sup>2</sup> (mean  $\pm$  SE,  $n = 151$ ); T00<sub>H</sub> networks:  $2402.8 \pm 40.1$  cells/mm<sup>2</sup> ( $n = 150$ ); T45<sub>L</sub> networks:  $445.0 \pm 24.1$  cells/mm<sup>2</sup> ( $n = 139$ ); T45<sub>H</sub> networks:  $582.0 \pm 24.5$  cells/mm<sup>2</sup> ( $n = 140$ ) (**Fig. 4 B**). Between 1 and 7 DIV, the PN density decreased by approximately 56.2 % in T45<sub>L</sub> networks and 63.3 % in T45<sub>H</sub> networks compared to their originally counted PN numbers, while in T00<sub>L</sub> and T00<sub>H</sub> networks, the density of PNs was respectively decreased by approximately 6.6% and 15.9% compared to the originally counted PN numbers. Apparently, the survival of PNs was better in both T00 networks (T00<sub>L</sub> and T00<sub>H</sub> networks). To further confirm whether IN content or total neuron density influence PN density, the data were normalized to their 1 DIV values. Then four sets were grouped: Low-density networks (T00<sub>L</sub> + T45<sub>L</sub> networks) and High-density networks (T00<sub>H</sub> + T45<sub>H</sub> networks), T00 networks (T00<sub>L</sub> + T00<sub>H</sub> networks) and T45 networks (T45<sub>L</sub> + T45<sub>H</sub> networks). Compared to the difference in IN content, PN density was less affected by the difference in total cell density (Low-density networks:  $n = 290$ ; High-density networks:  $n = 290$ ,  $p = 0.027$ , MW-RST; T00 networks:  $n = 301$ ; T45 networks:  $n = 379$ ,  $p \leq 0.001$ , MW-RST, **Fig. 4 C**). These findings suggest that PN survival is more likely determined by IN content than the total neuron density governing PN population size.

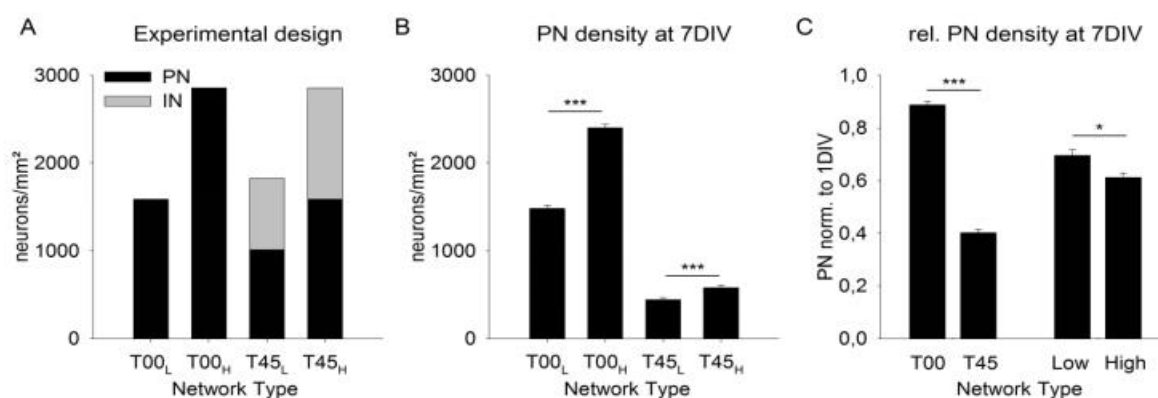


**Figure 4: MGE-derived INs regulate PN density at the developmental stage of 1<sup>st</sup> week in culture.**

(A) The total cell density of T00<sub>L</sub> and T45<sub>L</sub> networks was equal. The total cell density of T45<sub>H</sub> networks matched with T00<sub>H</sub> networks was much more than their counterparts. The number of PNs and INs was represented as black histograms and gray histograms, respectively. T45<sub>H</sub> networks contained the most INs. (B) In T45<sub>L</sub> and T45<sub>H</sub> networks, much more PNs were eliminated after 7 DIV, indicating that the survival of PNs was predominantly determined by IN density rather than total cell density during the initial week. (C) After normalizing PN densities to their 1 DIV values and pooling them into four sets (see text), the results showed that PN density declined more rapidly when INs were present (T00 vs. T45 networks). The results are presented as means  $\pm$  SE. The levels of significant differences between network types are present by asterisks (\*  $p \leq 0.05$ , \*\*\*  $p \leq 0.001$ ).

#### 4.3.2 Network-specific apoptosis rates

Based on our findings above, the data suggest that the density of INs substantially impacts PNs' survival. To identify this possibility, the occurrence of apoptosis in cultures during the first week was investigated. According to our protocol, the apoptotic cells were examined using caspase-3 immunocytochemistry. As a result of immunofluorescence staining, apoptotic PNs (red; activated caspase-3), neurons (green; NeuN), and cell nuclei (blue) were visualized in T25 networks (**Figs. 5 A-C**). Between 2-6 DIV, a quantitative analysis of the number of caspase-3-labeled PNs was shown in **Fig. 5 D**. The percentage of apoptotic PNs transiently increased at 3 DIV and then dramatically decreased after 3 DIV ( $p \leq 0.001$ ). The cell death observed to rise steeply at 2 DIV may be due to adding Ara-C (see chapter "3.3.6"). Taking into account that Ara-C induces apoptosis during cell mitosis (Banker and Goslin 1998), the following experiment would examine if the density of INs may affect the proliferation rates of PNs in this early stage of neuronal development.

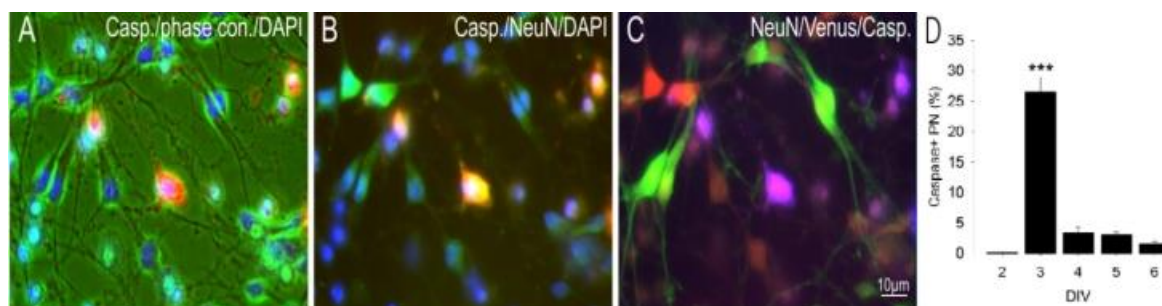


**Figure 5: Caspase-3-immunoreactive cells in T25 networks.**

(A-C) Caspase-3 immunoreactivity in chemically identified cells in T25 networks at 3 DIV. (A) phase contrast (green), caspase-3-positive cells (red), DAPI (blue). (B) NeuN (green), caspase-3-expressing cells (red), DAPI (blue). (C) eGFP-expressing cells (green), NeuN (red), caspase-3-immunoreactive cells (blue). (D) Quantitative analysis of caspase-3-labeled PNs in T25 networks was performed on the distribution histograms from 2 DIV to 6 DIV. After adding Ara-C to the networks at 2 DIV, the number of caspase-3-labeled PNs showed a significant increase at 3 DIV (\*\*\*)  $p \leq 0.001$  and declined at 4, 5, 6 DIV. The results are presented as means  $\pm$  SEM. The scale bar in C applies in A-C.

#### 4.3.3 INs influence PNs proliferation in a density-dependent manner

To examine the PNs and INs proliferation rates, BrdU immunocytochemistry was used. The experimental design was the same as the caspase-3 experiment, except that BrdU instead of Ara-C was added to the cultures 48-72 h after transplanting MGE-derived INs. The proliferating PNs were single-immunolabeled with anti-BrdU (red) and DAPI (blue) (Figs. 6 A-C). The proliferating INs were double-immunolabeled with anti-BrdU (red), anti-eGFP (Venus; green), and DAPI (blue) (Figs. 6 A-C). In the IN-depleted T00 networks, the proportion of BrdU-positive PNs among total counted cells was 68.3%. PN proliferation rates with increasing IN content gradually increased to 73.2%, 80.6%, and 83.5% in the T05 networks, T25 networks, and T45 networks, respectively ( $p \leq 0.001$ , chi-square-test; Fig. 6 D). The number of single-labeled or double-labeled cells in each network type was calculated: 9388 PNs in the T00 networks were counted; 9715 PNs and 1485 INs in the T05 networks; 10320 PNs and 421 INs in the T25 networks; 10716 PNs and 736 INs in the T45 networks.

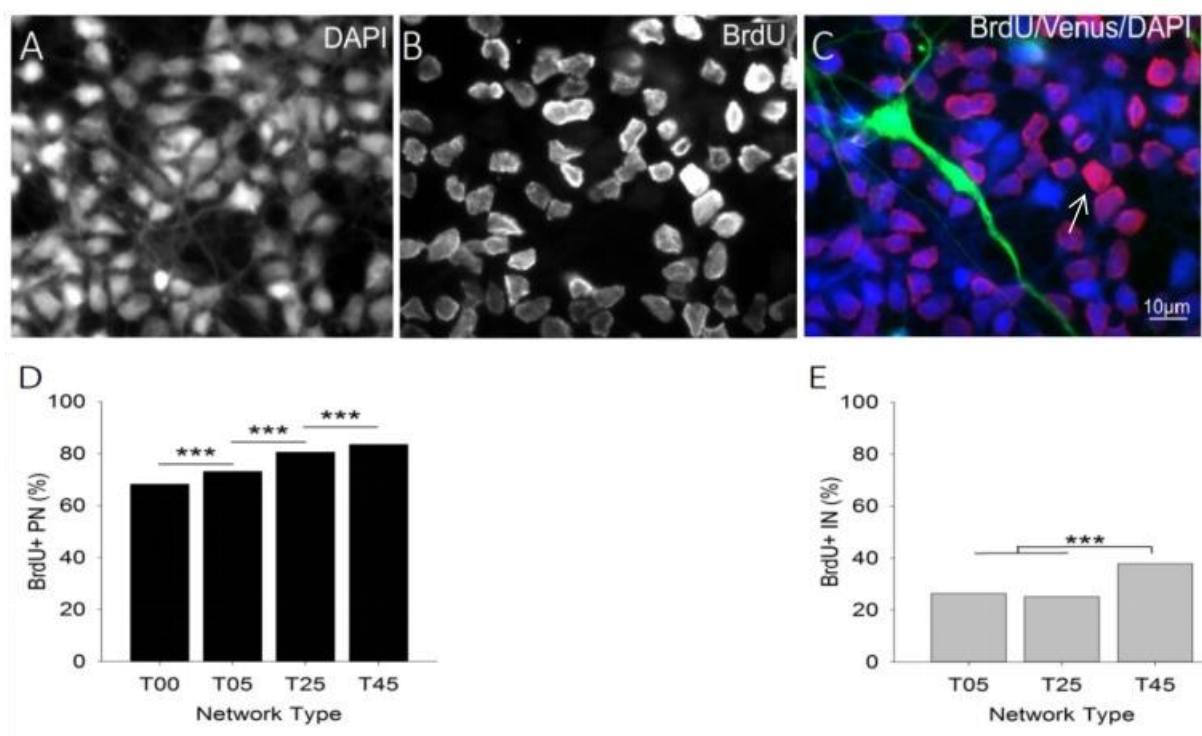


**Figure 6: IN density influence on PN cell proliferation rates.**

(A-C) Double immunostaining with anti-BrdU (red) and anti-eGFP (green) antibodies to identify proliferating cells in T25 networks 24 h after exposure to BrdU. BrdU was confined to nuclei and demonstrated by co-localization with DAPI (blue). Arrow points to an already dividing cell. (D and E) Quantifying the proliferating PNs or INs in different network types. (D) Fraction of BrdU-labeled PNs. The high IN density networks showed an increasing number of proliferating PNs. (E) Fraction of BrdU-labeled INs. We observed only T45 networks showing a significant increase in the number of proliferating INs. The results are presented as means  $\pm$  SE. The levels of significant differences between network types are present by asterisks (\*\*\*)  $p \leq 0.001$ ). The scale bar in C applies in A-C.

Compared to the IN-depleted T00 networks, as we have seen, T05 networks with even low IN content can significantly increase PN proliferation rates (Fig. 6 D). Therefore, these results suggest that the presence of INs activates PN population proliferation. Furthermore, the variation of PN density observed at 7 DIV among network types can also be explained by these findings (Fig. 3 B). Because Ara-C leads to apoptosis during cell mitosis, INs promoted PN proliferation, and thus, networks with higher IN content inevitably eliminated the most PNs (T45 networks) than networks with no MGE-transplanted INs (T00 networks).

#### 4.3.4 Regulation of IN proliferation rates

Having a strong correlation between IN density and PN proliferation rates, the question remains if INs themselves influence their own proliferation rates. As shown in Fig. 6 E, the proliferation

rates of INs between T05 and T25 networks did not differ significantly. However, there was a considerable increase in IN proliferation rates in T45 networks compared to the other network types. Thus, we deduced that for PN/IN ratios found in the intact rat neocortex, GABA density might not influence their own proliferation rates, but for higher ratios (e.g., T45 networks) might be in the MGE, the high density of GABA might have a proliferative effect on themselves population. The aspects may be irrelevant for the post-mitotic INs that migrate into the cortex. In high GABA density networks, cell proliferation may increase. Still, the future study of whether high GABA density is relevant for adjusting the proliferation of cells in the MGE remains to be tested.

#### 4.4 Analysis of the development of cell density in networks with different PN/IN ratios

##### 4.4.1 Developmental dynamics and estimating the long-term changes in MGE-dCtx networks

We next investigated the long-term developmental dynamics in the developing networks with designed PN/IN ratios over a wide range of developmental ages (7-28 DIV). The density of PNs or INs in the same network type was quantified by week. We observed similar dynamics in cell elimination in both neuron types (**Figs. 7 D-E**). Furthermore, a substantial reduction in cell numbers occurred during the second week, and then the cell elimination slowly went down during the third and fourth weeks (**Figs. 7 D-E**). At 7 DIV, the IN proportions in different-type networks were as follows: [T00 networks: 0.06%  $\pm$  0.02,  $n = 149$  fields; T05 networks: 5.1%  $\pm$  0.3,  $n = 149$ ; T25 networks: 24.4%  $\pm$  0.7,  $n = 240$ ; T45 networks: 49.3%  $\pm$  1.6 ( $n = 113$ ), and MGE networks: 90.6%  $\pm$  0.7 ( $n = 40$ ); **Fig. 7 F**]. Surprisingly, the differences in IN proportions among different network types constantly remained from 7 DIV through the rest of age development. As the earliest ages have been analyzed (before 7 DIV), the proportion of INs remained constant over one month in all investigated network types. It closely reflected those IN fractions set in the networks at the time of plating. The fraction of INs in T00 networks ( $p = 0.127$ , KW-ANOVA) or T25 networks ( $p = 0.086$ , KW-ANOVA) showed no age variation, while the fraction of INs in T05 networks showed a slight increase ( $p = 0.004$ , KW-ANOVA) (**Fig. 7 F**). The fraction of INs in T45 networks raised until 14 DIV ( $p = 0.005$ , Holm-Sidak) and then declined to levels comparable to the 7 DIV (**Fig. 7 F**). Noticeably, the cultures of MGE neurons (in the absence of cortical neurons) were initially prepared alongside other network types and cultivated under the same culture conditions as other network types. Surprisingly, these cultures had survived one month with a slight decline with age ( $p \leq 0.001$ , KW-ANOVA; **Fig. 7 F**, red dashed line), indicating that a stable network can be formed even with an unusually high GABA content.

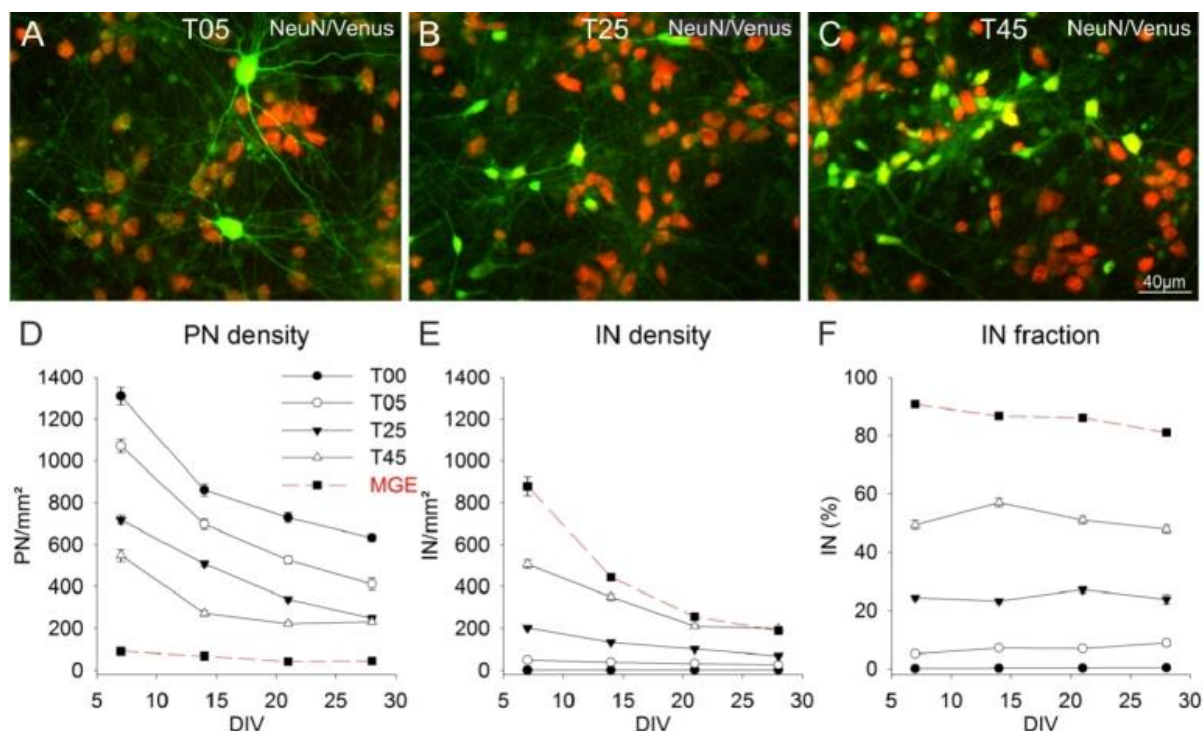


**Figure 7: Population dynamics in different types of networks.**

The merged images of Venus (green) and NeuN (red) s were from 14-day-old T05 (A), T25 (B), and T45 (C), respectively. **Figs. A-C** show the exemplary fields of merged images. **(D-F)** Developmental changes in the PNs **(D)** and INs **(E)** densities as well as IN fractions **(F)** between 7 and 28 DIV. The ordinate is for the neuron density **(D-E)** and fraction **(F)** in MGE networks (filled squares), T00 networks (black circles), T05 networks (open circles), T25 networks (filled triangles), and T45 networks (open triangles). The abscissa is developmental age (days *in vitro*). Note that MGE networks instead of PN density are shown in **Fig. D**. The results are presented as means  $\pm$  SEM. The scale bar of **Figs. A-C** is 04 cm.

The neuron density of T05, T05, T25, and T45 networks were normalized to their 7 DIV cell density values to compare the developmental changes among these network types (**Figs. 8 A-C**). Different network types showed comparable declines in PNs (**Fig. 8 A**). Furthermore, in T45 networks, PN density decreased faster from 14 to 21 DIV than in T05 and T25 networks ( $p \leq 0.001$ , KW-ANOVA; **Fig. 8 A**), but at 28 DIV, among different network types, no difference was detected in PN density ( $p = 0.062$ , KW-ANOVA). For normalized IN densities, INs in T05 networks had a higher survival rate ( $p = 0.012$  at 14 DIV;  $p \leq 0.001$  at 21 and 28 DIV, KW-ANOVA; **Fig. 8 B**). Only 21 DIV, T25, and T45 networks showed differences in normalized IN density ( $p \leq 0.001$ , KW-ANOVA; **Fig. 8 B**). During 7 to 28 days *in vitro*, the normalized IN fraction increased in low-GABA-density T05 networks, whereas it remained stable in high-GABA-density T25 and T45 networks (**Fig. 8 C**).

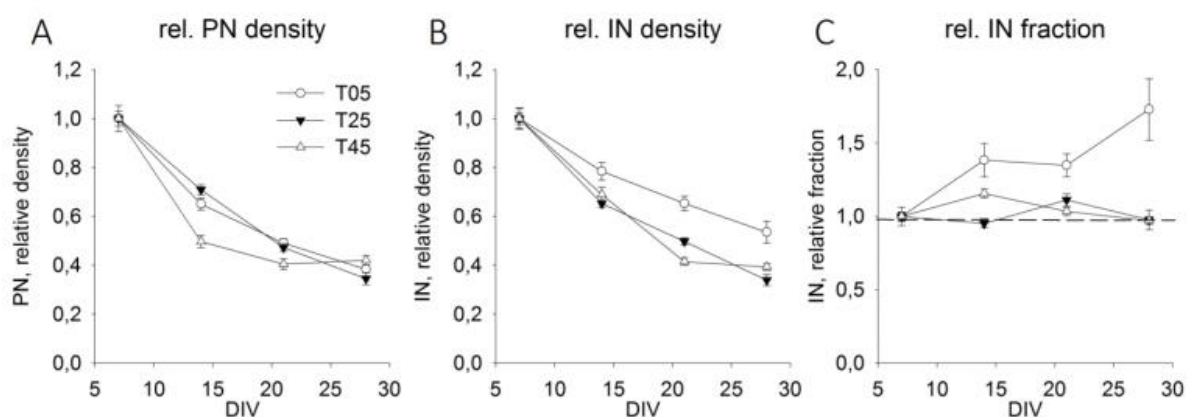


**Figure 8: Developmental changes of normalized neuronal densities in different network types.**

We used the neuronal density of T05, T25, and T45 networks collected at 7 DIV as the reference data. Then, data collected on experimental days in each network type were normalized to their 7 DIV values (A-C). The ordinate is for normalized the density (A-B) and the fraction (C) of neurons in T05 networks (filled circles), in T30 networks (open circles), in T45 networks (filled triangles), and the abscissa is developmental age (days *in vitro*). The results are presented as means  $\pm$  SEM.

#### 4.4.2 Developmental dynamics and estimating the long-term changes in MGE-wCtx networks

To extend our understanding of the long-term developmental dynamics in the developing networks, we chose the dissociated wCtx as receiving networks and investigated the developmental changes in neuron populations in the wCtx networks between 7 and 28 DIV. We doubted if the changes in cell density we observed in dCtx networks are the same as those in wCtx networks or if wCtx networks contribute to new changes. In the experiments above, we built T00 networks using dissociated neurons of E16 dCtx; as mentioned in the introduction, the migrating INs did not invade the developing rat dorsal cortex at E16, whereas the lateral portion had the invaded INs. Thus, these generated networks did not contain INs or only contained a few isolated ones ( $0.07\% \pm 0.02$ , means  $\pm$  SEM,  $n = 149$  fields, 7 DIV; **Fig. 9 A**). Compared to dCtx preparation, the preparation of dissociated wCtx at E16 contained not only a higher amount of post-mitotic PNs but also a tiny percentage of early-born INs ( $1.3\% \pm 0.1$ ,  $n = 127$  fields, 7 DIV; **Fig. 9 A**). When we compared the fraction of INs in dCtx networks and wCtx networks, we found the values in dCtx networks increased or remained unchanged (**Figs. 8 C, 9 B-D**). In contrast, a greater loss of INs in wCtx networks (**Figs. 9 E, F**) results in IN fractions dropping in all networks of this type (**Figs. 9 B-D**, open circles). In additional experiments, wCtx networks were cultivated with gabazine, a GABA<sub>A</sub> receptor antagonist. Interestingly, the profile of rapid decline in IN fraction in wCtx was not observed (**Figs. 9 G, H**).

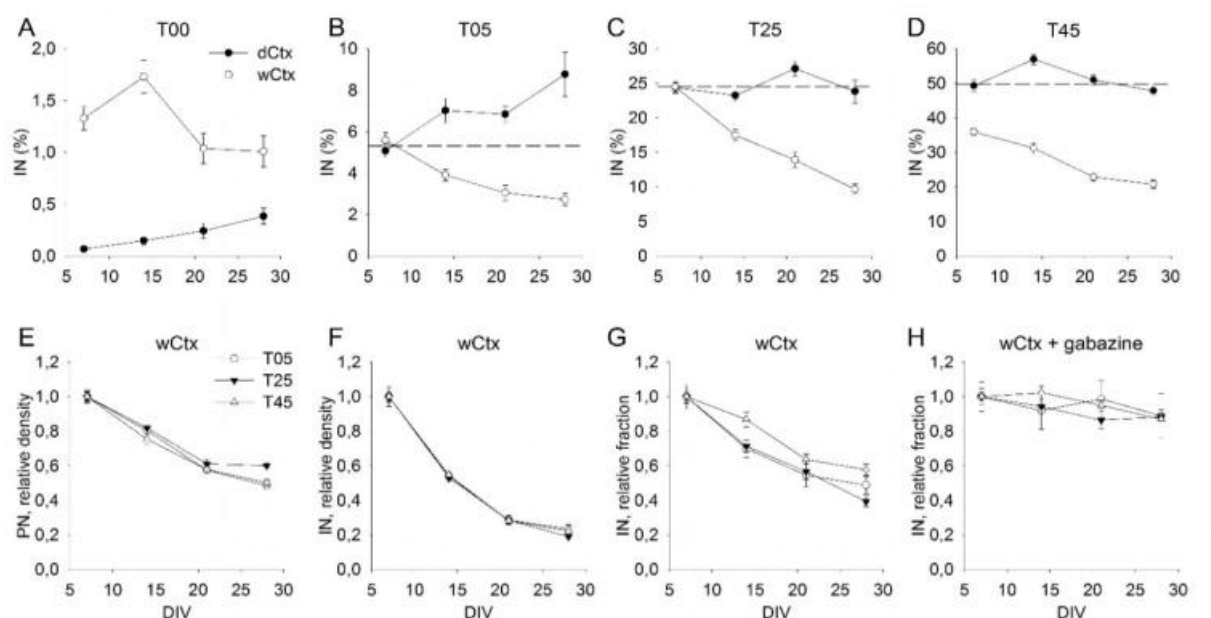


**Figure 9: Analysis of the structure differences in dCtx and wCtx networks during network development.**

(A-D) Comparing the fraction of MGE-INs in dCtx and wCtx networks for T00 (A), T05 (B), T25 (C), and T45 (D) cultures. Figures (E-F) illustrate the developmental changes of the PN and IN populations in the T05, T25, and T45 networks. (G) Plots of the fraction of INs in T05-, T25-, and T45-wCtx networks. After Gabazine (H) (a GABA antagonist) was added to wCtx networks, the rapid drop in the IN fraction (E-G) was observed to abolish, indicating that INs might modulate themselves by GABA receptors. All data in A-H show the normalized values (using their respective 7 DIV value as reference). The results are presented as means  $\pm$  SEM.

#### 4.5 Measurement of PN and IN soma size

To test if the morphological alterations of neurons are correlated with IN content, we compared the different aspects of neuronal morphologies in our cultures. Compared to the INs in T25 and T45 networks (Figs. 7 B, C), a large number of INs in T05 networks was found to possess bigger soma, and their axons are ramified (Fig. 7 A). It suggests that INs in GABA content deficit environments may develop longer and more extensively ramified axons and more giant fibred dendritic trees. Furthermore, the survival of INs in T05 networks was higher at each age than those in other network types (Fig. 8 B). Moreover, the fraction of INs in T05 networks, in T25 or T45 networks increased with neural maturation (Fig. 8 C). Thus, in very lower IN density networks, INs may rely on growing cell bodies and improving their fractions in the networks to compensate for cell number deficit.

We then measured the PN and IN soma size in our experimental cultures. When compared with those in T20 and T30 networks, the soma size INs in T05 showed detectable changes (7 DIV:  $p = 0.001$ ; 14 DIV:  $p < 0.001$ ; and 21 DIV:  $p < 0.001$ ; KW-ANOVA). Already at 7 DIV, the soma size of INs in T05 was slightly larger than those in other network types (T05 network vs. T20 networks:  $p = 0.002$ ; T05 network vs. T30 networks:  $p = 0.045$ ; MW-RST; **Fig. 10 A**). At 14 DIV and 21 DIV, the soma size differences became apparent (14 DIV:  $p < 0.001$  and 21 DIV:  $p < 0.001$ , MW-RST; **Fig. 10 A**). Compared to the IN soma size between T20 and T30 networks, the difference gradually vanished (14 DIV:  $p < 0.001$ ; 21 DIV: 0,077, MW-RST; **Fig. 10 A**). However, among PN network types, no size differences were founded ( $p = 0,794$ , KW-ANOVA; **Fig. 10 B**).

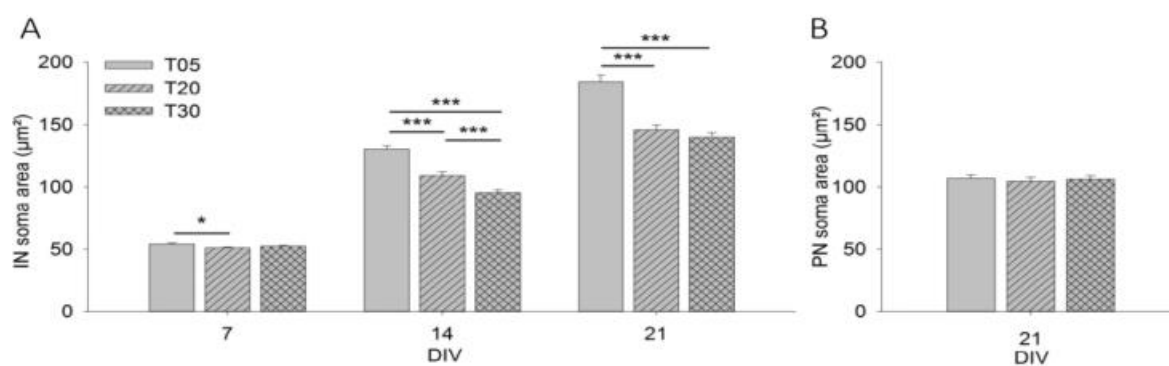


**Figure 10: Soma size analysis.**

The soma size of INs (**A**) and PNs (**B**) of T05, T20, and T30 networks were displayed in histograms at 7, 14, and 21 DIV. The soma size of INs decreased with increasing IN content and was the largest in T05 networks (**A**), whereas the soma size of PNs in all network types was not affected by GABA content (**B**). The results are presented as means  $\pm$  SEM. An asterisk indicates  $p \leq 0.05$ , and three asterisks denote  $p \leq 0.001$ .

In conclusion, PNs might be innervated by INs, each of which may probably innervate more PNs in low IN density networks.

#### 4.6 IN density determines cortical network activity

As revealed by the analysis of the neuronal population, dorsal cortices with a wide range of IN ratios could cultivate *in vitro* for several weeks. We wondered if these networks with different IN densities differ in physiological aspects. To seek this question, we recorded spontaneous  $\text{Ca}^{2+}$  transients in T05, T25, and T45 networks between 14-28 DIV.

Networks with higher IN density showed a significantly higher network burst frequency ( $p \leq 0.001$ , KW-ANOVA). Values amounted to 4 bursts/min (median;  $n = 82$ ) in T05 networks, 6.3 bursts/min ( $n = 9$ ) in T25 networks, and 15.7 bursts/min ( $n = 87$ ) in T45 networks (**Fig. 11 A**). The cumulative distribution frequency plot (CDF plot) of the single-cell frequency in T05 networks was 4 bursts/min (median;  $n = 7807$ ; **Fig. 11 B**). With increasing IN content, single-cell frequency in the networks increased (5.7 bursts/min in T05 networks,  $n = 5674$ ; 9.5 bursts/min in T45 networks,  $n = 5256$ ;  $p \leq 0.001$ , KW-ANOVA; **Fig. 11 B**). Conversely, cells in a network with higher IN content were less likely to participate in a network burst (T05 networks 100%  $n = 1538$ , burst events; T25 networks: 94%,  $n = 1538$ ; T45 networks: 72.2%,  $n = 1538$ ,  $p \leq 0.001$ , KW-ANOVA; data show the median value of the neuronal burst participation; **Fig. 11 C**).

The network activity recordings of 28 DIV T05, T25, and T45 networks are illustrated in exemplary fields shown in **Figures 11 D-E**. T05 networks showed large and stereotypical bursts (**Fig. 11 D**, left side) in which most cells were synchronously active with 100% cell participation (**Fig. 11 D**, right side). Compared with T05 networks, T45 networks showed an excess of smaller bursts (**Fig. 11 F**, left side), and nearly all neurons were active simultaneously (**Fig. 11 F**, right side). The activity pattern of the T05 network is typical for immature networks when synaptic GABA transmission is excitatory or for older networks lacking sufficient GABA inhibition (Baltz et al., 2010). With increasing IN density, neurons participated in the network activity in a desynchronized manner. CDF plots show that the neuronal burst participation dropped with increasing IN content in a given field (**Figs. 11 D-F**, right side).

In summary, calcium imaging showed networks with different IN content developed different network activity patterns. In lower IN density networks, burst activity was highly synchronized. In contrast, networks with higher GABA content exhibited desynchronized patterns, and fewer cells participated in a burst.

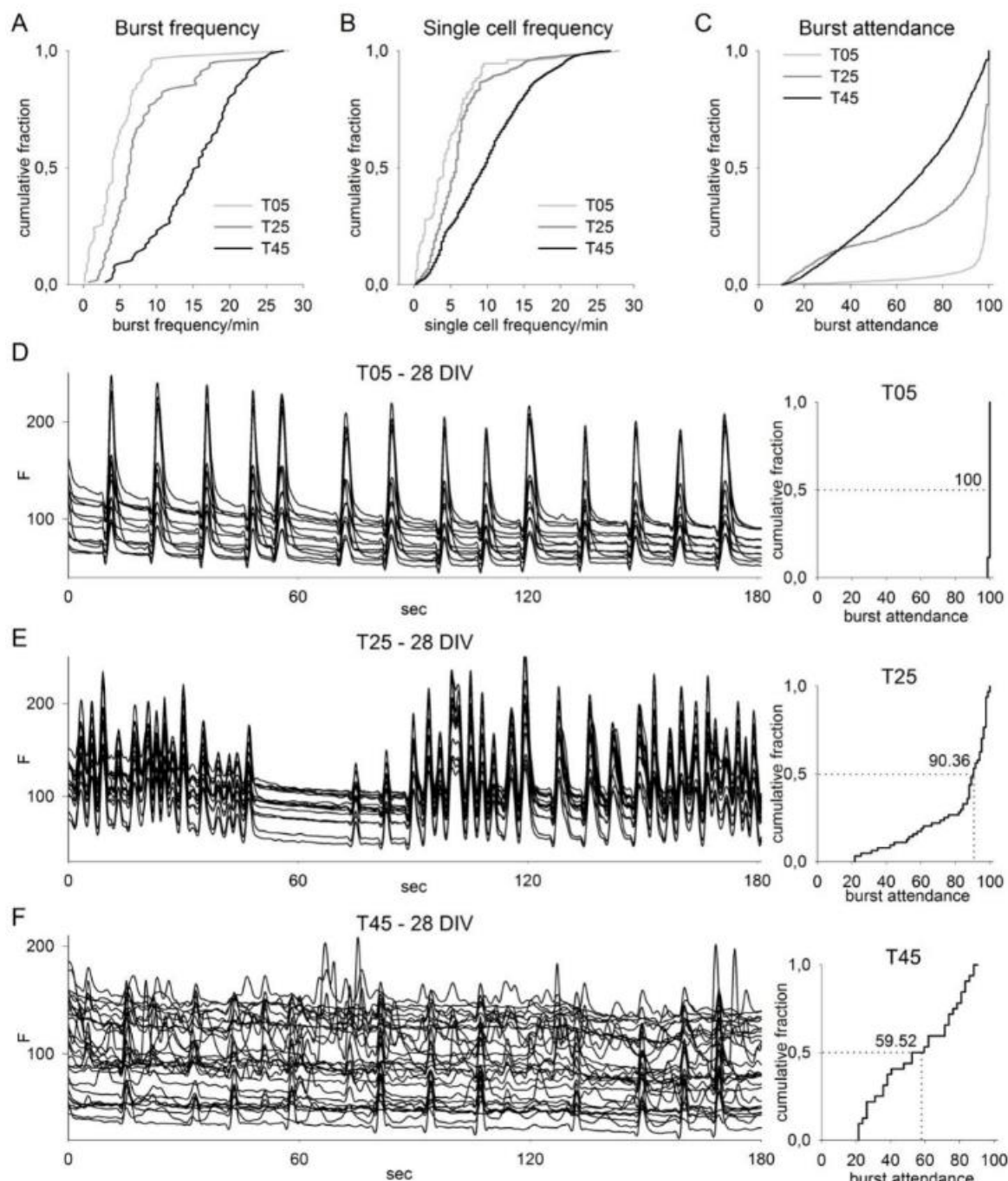


**Figure 11: Analysis of calcium imaging data in T05, T25, T30 networks.**

The cumulative probability plots of burst frequency, single burst frequency, and burst attendance for T05, T25, and T45 networks. Burst frequency (A) and single-cell frequency (B) increased with increasing MGE-derived IN content, but the number of cells participating in a burst decreased (burst attendance, C) (T05 network:  $n = 82$ ; T25 networks:  $n = 90$ ; T45 networks:  $n = 87$ ). “ $n$ ” represents the sum of data, which were collected from ten randomly selected fields in each of three cultures from each of three independent experiments between 14 and 28 DIV. Based on the background-corrected  $dF/F_0$  values, we calculated the burst attendance (right). During 4 min recording period, the data were recorded for all active neurons in a given field. D-F Traces show the changes in intracellular calcium levels in neurons

in a given field of 28 DIV T05, T25, and T45 networks, respectively. Burst attendance dropped from 100% in the T05 network to 90.36% (median value) in T25 networks and 59.52% in T45 networks.

## 4.7 Whole-cell patch-clamp recordings

### 4.7.1 Physiological impact of IN ratio variation on synaptic transmission

The results above showed that burst frequency and burst attendance varied among networks with different IN ratios. These findings motivated us to ask if these neuronal networks differ from their other physiological properties. To address this question, we examined patch-clamp recordings starting from T00 networks to evaluate the influence of INs' inputs on PNs in networks of this type (**Fig. 12**). Then, we determined and compared the development of synaptic changes of INs and PNs in the dorsal cortex with a low and high density of MGE-transplanted INs (T05 and T45 networks) over a one-month period (**Figs. 14-17**).

The first INs entering the rat cerebral cortex are born as early as E12. Even at a much lower density of these INs, they could profusely innervate other neurons (Voigt et al., 2001; Baltz et al., 2010). Our T00 networks were prepared from dCtx with no MGE-INs transplantation. However, a small amount of INs was confirmed in networks of this type (**Fig. 7 E**). Therefore, estimating the influence of INs' inputs on PNs in IN-depleted T00 networks is necessary.

Between 6-30 DIV, we recorded a total of 65 PNs. According to the protocol, during the  $2 \times 5$ -min recording period, the majority of the recorded neurons ( $n = 51$ ) showed only sEPSCs ( $\geq 30$ ) and no sIPSCs. These neurons were pooled as IPSC<sup>-</sup>-population. The remaining 14 PNs had exceeded 30 sEPSCs ( $\geq 30$ ) and at least 10 sIPSCs ( $\geq 10$ ). These neurons were pooled as IPSC<sup>+</sup>-population. Since all neurons were cultured in the same condition and developed in the same network type, it was possible to reliably evaluate the effect of sIPSCs on sEPSC parameters (**Fig. 12**).

The electrophysiological properties of PNs were estimated with a focus on the four parameters, including amplitude, rise time, decay time, and charge transfer, of sEPSCs for IPSC<sup>+</sup> and IPSC<sup>-</sup>-populations (**Fig. 12**). Over the inspected cultivation period, the four parameters of sEPSCs for each sub-population did not change with the age of development (IPSC<sup>-</sup>-population:  $n = 51$ , amplitude:  $p = 0.200$ ; rise time:  $p = 0.238$ ; decay time:  $p = 0.172$ ; charge transfer:  $p = 0.140$ , KW-ANOVA; IPSC<sup>+</sup>-population:  $n = 14$ , amplitude:  $p = 0.675$ ; rise time:  $p = 0.945$ ; decay time:  $p = 0.542$ , charge transfer:  $p = 0.821$ , KW-ANOVA). After comparing the individual sEPSC parameter between the IPSC<sup>+</sup> and IPSC<sup>-</sup>-population, no marked difference was founded in sEPSC amplitude, but sEPSC rise time, decay time, and charge transfer were significantly larger

in the IPSC<sup>+</sup>-population (amplitude:  $p = 0.88$ ; rise time:  $p = 0.010$ ; decay time:  $p \leq 0.001$ ; charge transfer:  $p = 0.023$ , KW-ANOVA).

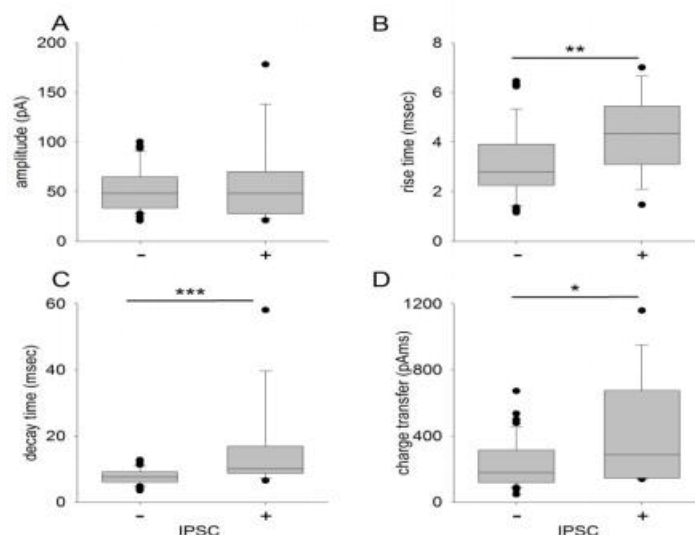


**Figure 12: Influence of GABAergic inputs on sEPSC parameters in PNs.**

Box plots show the differences in sEPSC properties between IPSC<sup>-</sup>-population ( $n = 51$ ) and IPSC<sup>+</sup>-population ( $n = 14$ ). IPSC<sup>-</sup>-population was characterized by the recorded neurons showing only sEPSCs, while the recorded neurons showing both sEPSCs and sIPSCs were pooled as IPSC<sup>+</sup>-population. Except for amplitude (A), all other sEPSC parameters were significantly increased in IPSC<sup>+</sup>-population (B-D). Significant levels are indicated with asterisks. \*  $p \leq 0.05$ , \*\*  $p \leq 0.01$ , \*\*\*  $p \leq 0.001$ .

Based on these findings, we confirmed that in T00 networks, the majority of PNs did not receive inhibitory synaptic inputs. Thus, the vast majority of GABAergic innervation in the networks of T05 and T45 was supplied by the MGE-transplanted INs. We next investigated the influence of IN density on sPSCs in PNs and INs in the developing T05 and T45 networks.

Between 6-30 DIV, we recorded 167 PNs and 229 INs from T05 and T45 networks. In every cell, the recordings of spontaneous currents included single sEPSCs and sIPSCs (Figs. 13 A-B, arrows in D), short multiple post-synaptic events (Fig. 13 D, asterisk), and network bursts. Network bursts are characterized by a high number of synaptic inputs over several hundred msec with several hundred pA amplitudes (Figs. 13 D-F), which can be recorded by calcium imaging (Opitz et al., 2002).

While in most neurons isolated spontaneous single PSCs and network bursts were easy to distinguish, multiple synaptic events formed a continuum from two to many superimposed single sPSCs making it difficult to quantify them. For this reason, in our current work, only isolated single sEPSCs and sIPSCs (Figs. 13 A, B, arrows in D) and large network bursts (Figs.

**13 D-F)** were analyzed. Some neurons recorded during the first week in culture (6-9 DIV) were immature. They lacked either sEPSC or sIPSC inputs or both. Thus, we needed to evaluate the number of neurons with both sEPSCs and sIPSCs at the initial stages of neuronal development of 6-9 DIV: PNs in T05 networks:  $n = 6$ ; PNs in T45 networks:  $n = 7$ ; INs in T05 networks:  $n = 12$ , and INs in T45 networks:  $n = 17$ . From 12 DIV, all neurons were well integrated into the network and showed reliable excitatory and inhibitory currents during 10 min recording, indicating that cells were mature at the beginning of at 2<sup>nd</sup> week. The recording period is from 12 to 30 DIV; we grouped the recorded cells by network types and week to analyze. 12-16 DIV, PNs,  $n = 24$ ; INs,  $n = 39$  in T05 networks; PNs,  $n = 20$ ; INs,  $n = 35$  in T45 networks; 19-23 DIV, PNs,  $n = 30$ ; INs,  $n = 30$  in T05 networks; PNs,  $n = 26$ ; INs,  $n = 31$  in T45 networks; 26-30 DIV, PNs,  $n = 29$ ; INs,  $n = 32$  in T05 networks; PNs,  $n = 25$ ; INs,  $n = 33$  in T45 networks. A summary of the analysis of isolated sPSC events is presented in **Figures 14-16** and **Table 2**. For the number of cells and statistically significant age-related differences see, **Table 2**.

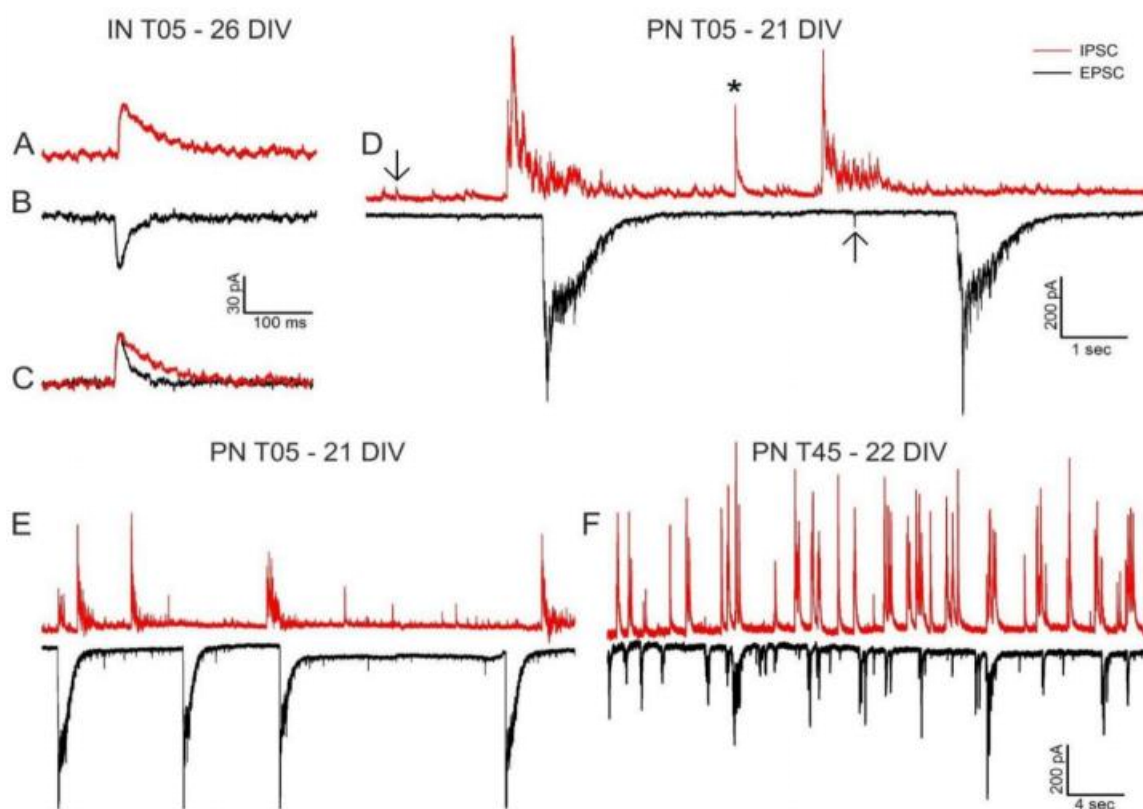


**Figure 13: Analysis of spontaneous post-synaptic currents in the intracellular voltage-clamp recordings.**

The exemplary sIPSCs (**A**, red trace) and sEPSCs (**B**, black trace) were recorded at 26 DIV in an IN of T05 networks. sEPSCs (**A**) and sIPSCs (**B**) were scaled to the same peak height (**C**). Exemplary original traces were recorded at 21 DIV in a PN of T05 networks, exhibiting single sPSCs (**D**, arrows), short

multi-synaptic events (**D**, asterisk), and large network bursts (**D**). Exemplary original traces of sIPSCs and sEPSCs were obtained from the same neuron type (PN) in T05 (21 DIV, **E**) and T45 networks (22 DIV, **F**), showing different spontaneous burst currents.

#### 4.7.2 Characterization of sPSC bursts

The synchronized bursting activity appears to be triggered by large inwardly-directed (EPSC bursts) or outwardly-directed (IPSC bursts) barrages of synaptic currents at a low frequency (**Figs. 13 D-F**). We calculated the burst charge transfer in individual PN and IN of T05 and T45 networks from 12 to 30 DIV as a complementary to the study of imaging bursts. Age-related differences in neuronal activity were examined. Results are illustrated in **Figures 14 A-F**. The number of cells we analyzed in each network type at different development stages, see **Table 1**.

**Table 1: A summary of analysis of the number of cells in network burst.**

		12-16 DIV	19-23 DIV	26-30 DIV
PNs	T05 networks	23	27	26
	T45 networks	19	25	26
INs	T05 networks	17	31	25
	T45 networks	21	38	40

The burst charge transfer of sEPSCs in PNs and INs of T05 and T45 networks significantly increased during the 2<sup>nd</sup> and 3<sup>rd</sup> week (in all cases,  $p < 0.001$ , MW-RST; **Figs. 14 A, D**). We then compared the sEPSC burst charge transfer between network types. We found it decreased in both cell types of T45 networks (PNs: 2<sup>nd</sup> week  $p < 0.001$  and 3<sup>rd</sup> week  $p < 0.001$ ; **Fig. 14 A**; INs: 3<sup>rd</sup> week  $p < 0.001$  and 4<sup>th</sup> week  $p = 0.002$ ; **Fig. 14 D**).

The burst charge transfer of sIPSCs in PNs of T05 networks showed no age difference ( $p = 0.086$ , MW-RST; **Fig. 14 B**, light grey boxes). In contrast, in PNs of T45 networks, the sIPSC burst charge transfer revealed an increase in the 4<sup>th</sup> week ( $p = 0.02$ , MW-RST; **Fig. 14 B**, dark grey boxes). It was only in the 4<sup>th</sup> week that the sIPSC burst charge transfer in PNs of T45 networks was significantly larger than the T05 networks ( $p = 0.043$ , MW-RST; **Fig. 14 B**). Similar to sEPSC burst charge transfer in PNs and INs of T05 and T45 networks, sIPSC burst charge transfer significantly increased in INs in the 3<sup>rd</sup> week in both networks of T05 and T45 ( $p < 0.001$  for INs in both network types, MW-RST; **Fig. 14 E**). In INs, no significant

developmental change was founded in sIPSC burst charge between age groups for both network types (**Fig. 14 E**).

To test the presence of GABA regulate the balance of excitation to inhibition in the developing networks, we used the formula of sIPSC burst charge transfer/(sIPSC burst charge transfer + sEPSC burst charge transfer) to calculate the burst charge transfer ratios (E/I balance) for each cell from averaged values.

We first compared the E/I balance for burst charge transfer in the PNs of the T05 and T45 networks. Age variation was observed in the PNs of T45 networks [PNs of T05 networks, 2<sup>nd</sup> week: E/I ratio =  $0.47 \pm 0.04$  (mean  $\pm$  SEM),  $n = 23$ ; 3<sup>rd</sup> week: E/I ratio =  $0.35 \pm 0.04$ ,  $n = 23$ ; 4<sup>th</sup> week: E/I ratio =  $0.42 \pm 0.05$ ,  $n = 26$ ,  $p = 0.092$ , one-way ANOVA; **Fig. 14 C**, light gray boxes) vs. PNs of T45 networks: 2<sup>nd</sup> week: E/I ratio =  $0.62 \pm 0.44$ ,  $n = 19$ ; 3<sup>rd</sup> week: E/I ratio =  $0.62 \pm 0.03$ ,  $n = 25$ ; 4<sup>th</sup> week: E/I ratio =  $0.50 \pm 0.04$ ,  $n = 26$ ,  $p = 0.031$ , one-way; **Fig. 14 C**, dark gray boxes)]. We next compared the E/I balance in the INs of T05 and T45 networks. In INs of T05 networks, the ratio of excitatory burst charge transfer to inhibitory burst charge transfer showed age variation ( $p < 0.05$ , **Fig. 14 F**, light gray boxes). The values decreased from  $0.54 \pm 0.06$  (mean  $\pm$  SEM,  $n = 17$ ) at 2<sup>nd</sup> week to  $0.31 \pm 0.04$  ( $n = 31$ ) in the 3<sup>rd</sup> week ( $p = 0.027$ , MW-RST, compared with 2<sup>nd</sup> week) and then increased to  $0.41 \pm 0.04$  ( $n = 25$ ) in the 4<sup>th</sup> week ( $p = 0.027$ , MW-RST, compared with 3<sup>rd</sup> week; **Fig. 14 F**, light gray boxes). In INs of T45 networks, the E/I balance showed no age variation (2<sup>nd</sup> week: E/I =  $0.59 \pm 0.04$ ,  $n = 21$ ; 3<sup>rd</sup> week: E/I =  $0.55 \pm 0.03$ ,  $n = 38$ ; 4<sup>th</sup> week: E/I =  $0.57 \pm 0.02$ ,  $n = 40$ ,  $p = 0.634$ , one-way ANOVA, mean  $\pm$  SEM; **Fig. 14 F**, dark gray boxes).

The E/I balance for burst charge transfer in PNs and INs of T05 networks significantly decreased when compared to those in neurons of T45 networks [PNs: 2<sup>nd</sup> week ( $p = 0.012$ ) and 3<sup>rd</sup> week ( $p \leq 0.001$ ); **Fig. 14 C**; INs: 3<sup>rd</sup> week ( $p \leq 0.001$ ) and 4<sup>th</sup> week ( $p \leq 0.001$ ); **Fig. 14 F**], which reflected an overall reduction in GABAergic synaptic inputs in both cell types of T05 networks. The results indicate that the hyperactivity generated by INs in the network with lower GABA density can not offset the excessive excitation that was provided by the PNs' synapses during the burst of synaptic activity.

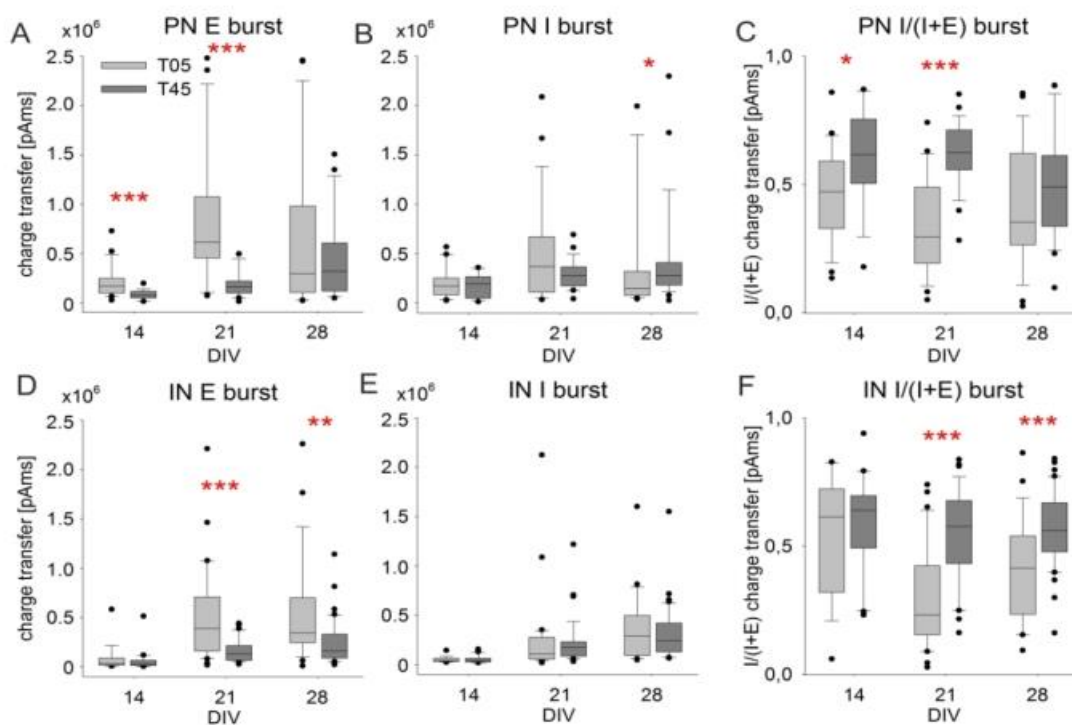


**Figure 14: Spontaneous PSC Bursts.**

Developmental changes in network burst charge transfer and excitation-inhibition balance in PNs (A-C) and INs (D-F) of T05 (light gray boxes) and T45 (dark gray boxes) networks. Both neuron types of T05 and T45 networks displayed increased sEPSC charge transfer in the 3<sup>rd</sup> week (A, D). Asterisks in A and D indicate the burst charge transfer in the T05 networks is significantly larger than in the T45 networks. Although the sIPSC burst charge transfer increased in PNs and INs of T05 and T45 networks, no differences in sIPSC burst charge transfer between network types were found (B, E) except PNs in the 4<sup>th</sup> week (B). As a result, the values of E/I balance in T05 networks were lower than that in the T45 networks (E, F), reflecting in both neuron types of T05 networks, the synaptic inhibitory drive is deficits. The levels of significant differences between network types are present by asterisks (\* $p \leq 0.05$ , \*\* $p \leq 0.01$ , \*\*\* $p \leq 0.001$ ).

### 4.7.3 Characterizations of post-synaptic currents in our cultures

#### 4.7.3.1 sEPSC events

To characterize the developmental changes in excitatory and inhibitory spontaneous post-synaptic currents in PNs and INs of T05 and T45 networks, we recorded sPSCs in 167 PNs and 229 INs between 6 and 30 DIV and compared the amplitude, rise time, decay time, and charge transfer of sPSCs at different developmental ages and between network types (**Table 2, Figs. 15 A-F, Figs. 16 A-F**). We then estimated the changes in the balance of excitation and inhibition (**Table 2, Figs. 17 A-F**).

In T45 networks, amplitudes of sEPSCs significantly increased in both neuron types during development (PNs:  $p = 0.009$ , ANOVA; INs:  $p < 0.001$ , ANOVA; **Figs. 15 A, B**, dark grey boxes), while in T05 networks, a significant increase with neuron maturation was detected only in INs (INs:  $p = 0.001$ , ANOVA; **Fig. 15 B**, light gray boxes). Compared to T05 networks, the amplitude of sEPSCs in PNs of T45 networks was slightly higher in the first two weeks [T45 networks: 25.23 (median) vs. T05 networks: 22.10 at 1<sup>st</sup> week,  $p = 0.366$ , MW-RST; T45 networks: 43.85 (median) vs. T05 networks: 33.73 at 2<sup>nd</sup> week,  $p = 0.106$ , MW-RST; **Fig. 15 A**], and was significantly higher in the last two weeks (3<sup>rd</sup> week:  $p < 0.001$ ; 4<sup>th</sup> week:  $p < 0.001$ , MW-RST; **Fig. 15 A**). However, the amplitude of sEPSCs in INs of T45 networks was significantly higher than that in T05 networks, only in the 3<sup>rd</sup> and 4<sup>th</sup> week (3<sup>rd</sup> week:  $p = 0.002$ ; 4<sup>th</sup> week:  $p = 0.009$ , MW-RST; **Fig. 15 B**). In T45 networks, the rise time of sEPSCs in PNs increased to the 2<sup>nd</sup> week and decreased during the time of the 2<sup>nd</sup> and 4<sup>th</sup> week (**Table 2, Fig. 15 C**, dark grey boxes), while the rise time of sEPSCs in INs increased over age ( $p < 0.001$ , ANOVA; **Fig. 15 D**, dark grey boxes). Similar to the rise time of sEPSCs in PNs of T45 networks, the decay time of sEPSCs in PNs of T45 networks was the largest by the 2<sup>nd</sup> week and then decreased (**Table 2, Fig. 15 E**, dark grey boxes). In PNs, the difference in the decay time of sEPSCs between T05 and T45 networks was only detected in the 2<sup>nd</sup> week ( $p = 0.024$ , MW-RST; **Fig. 15 E**). Similar to the rise time of sEPSCs in INs of T45 networks, the decay time of sEPSCs in INs of T45 networks was the largest by the 3<sup>rd</sup> week and then a small but not a significant decrease in the 4<sup>th</sup> week (**Table 2, Fig. 15 F**, dark grey boxes). The decay time of sEPSCs in INs did not differ between network types (**Table 2, Fig. 15 F**).

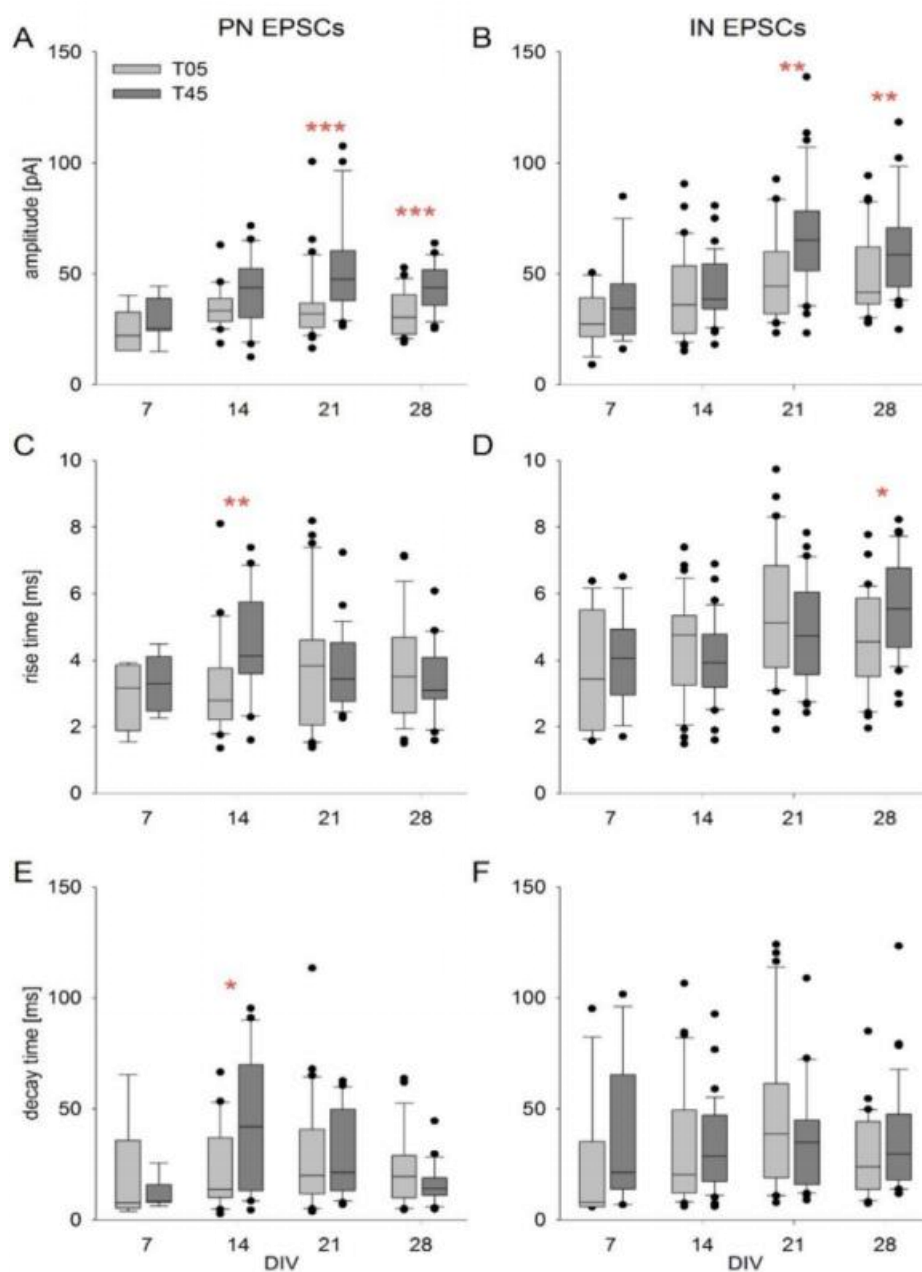


**Figure 15: Developmental changes in sEPSCs in neurons of T05 and T45 networks.**

Box plots show amplitude (A, B), rise time (C, D), and decay time (E, F) of spontaneous EPSCs for PNs and INs in T05 (light gray boxes) and T45 networks (dark gray boxes) at each age. The levels of significant differences between network types are present by asterisks ( $*p \leq 0.05$ ,  $**p \leq 0.01$ ,  $***p \leq 0.001$ ).

In conclusion, these findings demonstrated that all sEPSC parameters in PNs exhibited substantial age variations only in the network type of T45. In contrast, the four parameters of sEPSCs in INs revealed age variations in both network types of T05 and T45.

#### 4.7.3.2 sIPSC events

In T45 networks, amplitudes of sIPSCs increased in the first three weeks in both neuron types (**Table 2, Figs. 16 A, B**, dark grey boxes), while in T05 networks, a detectable increase was only observed in INs ( $p < 0.001$ , ANOVA; **Fig. 16 B**, light grey boxes). The sIPSC amplitude in PNs and INs of the T45 networks was larger in T05 networks (PNs: 2<sup>nd</sup> week,  $p = 0.024$  and 3<sup>rd</sup> week,  $p = 0.016$ ; INs: 2<sup>nd</sup> week  $p = 0.006$  and 4<sup>th</sup> week,  $p = 0.015$ , KW-MRT; **Table 2** and **Figs. 16 A, B**). In T45 networks, the rise time of sIPSCs in PNs was the largest in the 2<sup>nd</sup> week (**Table 2, Fig. 16 C**, dark grey boxes), while in INs of T05 and T45 networks, the maximum value was in the 3<sup>rd</sup> week or 4<sup>th</sup> week (INs: T05 networks in the 3<sup>rd</sup> week; T45 networks in the 4<sup>th</sup> week; **Table 2, Fig. 16 D**). In both neuron types, the sIPSC rise time did not differ between network types (**Table 2, Fig. 16 D**). In PNs, sIPSC decay time decreased from the 2<sup>nd</sup> week in both T05 and T45 networks (T05 networks:  $p < 0.001$ , ANOVA; T45 networks:  $p < 0.001$ ; **Fig. 16 E**). In contrast, the decay time of sIPSCs in INs decreased from the initial week in both network types (for both network types:  $p < 0.001$ , ANOVA; **Fig. 16 F**). The sIPSC decay time was shorter in PNs and INs of T45 networks (PNs: 3<sup>rd</sup> week,  $p = 0.026$  and 4<sup>th</sup> week,  $p < 0.001$ ; INs: 2<sup>nd</sup> week  $p = 0.049$ , KW-MRT; **Table 2, Figs. 16 E, F**).

In conclusion, the results revealed that all sIPSCs in T45 networks showed significant age variations in PNs and INs; in both neuron types of T05 networks, age variations were detected only in amplitude and decay time.

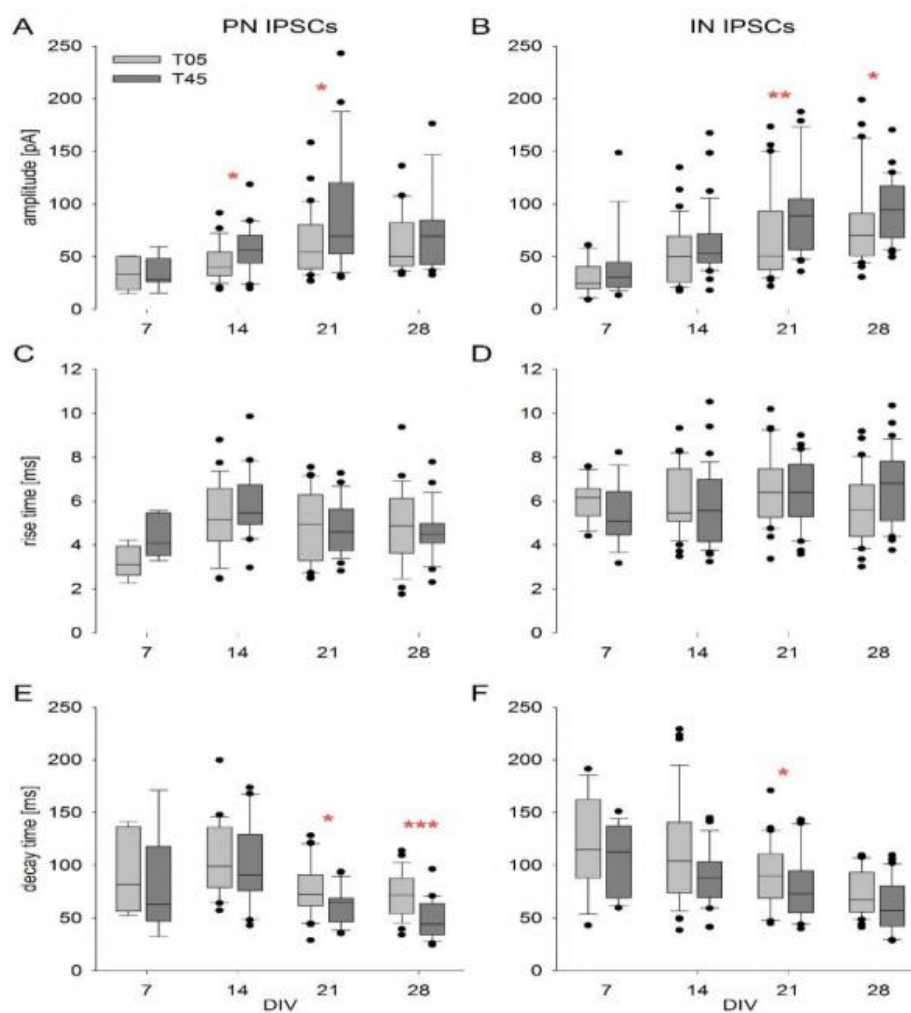


**Figure 16: Developmental changes in sIPSCs in neurons of T05 and T45 networks.**

Box plots show amplitude (A, B), rise time (C, D), and decay time (E, F) of spontaneous IPSCs for PNs and INs in T05 (light gray boxes) and T45 networks (dark gray boxes) at each age. The levels of significant differences between network types are present by asterisks ( $*p \leq 0.05$ ,  $**p \leq 0.01$ ,  $***p \leq 0.001$ ).

#### 4.7.4 Charge transfer balance between sEPSCs and sIPSCs

In PNs of T45 networks, the charge transfer of sEPSCs reached the maximum at the 2<sup>nd</sup> week (Table 2, Fig. 17 A, dark gray boxes), while in INs, the charge transfer of sEPSCs showed its peak value in both network types at the 3<sup>rd</sup> week (Table 2, Figs. 17 A, D). In addition, we found the changes in amplitude and decay time are similar to the variations in sEPSC charge transfer (see above) regardless of neuron types. Only a slight difference in the sEPSC charge transfer between network types was detected (Figs. 17 A, B). The charge transfer of sEPSCs in T45 networks was larger than in T05 networks in PNs in the 2<sup>nd</sup> week ( $p = 0.001$ , KW-MRT; Fig. 17 A) and in INs in the 4<sup>th</sup> week ( $p = 0.039$ , KW-MRT; Fig. 17 B). The charge transfer of sIPSCs in INs of T45 networks significantly increased during development, reaching its peak in the 3<sup>rd</sup>

week ( $p < 0.001$ , ANOVA; **Table 2**, **Fig. 17 E**, dark grey boxes). In both neuron types, the charge transfer of sIPSCs between T05 and T45 networks did not show a difference (**Table 2**, **Figs. 17 B** and **E**).

The cellular E/I balance [sIPSC charge transfer/(sIPSC charge transfer + sEPSC charge transfer)] was calculated for each cell from the charge transfer obtained from MiniAnalysis. In rat cortical cultures, we found the charge transfer of isolated sEPSCs (**Figs. 17 A, B**) was always smaller than the charge transfer of isolated sIPSCs (**Figs. 17 D, E**) regardless of the number of MGE-transplanted INs in the networks. According to the formula above, the E/I balance for charge transfer was over 0.5. This discovery is inconsistent with the mice cortical cultures data (Klueva et al., 2008). The charge transfer ratio remained unchanged over the recording period in PNs of both T05 and T45 networks as well as in INs of T45 networks (PNs T05 network:  $p = 0.389$ ; T45 networks:  $p = 0.223$ , INs T45 networks:  $p = 0.118$ , ANOVA; **Figs. 17 C, F**). During the whole recording period, the charge transfer ratio in INs of T05 cultures showed a slight decrease only in the 3<sup>rd</sup> week (**Table 2**, **Fig. 17 F**). In PNs and INs, the charge transfer ratio between T05 and T45 networks did not reveal differences (PNs:  $p = 0.178$ ; INs:  $p = 0.058$ , two-way ANOVA). However, we found few differences when comparing networks with isolated age groups. In the 2<sup>nd</sup> week in PNs ( $p = 0.018$ , MW-RST; **Fig. 17 C**) and the 4<sup>th</sup> week in INs ( $p = 0.010$ , MW-RST; **Fig. 17 F**), the E/I ratio of the charge transfer was higher in T45 networks than T05 networks.

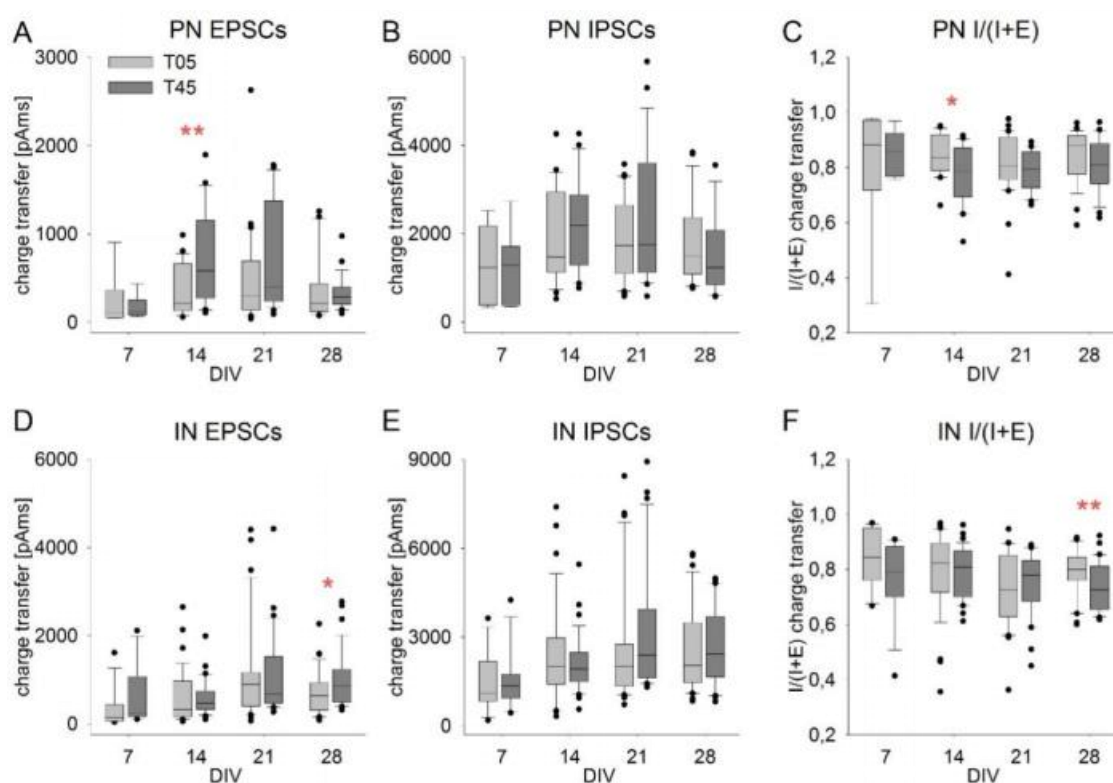


**Figure 17: Charge transfer and charge transfer ratios for single sPSCs.**

The developmental changes in single sPSC charge transfer and in charge transfer ratio of PNs (A-C) and INs (D-F) in T05 (light gray boxes) and T45 (dark gray boxes) networks. In contrast to network burst charge transfer (Figs. 14 A, B, D, E), the charge transfer of single sPSCs showed less variation over time and across network types (A, B, D, E). The significant differences between network types are present by asterisks (\*  $p \leq 0.05$ , \*\*  $p \leq 0.01$ , \*\*\*  $p \leq 0.001$ ).

In summary, we concluded that the E/I balance for isolated sPSCs remained relatively constant despite the PN/IN ratios in the network. When multi-synaptic network events are considered, differences in IN content become apparent. This indicates that for single synaptic events, each cell balances its excitatory and inhibitory synaptic inputs during development and within a wide range of network conditions, but this can, however, not compensate for inhibitory neuron deficiency.

## 5. Discussion

### 5.1 IN classification

To investigate the interneuronal subtypes in our cultures, cells were double-immunostained with anti-eGFP and either anti-CR (**Fig. 2 A**), anti-PV (**Fig. 2 B**), or anti-SOM (**Fig. 2 C**) antibodies. In our cultures, the proportion of PV-, SOM-, and CR-positive cells among the INs was 6.9%, 17.3%, and 13.4%, respectively. These three subtypes together account for about 37% of all GABAergic cells. PV<sup>+</sup>, SOM<sup>+</sup>, and CR<sup>+</sup> interneurons in rat cortex represent three non-overlapping populations (Kubota et al., 1994; Gonchar and Burkhalter 1997). In the rat visual cortex, PV<sup>+</sup> cells are the most numerous, making up about 51% of the GABAergic population; SOM<sup>+</sup> cells and CR<sup>+</sup> cells account for equal about 17% (Gonchar and Burkhalter 1997). The data we obtained differed from previous findings can be explained as follows: First, a previous study had shown that *in vivo*, all PV<sup>+</sup> neurons were already present at P20, but the proportion of PV<sup>+</sup> cells achieved only 6% at 50-70 DIV (Patz et al., 2004). Due to the developmental delay in the somatosensory and visual cortex (Alcántara et al., 1996; Patz et al., 2004), PV-positive cells developed slowly in our 28-day-old cultures. Second, the expression of PV is highly activity-dependent. That is, the levels of PV mRNA were affected by thalamic inputs. The PV expression could be completely prevented by blocking thalamic inputs (Alcántara et al., 1996; Patz et al., 2004). However, our cultures lacked thalamic inputs. Third, according to our protocol, astrocytes were present in our culture before neuron plating. It has been confirmed that the present glial cells inhibit the proliferation of precursor cells (de Lima and Voigt 1999), which results in the proportion of each subtype being lower than *in vivo* cortex. Forth, *in vivo* transplantation studies have identified that MGE generates only a small number of CR (Wichterle et al., 2001; Nery et al., 2002; Valcanis and Tan 2003; Lopez-Bendito et al., 2004; Xu et al., 2004; Butt et al., 2005). In contrast, the majority of CR<sup>+</sup> interneurons (sometimes VIP<sup>+</sup>) are generated from the CGE (Nery et al., 2002; Xu et al., 2004; Butt et al., 2005; Fogarty et al., 2005; Cobos et al., 2006; Miyoshi et al., 2007; Miyoshi et al., 2010).

The MGE is the origin of most INs expressing PV or SOM, which together account for ~60% of cortical INs (Wonders and Anderson 2006; Batista-Brito and Fishell 2009). The CGE is the origin of ~30% of the INs in the cerebral cortex (Wonders and Anderson 2006; Batista-Brito and Fishell 2009; Gelman and Marin 2010). The remaining 10% of cortical INs are generated from the preoptic region (Gelman et al., 2009; Gelman and Marin 2010). The INs present in our cultures were only from the MGE-INs from the E14 transgenic rats. At embryonic days E14, only a small fraction of INs that normally migrate into the neocortex *in vivo*; thus, the number and the subclass of INs in our cultures can not match the INs in the mature cortical; this may explain the low proportion of IN subtypes in our cultures.

## 5.2 INs impact on the survival of PNs

In our study, we used precursor cells from the dissociated dorsal cortex of E16 wild-type rats together with E14 MGE-INs to build cortical networks. We found an increase in PNs proliferating with the presence of co-cultured INs during the first days (**Fig. 6 D**). The results suggest that migrating INs may play an essential role in setting up the cellular ratio between INs and PNs by modulating the proliferation rate of PNs in their target area. Thus, a regulatory coupling between the number of INs and the number of generated PNs is likely to allow the initial adjustment of the PN/IN ratio based on cell proliferation before activity-dependent cell elimination takes over for fine adjustments at later developmental stages.

INs migrate into the MZ or SVZ are the two horizontal streams of IN migration into the cortex (see more detail in chapter “2.1.2”). Noteworthy, those neurons migrating within the SVZ are located close to the proliferating progenitor cells in the ventricular zone (VZ). On the one hand, the proliferating neurons in the VZ and the SVZ express at least the KA-2 subunit of glutamatergic receptors and several subunits of GABA<sub>A</sub> receptors, including ionotropic and metabotropic subunits (Herb et al., 1992; Laurie et al., 1992; Owens et al., 1999; Lujan et al., 2005). On the other hand, before synapse formation, glutamate and GABA were released by a Ca<sup>+</sup>- and SNA-independent paracrine system into the environment (Demarque et al., 2002). Thus, neurons in the VZ and SVZ are capable of responding to GABA and glutamate. LoTurco et al., (1995) reported both GABA and glutamate reduced cell proliferation rates. Two years later, Antonopoulos and his colleagues (1997) confirmed this discovery. However, in 2002, Haydar et al. pointed out the functions of ambient GABA in the progenitor proliferation rates in the SVZ and VZ is conversed. Decrease in the later formed SVZ while an increase in the early formed VZ. Young et al., (2012) and Bordey (2007) hold the idea that the depolarizing GABA<sub>A</sub> receptors triggered Ca<sup>2+</sup> entry into the cell resulting in the reduction of the cell proliferation of the SVZ. Moreover, in the mammalian embryonic stem (ES) cells, the progress of the cell-cycle was inhibited due to the fact that GABA<sub>A</sub> receptors are involved in the ‘DNA damage’ S/G2 cell cycle checkpoint pathway. The activation of GABA<sub>A</sub> receptors hyperpolarizes the membrane of ES cells, and thus the cell volume increases, and a large number of ES cells are accumulated in the S phase, which leads to the proliferation of ES cells decrease (Andang et al., 2008). However, the mouse model has shown an increase in the cellular proliferation of VZ results from GABA<sub>A</sub> or GABA<sub>B</sub> receptors recruiting different growth factors. Modulating cellular proliferation and differentiation through GABA<sub>B</sub> receptors was expressed by undifferentiated neural progenitor cells isolated from the fetal mouse brain (Fukui et al., 2008; Fukui et al., 2008).

Understanding how the cell cycle modulates the projection cells allocated for the different layers is more important (Takahashi et al., 1999; Verney et al., 2000). In our study, dCtx from E16 consists primarily of progenitor projection cells of VZ [for review, see (Nadarajah et al., 2002)]. When the first wave of INs migrates into the neocortex, the precursors of VZ are born [for review, see (Nadarajah et al., 2002)]. Based on the knowledge presented above, the adjustment of PN/IN ratios prior to any synapse formation is regulated by three crucial elements: ingrowing INs, ambient GABA, and GABA-dependent cell-cycle modulation of precursors.

### 5.3 dCtx networks vs. wCtx networks

When we examined the developmental dynamics of neuronal populations in our cultures, we found both PNs and INs declined between 7 and 28 DIV in the dorsal cortex networks (**Figs. 7 D-E, 8 A-B**) and the whole cortex networks (**Figs. 9 E-F**). Activity-dependent cell apoptosis may trigger the reduction in neuron numbers (Nadarajah et al., 2002). We also found the development of neurons in our cultures followed a similar timeline to that of the cultures of other species or intact rodent brains (Southwell et al., 2010; Wong and Marin 2019). In the dCtx cultures enriched with MGE-INs, there was a similar dynamic of cell elimination between PNs and INs populations (**Figs. 7 D-E**), and the IN proportions in the networks with predefined ratios did not change over three weeks (dCtx; **Fig. 7 F**). However, in the wCtx cultures cultivated with MGE-INs, the IN population declined (**Fig. 9 F**) faster than the PN population (**Fig. 9 E**). Interestingly, cultures grown with gabazine did not show a faster reduction in the IN fraction of wCtx (**Fig. 9 H**), suggesting that GABA-mediated neurotransmission is the key to the long-term integration of INs into the network.

The differences in developmental dynamics in the dCtx and wCtx may be ascribed to the different cellular structures of dCtx and wCtx. At E16, a rat's dCtx is mainly composed of the VZ and layer 1 [for review, see (Nadarajah et al., 2002)]. At this age, other cortical layers have not formed, and the entire upper portion has not been invaded by the migrating MGE-derived INs (see IN-depleted T00 networks; **Figs. 1 A, 7 E**). In contrast, the lateral cortex has already been invaded by the first cohort of early-born MGE-INs (Voigt et al., 2001). Since the development of the cortical cortex is from lateral to dorsal, the neurons in the upper cortical layers are still proliferating. In contrast, the neurons in the most lateral cortex are already post-mitotic (Berry and Rogers 1965). Thus, when we used the cells of dissociated E16 dCtx to build cortical networks (**Fig. 1 A**), these generated networks did not contain INs or contained a few isolated ones (dCtx; **Fig. 9 A**), but a wCtx preparation at E16 included a small number of early-born INs (wCtx; **Fig. 9 A**) and a large number of post-mitotic PNs. In rats, the first INs are born

at E12-E15, and these INs include those that participate in initially regulating early network activities (Voigt et al., 2001).

The functional SP is a significant transient layer during neuronal development. Multiple lines of evidence have shown that the SP serves diverse organizational functions throughout cortical development (Kanold and Luhmann 2010; Luhmann et al., 2018).

These functions include propagating activation signals and consolidating synaptic connections in the immature network activity (Voigt et al., 2005; Young et al., 2012). Thus, the difference between dCtx and wCtx preparations reflects whether the networks contain those INs that have been integrated into the SP layer.

In our cultures, electrically active INs were found in both dCtx and wCtx networks. However, PN/IN ratios were adjusted only in wCtx networks with early-born INs (**Figs. 9 B-D**). Thus, our findings strongly suggest that these early-born INs play a unique role not only in initiating early synchronous network activity (Voigt et al., 2001; Opitz et al., 2002; Luhmann et al., 2018) but also in adjusting the PN/IN ratios.

The analysis of the long-term culture experiments suggests the regulation of the PN/IN ratio seems to be dependent on the network structure at the time activity-dependent cell elimination occurs. When the structure of the developing cortex is very young (e.g., dCtx), the proportion of INs in each network type remains constant. In contrast, a reduction in the fraction of INs was observed when the MGE-INs were transplanted into a network that had developed to a critical structural maturity (e.g., wCtx) indicating an additional, at least partially, GABA-dependent mechanism for population adjustment take place.

#### **5.4 Intrinsically determined cell death of developing cortical INs.**

During the formation of neuronal networks, cell death is considered a prominent factor in regulating neuronal incorporation (Katz and Shatz 1996; Voyvodic 1996). The transplantation experiments have revealed that the death of cortical INs in the early postnatal mouse cortex is under intrinsic control (Southwell et al., 2012). Southwell and colleagues (2012) have observed that the majority of cortical INs undergo programmed cell death *in vivo* between P7 and P18. When INs are transplanted into older cortices (P3), they undergo programmed cell death, however, later than normal (~P15), which demonstrates that this process is intrinsically linked to the cellular age of INs. Consistently, cortical INs undergo programmed cell death *in vitro* with the same temporal dynamics as *in vivo*. Further evidence supporting the existence of an

intrinsic clock that controls the sequence of neuron elimination in the mouse cortex comes from Wong and his colleagues' research (2018). Their research has revealed that the PN/IN ratio is established in a two-phase process. The first-phase process occurs between P2-P5, during which the number of PNs declines first. The second-phase process occurs between P5-P10. In this phase, apoptosis occurs predominantly in INs. INs undergo apoptosis in response to PN activity. In IN selection phase, the required ratio is established by well-connected INs being recruited into the electrically active PN networks in an activity-dependent manner (Wong et al., 2018). Cortical development in rats takes slightly longer than in mice. In the present study, we found apoptosis extended over three weeks in cultured networks of rat cortical neurons (a developmental age of P14 is roughly equivalent to 21 DIV) and a similar sequence of neuron elimination in the networks with high IN content. **Figs. 8 A-B** show the declination of PNs preceded that of INs in the T45 networks during the developmental age of 7-21 DIV.

### 5.5 Contribution of INs in spontaneous network activity

As one of the earliest fundamental processes in a network, spontaneous activity has significant implications for plasticity and adaptability. Its subsequent maturation is thought to contribute to the further evolution of functional networks (Feller 1999; O'Donovan 1999; Ben-Ari 2001; Opitz et al., 2002).

The present work showed that networks with different INs content developed different network activity patterns (**Fig. 11**). When networks were grown with a small number of INs, the spontaneous activity of neurons in cortical networks was characterized by large bursts separated by long periods of silence (**Fig. 11 D**). Neally, all active neurons participated in the network events. Immature networks with depolarized GABA or old networks without sufficient GABAergic inhibition exhibit this participation pattern (Opitz et al., 2002; Baltz et al., 2010).

With increasing IN content, networks displayed higher burst frequencies and increased bursts with low neuron participation (**Figs. 11 A, C**). *In vitro* pharmacological evidence has revealed that cells co-activated with other neurons have a greater chance of survival than those not participating in synchronized events (Voigt et al., 1997; Wagner-Golbs and Luhmann 2012). The analysis of whole-cell recordings demonstrated that the inhibition in IN low-density T05 networks could not compensate for the overproduced excitatory, which are provided by the PNs' synapses (**Figs. 14 D, F**). Therefore, to avoid excitotoxic cell death (Choi 1992), in the networks with low-density IN content, all cells are participated in synchronous network activity to increase their survival.

During the first cultured week, networks develop synchronous network activity, and the large-scale network bursts appear at the end of the first week (Muramoto et al., 1993; Voigt et al., 2005). During the second week *in vitro*, the number of cells participating in a burst reaches the maximum (Voigt et al., 2005). Despite the depolarizing GABAergic neurons facilitating the early emergence of the synchronized activity and generating different burst patterns, ionotropic glutamatergic receptors drive these activities (Ben-Ari et al., 1997; Ben-Ari 2002; Opitz et al., 2002). In the 2<sup>nd</sup> and 3<sup>rd</sup> weeks *in vitro*, the frequency of burst activity increases, and the larger burst pattern is often enriched with a higher amount of shorter burst in the Large-INs present cultures, which can be blocked by GABA<sub>A</sub> antagonists (Opitz et al., 2002). A burst activity can be first observed roughly at 21 DIV. Except for the characterization of burst activity by alternating periods of higher and lower burst incidence (Baker et al., 2006; Wagenaar et al., 2006; Baltz et al., 2010), it also corresponds to slow changes in network excitability (Baltz and Voigt 2015). However, in GABA-depleted dCtx cultures or cultures grown with GABA<sub>A</sub> receptor antagonists, the small developmental changes of the burst activity can not be observed, suggesting that GABA is involved in small changes in network excitability (Baltz et al., 2010). Consistent with previous findings of calcium imaging and MEA recordings (Baltz et al., 2010; Baltz et al., 2011; Baltz and Voigt 2015; Haroush and Marom 2019), our results show that networks relying on GABA activity develop the complex activity patterns.

Thus, sufficient INs, on the one hand, contribute to synchronization during the initial period of network activity. On the other hand, they are also essential for forming desynchronized patterns of network activity during their later development.

## 5.6 Morphology changes are correlated with synaptic network activity

The present work of analyzing the charge transfer ratios (E/I balance) included analyzing the E/I balance for single synaptic events (**Figs. 17 C, F**) and multi-synaptic network bursts (**Figs. 14 C, F**). It was found that the E/I balance for isolated sPSCs did not vary significantly with neuron maturation and over a wide range of PN/IN ratios (**Figs. 17 C, F**).

Compared with isolated sPSCs measurement, network bursts reflected many neurons being active simultaneously. Coinciding with the calcium imaging analysis (**Fig. 11**), network bursts revealed pronounced differences between T05 and T45 networks (**Fig. 14**). Previous studies have independently identified that neuronal synaptic strength is modified in a neuronal activity-dependent manner (Redmond et al., 2002; Turrigiano 2007; Seeburg and Sheng 2008). Consistent with these studies, we found networks with a lower frequency of burst activity (**Fig. 11**) had a relatively lower inhibitory current strength in single PNs or INs (**Figs. 14 C, F**).

Meanwhile, we also found that INs in the networks with low GABA content showed larger soma sizes (**Fig. 10 A**) and higher survival rates (**Figs. 7 F, 8 C**). Thus, we deduced that in the GABA deficient networks, INs might alter their morphologies to prevent over-excitability and increase survival. These morphology changes are dependent on an activity-dependent manner.

In conclusion, although networks were generated with a wide range of PN/IN ratios, the development of E/I balance for single synaptic events varied minimally (**Figs. 17 C, F**). However, if multi-synaptic network activity is considered (**Figs. 11, 14 C, F**), networks with different IN content result in different network behaviors. Even if networks with a few IN exhibit cellular E/I balance, the patterns of network activity reflect the structural deficiencies. Morphology change is an interesting and important property of neuronal networks. The relationship between morphology and the number of potential afferent input partners may be an essential rule for neurons in a network. When INs receive much more excitatory inputs from other INs and PNs in the networks with low GABA density, INs show a surprising ability to increase arborization to avoid toxicity and overexcitability (**Fig. 10 A**). However, neither subcellular remodeling nor synaptic plastic changes can offset the scarcity of INs or the lack of certain types of INs.

**Table 2: Summary of sEPSC and sIPSC parameters in PNs and INs of T05 and T45 networks.**

		PN						IN			
		T05		T45			T05		T45		
DIV	<i>n</i>	Median	<i>n</i>	Median	<i>p</i> <sup>&amp;</sup>	<i>N</i>	Median	<i>n</i>	Median	<i>p</i> <sup>&amp;</sup>	
<b>EPSCs</b>											
<b>Amplitude (pA)</b>											
6-9	6	22.10	7	25.23	0.366	12	27.28	17	34.38	0.438	
12-16	24	33.73	20	43.85	0.106	39	35.98	35	38.69*	0.147	
19-23	30	31.89	26	47.69*	<0.001	30	44.53*	31	65.19	0.002	
26-30	29	30.42	25	43.79	<0.001	32	41.67	33	58.81*	0.009	
<i>p</i> <sup>*</sup>		0.096		0.009			0.001		<0.001		
<b>Rise Time (ms)</b>											
6-9		3.16		3.30	0.534		3.43		4.05	0.642	
12-16		2.79		4.13	0.004		4.75		3.93	0.299	
19-23		3.83		3.43	0.915		5.13*		4.75	0.323	
26-30		3.50		3.10*	0.716		4.55		5.54*	0.015	
<i>p</i> <sup>*</sup>		0.450		0.027			0.016		<0.001		
<b>Decay (ms)</b>											
6-9		7.67		8.26			7.84		21.24	0.073	
12-16		13.61		41.97*	0.024		20.21		28.64	0.369	
19-23		19.86		21.30	0.712		38.82*		34.85	0.302	
26-30		19.43		13.96*	0.306		23.99		29.78	0.273	
<i>p</i> <sup>*</sup>		0.425		0.002			0.010		0.869		
<b>Charge Transfer (pAms)</b>											
6-9		109.74		119.69	0.731		149.09		222.43	0.088	
12-16		218.74		585.54*	0.010		325.32		475.67	0.330	
19-23		294.97		405.62	0.086		892.94*		680.43*	0.629	
26-30		218.24		289.70	0.245		640.78		867.99	0.039	
<i>p</i> <sup>*</sup>		0.225		0.001			0.001		<0.001		
<b>IPSCs</b>											
<b>Amplitude (pA)</b>											
6-9	6	33.77	7	28.68	1.000	12	24.64	17	30.31	0.492	
12-16	24	40.34	20	56.77	0.024	39	50.06	35	53.08	0.083	
19-23	30	59.69	26	77.29*	0.015	30	50.43*	31	89.11*	0.006	

26-30	29	49.92	25	69.48	0.331	32	70.16	33	94.39	0.015
$p^*$		0.005		0.003			<0.001		<0.001	
<b>Rise Time (ms)</b>										
6-9		3.13		4.10	0.051		6.15		5.09	0.127
12-16		5.14		5.47	0.234		5.47		5.58	0.417
19-23		4.96		4.60	0.749		6.40		6.40	0.790
26-30		4.87		4.49	0.381		5.59		6.82	0.051
$p^*$		0.054		0.005			0.226		0.039	
<b>Decay (ms)</b>										
6-9		81.73		63.02	0.731		114.58		112.58	0.438
12-16		98.92		91.26	0.823		104.12		88.47	0.049
19-23		72.00*		65.28*	0.026		89.88		72.68*	0.197
26-30		71.18		44.15	<0.001		67.44		57.39*	0.055
$p^*$		<0.001		<0.001			<0.001		<0.001	
<b>Charge Transfer (pAms)</b>										
6-9		1230.41		1297.07	1.000		1117.23		1356.92	0.674
12-16		1474.04		2192.20	0.263		2002.62		1934.03	0.974
19-23		1731.17		1748.05	0.379		1997.69		2403.91*	0.102
26-30		1503.81		1240.23	0.160		2042.30		2432.01	0.315
$p^*$		0.620		0.034			0.118		<0.001	
<b>I/(E+I)</b>										
<b>E/I Charge Transfer</b>										
6-9	6	0.88	7	0.86	0.534	12	0.85	17	0.79	0.163
12-16	24	0.84	20	0.79	0.018	39	0.82	35	0.81	0.289
19-23	30	0.81	26	0.80	0.186	30	0.73*	31	0.78	0.375
26-30	29	0.88	25	0.81	0.071	32	0.80	33	0.73	0.010
$p^*$		0.389		0.223			0.012		0.118	

*DIV, days in vitro; n, number of neurons examined at each age and network set;  $p^*$  = p-values from ANOVA or Kruskal-Wallis-ANOVA (KW-ANOVA), comparing different ages.  $p^\&$  = p-values from Mann Whitney rank sum test (MW-RST) comparing the data from networks T05 and T45. The results of the multiple comparison tests for age differences (Holm-Sidak or Dunn's Tests,  $p < 0.05$ ) are indicated with an asterisk after the median, if this parameter at that age was significantly different from the one of the anterior age set (or more than one set, when these were not significantly different).*

## 6 Reference List

- Adelsberger, H., O. Garaschuk and A. Konnerth (2005). "Cortical calcium waves in resting newborn mice." Nat Neurosci **8**(8): 988-990.
- Akerman, C. J. and H. T. Cline (2006). "Depolarizing GABAergic conductances regulate the balance of excitation to inhibition in the developing retinotectal circuit in vivo." Journal of Neuroscience **26**(19): 5117-5130.
- Alcántara, S., E. Soriano and I. Ferrer (1996). "Thalamic and basal forebrain afferents modulate the development of parvalbumin and calbindin D28k immunoreactivity in the barrel cortex of the rat." European Journal of Neuroscience **8**(7): 1522-1534.
- Alvarez-Dolado, M., M. E. Calcagnotto, K. M. Karkar, D. G. Southwell, D. M. Jones-Davis, R. C. Estrada, J. L. Rubenstein, A. Alvarez-Buylla and S. C. Baraban (2006). "Cortical inhibition modified by embryonic neural precursors grafted into the postnatal brain." Journal of Neuroscience **26**(28): 7380-7389.
- Andang, M., J. Hjerling-Leffler, A. Moliner, T. K. Lundgren, G. Castelo-Branco, E. Nanou, E. Pozas, V. Bryja, S. Halliez, H. Nishimaru, J. Wilbertz, E. Arenas, M. Koltzenburg, P. Charnay, A. El Manira, C. F. Ibanez and P. Ernfors (2008). "Histone H2AX-dependent GABA(A) receptor regulation of stem cell proliferation." Nature **451**(7177): 460-464.
- Anderson, S., D. Eisenstat, L. Shi and J. Rubenstein (1997). "Interneuron migration from basal forebrain to neocortex: dependence on Dlx genes." Science **278**(5337): 474-476.
- Anderson, S. A., C. E. Kaznowski, C. Horn, J. L. Rubenstein and S. K. McConnell (2002). "Distinct origins of neocortical projection neurons and interneurons in vivo." Cereb Cortex **12**(7): 702-709.
- Angevine, J. and R. L. Sidman (1961). "Autoradiographic study of cell migration during histogenesis of cerebral cortex in the mouse." Nature **192**(4804): 766-768.
- Antonopoulos, J., I. S. Pappas and J. G. Parnavelas (1997). "Activation of the GABAA receptor inhibits the proliferative effects of bFGF in cortical progenitor cells." Eur J Neurosci **9**(2): 291-298.
- Avramescu, S., D. A. Nita and I. Timofeev (2009). "Neocortical post-traumatic epileptogenesis is associated with loss of GABAergic neurons." Journal of neurotrauma **26**(5): 799-812.
- Azim, E., D. Jabaudon, R. M. Fame and J. D. Macklis (2009). "SOX6 controls dorsal progenitor identity and interneuron diversity during neocortical development." Nature neuroscience **12**(10): 1238-1247.

- Baker, R. E., M. A. Corner and J. van Pelt (2006). "Spontaneous neuronal discharge patterns in developing organotypic mega-co-cultures of neonatal rat cerebral cortex." Brain Res **1101**(1): 29-35.
- Baltz, T., A. D. de Lima and T. Voigt (2010). "Contribution of GABAergic interneurons to the development of spontaneous activity patterns in cultured neocortical networks." Front Cell Neurosci **4**: 15.
- Baltz, T., A. Herzog and T. Voigt (2011). "Slow oscillating population activity in developing cortical networks: models and experimental results." J Neurophysiol **106**(3): 1500-1514.
- Baltz, T. and T. Voigt (2015). "Interaction of electrically evoked activity with intrinsic dynamics of cultured cortical networks with and without functional fast GABAergic synaptic transmission." Frontiers in cellular neuroscience **9**: 272.
- Banker, G. and K. Goslin (1998). Culturing nerve cells, MIT press.
- Batista-Brito, R. and G. Fishell (2009). "The developmental integration of cortical interneurons into a functional network." Current topics in developmental biology **87**: 81-118.
- Bayer, S. A. and J. Altman (1991). Neocortical development, Raven Press New York.
- Beaulieu, C. (1993). "Numerical data on neocortical neurons in adult rat, with special reference to the GABA population." Brain Res **609**(1-2): 284-292.
- Bekkers, J. M. and C. F. Stevens (1989). "NMDA and non-NMDA receptors are co-localized at individual excitatory synapses in cultured rat hippocampus." Nature **341**(6239): 230-233.
- Bellion, A. and C. Metin (2005). "Early regionalisation of the neocortex and the medial ganglionic eminence." Brain Res Bull **66**(4-6): 402-409.
- Bellion, A., M. Wassef and C. Métin (2003). "Early differences in axonal outgrowth, cell migration and GABAergic differentiation properties between the dorsal and lateral cortex." Cerebral Cortex **13**(2): 203-214.
- Ben-Ari, Y. (2001). "Developing networks play a similar melody." Trends Neurosci **24**(6): 353-360.
- Ben-Ari, Y. (2002). "Excitatory actions of gaba during development: the nature of the nurture." Nat Rev Neurosci **3**(9): 728-739.
- Ben-Ari, Y., E. Cherubini, R. Corradetti and J. L. Gaiarsa (1989). "Giant synaptic potentials in immature rat CA3 hippocampal neurones." J Physiol **416**: 303-325.
- Ben-Ari, Y., R. Khazipov, X. Leinekugel, O. Caillard and J.-L. Gaiarsa (1997). "GABAA, NMDA and AMPA receptors: a developmentally regulated menage a trois." Trends in

- neurosciences **20**(11): 523-529.
- Ben-Ari, Y., E. Cherubini, R. Corradetti and J. Gaiarsa (1989). "Giant synaptic potentials in immature rat CA3 hippocampal neurones." The Journal of physiology **416**(1): 303-325.
- Berg, R. W., A. Alaburda and J. Hounsgaard (2007). "Balanced inhibition and excitation drive spike activity in spinal half-centers." Science **315**(5810): 390-393.
- Berry, M. and A. Rogers (1965). "The migration of neuroblasts in the developing cerebral cortex." Journal of anatomy **99**(Pt 4): 691.
- Bjorklund, A. and O. Lindvall (2000). "Cell replacement therapies for central nervous system disorders." Nat Neurosci **3**(6): 537-544.
- Blankenship, A. G. and M. B. Feller (2010). "Mechanisms underlying spontaneous patterned activity in developing neural circuits." Nat Rev Neurosci **11**(1): 18-29.
- Bordey, A. (2007). "Enigmatic GABAergic networks in adult neurogenic zones." Brain Res Rev **53**(1): 124-134.
- Bortone, D. and F. Polleux (2009). "KCC2 expression promotes the termination of cortical interneuron migration in a voltage-sensitive calcium-dependent manner." Neuron **62**(1): 53-71.
- Bortone, D. S., S. R. Olsen and M. Scanziani (2014). "Translaminar inhibitory cells recruited by layer 6 corticothalamic neurons suppress visual cortex." Neuron **82**(2): 474-485.
- Buchanan, K. A., A. V. Blackman, A. W. Moreau, D. Elgar, R. P. Costa, T. Lalanne, A. A. Tudor Jones, J. Oyrer and P. J. Sjöström (2012). "Target-specific expression of presynaptic NMDA receptors in neocortical microcircuits." Neuron **75**(3): 451-466.
- Butt, S. J., M. Fuccillo, S. Nery, S. Noctor, A. Kriegstein, J. G. Corbin and G. Fishell (2005). "The temporal and spatial origins of cortical interneurons predict their physiological subtype." Neuron **48**(4): 591-604.
- Cavanagh, M. E. and J. G. Parnavelas (1989). "Development of vasoactive-intestinal-polypeptide-immunoreactive neurons in the rat occipital cortex: a combined immunohistochemical-autoradiographic study." J Comp Neurol **284**(4): 637-645.
- Caviness Jr, V. S. (1982). "Neocortical histogenesis in normal and reeler mice: a developmental study based upon [3H] thymidine autoradiography." Developmental Brain Research **4**(3): 293-302.
- Choi, D. W. (1992). "Excitotoxic cell death." Journal of neurobiology **23**(9): 1261-1276.
- Chu, J. and S. A. Anderson (2015). "Development of cortical interneurons."

- Neuropsychopharmacology **40**(1): 16-23.
- Chudotvorova, I., A. Ivanov, S. Rama, C. A. Hubner, C. Pellegrino, Y. Ben-Ari and I. Medina (2005). "Early expression of KCC2 in rat hippocampal cultures augments expression of functional GABA synapses." J Physiol **566**(Pt 3): 671-679.
- Cline, H. (2005). "Synaptogenesis: a balancing act between excitation and inhibition." Current Biology **15**(6): R203-R205.
- Close, J., H. Xu, N. D. M. García, R. Batista-Brito, E. Rossignol, B. Rudy and G. Fishell (2012). "Satb1 is an activity-modulated transcription factor required for the terminal differentiation and connectivity of medial ganglionic eminence-derived cortical interneurons." Journal of Neuroscience **32**(49): 17690-17705.
- Cobos, I., M. E. Calcagnotto, A. J. Vilaythong, M. T. Thwin, J. L. Noebels, S. C. Baraban and J. L. Rubenstein (2005). "Mice lacking Dlx1 show subtype-specific loss of interneurons, reduced inhibition and epilepsy." Nat Neurosci **8**(8): 1059-1068.
- Cobos, I., J. E. Long, M. T. Thwin and J. L. Rubenstein (2006). "Cellular patterns of transcription factor expression in developing cortical interneurons." Cereb Cortex **16 Suppl 1**: i82-88.
- Cohen, E., M. Ivenshitz, V. Amor-Baroukh, V. Greenberger and M. Segal (2008). "Determinants of spontaneous activity in networks of cultured hippocampus." Brain research **1235**: 21-30.
- Cossart, R. (2011). "The maturation of cortical interneuron diversity: how multiple developmental journeys shape the emergence of proper network function." Current opinion in neurobiology **21**(1): 160-168.
- Cossart, R., C. Bernard and Y. Ben-Ari (2005). "Multiple facets of GABAergic neurons and synapses: multiple fates of GABA signalling in epilepsies." Trends Neurosci **28**(2): 108-115.
- Crépel, V., D. Aronov, I. Jorquera, A. Represa, Y. Ben-Ari and R. Cossart (2007). "A parturition-associated nonsynaptic coherent activity pattern in the developing hippocampus." Neuron **54**(1): 105-120.
- Datta, S. R., H. Dudek, X. Tao, S. Masters, H. Fu, Y. Gotoh and M. E. Greenberg (1997). "Akt phosphorylation of BAD couples survival signals to the cell-intrinsic death machinery." Cell **91**(2): 231-241.
- de Lima, A. D., T. Opitz and T. Voigt (2004). "Irreversible loss of a subpopulation of cortical

- interneurons in the absence of glutamatergic network activity." Eur J Neurosci **19**(11): 2931-2943.
- de Lima, A. D. and T. Voigt (1997). "Identification of two distinct populations of gamma-aminobutyric acidergic neurons in cultures of the rat cerebral cortex." J Comp Neurol **388**(4): 526-540.
- de Lima, A. D. and T. Voigt (1999). "Astroglia inhibit the proliferation of neocortical cells and prevent the generation of small GABAergic neurons in vitro." Eur J Neurosci **11**(11): 3845-3856.
- Deidda, G., I. F. Bozarth and L. Cancedda (2014). "Modulation of GABAergic transmission in development and neurodevelopmental disorders: investigating physiology and pathology to gain therapeutic perspectives." Front Cell Neurosci **8**: 119.
- Del Rio, J. A., E. Soriano and I. Ferrer (1992). "Development of GABA-immunoreactivity in the neocortex of the mouse." Journal of Comparative Neurology **326**(4): 501-526.
- Demarque, M., A. Represa, H. Becq, I. Khalilov, Y. Ben-Ari and L. Aniksztejn (2002). "Paracrine intercellular communication by a Ca<sup>2+</sup>- and SNARE-independent release of GABA and glutamate prior to synapse formation." Neuron **36**(6): 1051-1061.
- Denaxa, M., M. Kalaitzidou, A. Garefalaki, A. Achimastou, R. Lasrado, T. Maes and V. Pachnis (2012). "Maturation-promoting activity of SATB1 in MGE-derived cortical interneurons." Cell Rep **2**(5): 1351-1362.
- Dorn, A. L., K. Yuan, A. J. Barker, C. E. Schreiner and R. C. Froemke (2010). "Developmental sensory experience balances cortical excitation and inhibition." Nature **465**(7300): 932-936.
- Dudek, H., S. R. Datta, T. F. Franke, M. J. Birnbaum, R. Yao, G. M. Cooper, R. A. Segal, D. R. Kaplan and M. E. Greenberg (1997). "Regulation of neuronal survival by the serine-threonine protein kinase Akt." Science **275**(5300): 661-665.
- Dunning, D. D., C. L. Hoover, I. Soltesz, M. A. Smith and D. K. O'Dowd (1999). "GABA(A) receptor-mediated miniature postsynaptic currents and alpha-subunit expression in developing cortical neurons." J Neurophysiol **82**(6): 3286-3297.
- Dzhala, V. I., D. M. Talos, D. A. Sdrulla, A. C. Brumback, G. C. Mathews, T. A. Benke, E. Delpire, F. E. Jensen and K. J. Staley (2005). "NKCC1 transporter facilitates seizures in the developing brain." Nat Med **11**(11): 1205-1213.
- Emsley, J. G., B. D. Mitchell, S. S. Magavi, P. Arlotta and J. D. Macklis (2004). "The repair of complex neuronal circuitry by transplanted and endogenous precursors." NeuroRx **1**(4):

452-471.

- Fairén, A., A. Cobas and M. Fonseca (1986). "Times of generation of glutamic acid decarboxylase immunoreactive neurons in mouse somatosensory cortex." Journal of Comparative Neurology **251**(1): 67-83.
- Feller, M. B. (1999). "Spontaneous correlated activity in developing neural circuits." Neuron **22**(4): 653-656.
- Fishell, G. and B. Rudy (2011). "Mechanisms of inhibition within the telencephalon: "where the wild things are"." Annual review of neuroscience **34**: 535.
- Fiumelli, H. and M. A. Woodin (2007). "Role of activity-dependent regulation of neuronal chloride homeostasis in development." Curr Opin Neurobiol **17**(1): 81-86.
- Fogarty, M., W. D. Richardson and N. Kessaris (2005). "A subset of oligodendrocytes generated from radial glia in the dorsal spinal cord."
- Friocourt, G. and J. G. Parnavelas (2010). "Mutations in ARX result in several defects involving GABAergic neurons." Frontiers in cellular neuroscience: 4.
- Froemke, R. C. (2015). "Plasticity of cortical excitatory-inhibitory balance." Annu Rev Neurosci **38**: 195-219.
- Fukui, M., N. Nakamichi, M. Yoneyama, S. Ozawa, S. Fujimori, Y. Takahata, N. Nakamura, H. Taniura and Y. Yoneda (2008). "Modulation of cellular proliferation and differentiation through GABAB receptors expressed by undifferentiated neural progenitor cells isolated from fetal mouse brain." Journal of cellular physiology **216**(2): 507-519.
- Fukui, M., N. Nakamichi, M. Yoneyama, K. Yoshida, S. Ozawa, T. Kitayama, N. Nakamura, H. Taniura and Y. Yoneda (2008). "Up-regulation of ciliary neurotrophic factor receptor expression by GABAA receptors in undifferentiated neural progenitors of fetal mouse brain." Journal of neuroscience research **86**(12): 2615-2623.
- Gabbott, P. L. and S. J. Bacon (1996). "Local circuit neurons in the medial prefrontal cortex (areas 24a,b,c, 25 and 32) in the monkey: I. Cell morphology and morphometrics." J Comp Neurol **364**(4): 567-608.
- Gabbott, P. L., B. G. Dickie, R. R. Vaid, A. J. Headlam and S. J. Bacon (1997). "Local-circuit neurones in the medial prefrontal cortex (areas 25, 32 and 24b) in the rat: morphology and quantitative distribution." J Comp Neurol **377**(4): 465-499.
- Ge, S., E. L. Goh, K. A. Sailor, Y. Kitabatake, G.-l. Ming and H. Song (2006). "GABA regulates synaptic integration of newly generated neurons in the adult brain." Nature **439**(7076): 589-

593.

- Gelman, D. M. and O. Marin (2010). "Generation of interneuron diversity in the mouse cerebral cortex." Eur J Neurosci **31**(12): 2136-2141.
- Gelman, D. M., F. J. Martini, S. Nobrega-Pereira, A. Pierani, N. Kessaris and O. Marin (2009). "The embryonic preoptic area is a novel source of cortical GABAergic interneurons." J Neurosci **29**(29): 9380-9389.
- Gelman, D. M., F. J. Martini, S. Nóbrega-Pereira, A. Pierani, N. Kessaris and O. Marín (2009). "The embryonic preoptic area is a novel source of cortical GABAergic interneurons." Journal of Neuroscience **29**(29): 9380-9389.
- Gill, D. A., S. L. Ramsay and R. A. Tasker (2010). "Selective reductions in subpopulations of GABAergic neurons in a developmental rat model of epilepsy." Brain Res **1331**: 114-123.
- Gogolla, N., J. J. Leblanc, K. B. Quast, T. C. Sudhof, M. Fagiolini and T. K. Hensch (2009). "Common circuit defect of excitatory-inhibitory balance in mouse models of autism." J Neurodev Disord **1**(2): 172-181.
- Gonchar, Y. and A. Burkhalter (1997). "Three distinct families of GABAergic neurons in rat visual cortex." Cereb Cortex **7**(4): 347-358.
- Gulledge, A. T. and G. J. Stuart (2003). "Excitatory actions of GABA in the cortex." Neuron **37**(2): 299-309.
- Halabisky, B., F. Shen, J. R. Huguenard and D. A. Prince (2006). "Electrophysiological classification of somatostatin-positive interneurons in mouse sensorimotor cortex." J Neurophysiol **96**(2): 834-845.
- Hammad, M., S. L. Schmidt, X. Zhang, R. Bray, F. Frohlich and H. T. Ghashghaei (2015). "Transplantation of GABAergic interneurons into the neonatal primary visual cortex reduces absence seizures in stargazer mice." Cerebral Cortex **25**(9): 2970-2979.
- Hanson, M. G. and L. T. Landmesser (2003). "Characterization of the circuits that generate spontaneous episodes of activity in the early embryonic mouse spinal cord." Journal of Neuroscience **23**(2): 587-600.
- Hanson, M. G. and L. T. Landmesser (2004). "Normal patterns of spontaneous activity are required for correct motor axon guidance and the expression of specific guidance molecules." Neuron **43**(5): 687-701.
- Haroush, N. and S. Marom (2019). "Inhibition increases response variability and reduces stimulus discrimination in random networks of cortical neurons." Sci Rep **9**(1): 4969.

- Haydar, T. F., F. Wang, M. L. Schwartz and P. Rakic (2000). "Differential modulation of proliferation in the neocortical ventricular and subventricular zones." J Neurosci **20**(15): 5764-5774.
- He, M., J. Tucciarone, S. Lee, M. J. Nigro, Y. Kim, J. M. Levine, S. M. Kelly, I. Krugikov, P. Wu, Y. Chen, L. Gong, Y. Hou, P. Osten, B. Rudy and Z. J. Huang (2016). "Strategies and Tools for Combinatorial Targeting of GABAergic Neurons in Mouse Cerebral Cortex." Neuron **92**(2): 555.
- Hendry, S. H., H. D. Schwark, E. G. Jones and J. Yan (1987). "Numbers and proportions of GABA-immunoreactive neurons in different areas of monkey cerebral cortex." J Neurosci **7**(5): 1503-1519.
- Herb, A., N. Burnashev, P. Werner, B. Sakmann, W. Wisden and P. H. Seeburg (1992). "The KA-2 subunit of excitatory amino acid receptors shows widespread expression in brain and forms ion channels with distantly related subunits." Neuron **8**(4): 775-785.
- Hilscher, M. M., R. N. Leao, S. J. Edwards, K. E. Leao and K. Kullander (2017). "Chrna2-Martinotti Cells Synchronize Layer 5 Type A Pyramidal Cells via Rebound Excitation." PLoS Biol **15**(2): e2001392.
- Hollrigel, G. S. and I. Soltesz (1997). "Slow kinetics of miniature IPSCs during early postnatal development in granule cells of the dentate gyrus." J Neurosci **17**(13): 5119-5128.
- Howard, M. A. and S. C. Baraban (2016). "Synaptic integration of transplanted interneuron progenitor cells into native cortical networks." Journal of Neurophysiology **116**(2): 472-478.
- Hu, H., J. Gan and P. Jonas (2014). "Interneurons. Fast-spiking, parvalbumin(+) GABAergic interneurons: from cellular design to microcircuit function." Science **345**(6196): 1255-1263.
- Huang, Z. J. (2009). "Activity-dependent development of inhibitory synapses and innervation pattern: role of GABA signalling and beyond." J Physiol **587**(Pt 9): 1881-1888.
- Hunt, R. F., K. M. Girsakis, J. L. Rubenstein, A. Alvarez-Buylla and S. C. Baraban (2013). "GABA progenitors grafted into the adult epileptic brain control seizures and abnormal behavior." Nature neuroscience **16**(6): 692-697.
- Itami, C., F. Kimura and S. Nakamura (2007). "Brain-derived neurotrophic factor regulates the maturation of layer 4 fast-spiking cells after the second postnatal week in the developing barrel cortex." Journal of Neuroscience **27**(9): 2241-2252.
- Jin, X., J. R. Huguenard and D. A. Prince (2011). "Reorganization of inhibitory synaptic circuits

- in rodent chronically injured epileptogenic neocortex." Cerebral cortex **21**(5): 1094-1104.
- Jones, E. G. (1975). "Varieties and distribution of non-pyramidal cells in the somatic sensory cortex of the squirrel monkey." J Comp Neurol **160**(2): 205-267.
- Kahle, K. T., K. J. Staley, B. V. Nahed, G. Gamba, S. C. Hebert, R. P. Lifton and D. B. Mount (2008). "Roles of the cation-chloride cotransporters in neurological disease." Nat Clin Pract Neurol **4**(9): 490-503.
- Kanold, P. O. and H. J. Luhmann (2010). "The subplate and early cortical circuits." Annu Rev Neurosci **33**: 23-48.
- Katz, L. C. and C. J. Shatz (1996). "Synaptic activity and the construction of cortical circuits." Science **274**(5290): 1133-1138.
- Katz, L. C. and C. J. Shatz (1996). "Synaptic activity and the construction of cortical circuits." Science **274**(5290): 1133-1138.
- Kawaguchi, Y. and S. Kondo (2002). "Parvalbumin, somatostatin and cholecystokinin as chemical markers for specific GABAergic interneuron types in the rat frontal cortex." Journal of neurocytology **31**(3): 277-287.
- Kawaguchi, Y. and Y. Kubota (1997). "GABAergic cell subtypes and their synaptic connections in rat frontal cortex." Cerebral cortex (New York, NY: 1991) **7**(6): 476-486.
- Kilb, W., S. Kirischuk and H. J. Luhmann (2011). "Electrical activity patterns and the functional maturation of the neocortex." Eur J Neurosci **34**(10): 1677-1686.
- Kilman, V., M. C. Van Rossum and G. G. Turrigiano (2002). "Activity deprivation reduces miniature IPSC amplitude by decreasing the number of postsynaptic GABAA receptors clustered at neocortical synapses." Journal of Neuroscience **22**(4): 1328-1337.
- Klausberger, T. and P. Somogyi (2008). "Neuronal diversity and temporal dynamics: the unity of hippocampal circuit operations." Science **321**(5885): 53-57.
- Klueva, J., S. Meis, A. D. de Lima, T. Voigt and T. Munsch (2008). "Developmental downregulation of GABAergic drive parallels formation of functional synapses in cultured mouse neocortical networks." Developmental Neurobiology **68**(7): 934-949.
- Kubota, Y., R. Hattori and Y. Yui (1994). "Three distinct subpopulations of GABAergic neurons in rat frontal agranular cortex." Brain Res **649**(1-2): 159-173.
- Laurie, D., W. Wisden and P. Seeburg (1992). "The distribution of thirteen GABAA receptor subunit mRNAs in the rat brain. III. Embryonic and postnatal development." Journal of Neuroscience **12**(11): 4151-4172.

- Leinekugel, X., I. Medina, I. Khalilov, Y. Ben-Ari and R. Khazipov (1997). "Ca<sup>2+</sup> oscillations mediated by the synergistic excitatory actions of GABA(A) and NMDA receptors in the neonatal hippocampus." Neuron **18**(2): 243-255.
- Lim, L., D. Mi, A. Llorca and O. Marin (2018). "Development and Functional Diversification of Cortical Interneurons." Neuron **100**(2): 294-313.
- Liodis, P., M. Denaxa, M. Grigoriou, C. Akufo-Addo, Y. Yanagawa and V. Pachnis (2007). "Lhx6 activity is required for the normal migration and specification of cortical interneuron subtypes." J Neurosci **27**(12): 3078-3089.
- Liu, G. (2004). "Local structural balance and functional interaction of excitatory and inhibitory synapses in hippocampal dendrites." Nat Neurosci **7**(4): 373-379.
- Liu, X., Q. Wang, T. F. Haydar and A. Bordey (2005). "Nonsynaptic GABA signaling in postnatal subventricular zone controls proliferation of GFAP-expressing progenitors." Nat Neurosci **8**(9): 1179-1187.
- Lodato, S., C. Rouaux, K. B. Quast, C. Jantrachotechatchawan, M. Studer, T. K. Hensch and P. Arlotta (2011). "Excitatory projection neuron subtypes control the distribution of local inhibitory interneurons in the cerebral cortex." Neuron **69**(4): 763-779.
- Lopez-Bendito, G., K. Sturgess, F. Erdelyi, G. Szabo, Z. Molnar and O. Paulsen (2004). "Preferential origin and layer destination of GAD65-GFP cortical interneurons." Cereb Cortex **14**(10): 1122-1133.
- LoTurco, J. J., D. F. Owens, M. J. Heath, M. B. Davis and A. R. Kriegstein (1995). "GABA and glutamate depolarize cortical progenitor cells and inhibit DNA synthesis." Neuron **15**(6): 1287-1298.
- Luhmann, H. J., A. Fukuda and W. Kilb (2015). "Control of cortical neuronal migration by glutamate and GABA." Front Cell Neurosci **9**: 4.
- Luhmann, H. J., S. Kirischuk and W. Kilb (2018). "The Superior Function of the Subplate in Early Neocortical Development." Front Neuroanat **12**: 97.
- Lujan, R., R. Shigemoto and G. Lopez-Bendito (2005). "Glutamate and GABA receptor signalling in the developing brain." Neuroscience **130**(3): 567-580.
- Ma, Y., H. Hu, A. S. Berrebi, P. H. Mathers and A. Agmon (2006). "Distinct subtypes of somatostatin-containing neocortical interneurons revealed in transgenic mice." J Neurosci **26**(19): 5069-5082.
- Mao, B. Q., F. Hamzei-Sichani, D. Aronov, R. C. Froemke and R. Yuste (2001). "Dynamics of

- spontaneous activity in neocortical slices." Neuron **32**(5): 883-898.
- Marin-Padilla, M. (1990). "The pyramidal cell and its local-circuit interneurons: a hypothetical unit of the Mammalian cerebral cortex." J Cogn Neurosci **2**(3): 180-194.
- Marin, O. (2013). "Cellular and molecular mechanisms controlling the migration of neocortical interneurons." Eur J Neurosci **38**(1): 2019-2029.
- Martina, M., S. Royer and D. Pare (2001). "Cell-type-specific GABA responses and chloride homeostasis in the cortex and amygdala." J Neurophysiol **86**(6): 2887-2895.
- Martini, F. J., T. Guillamon-Vivancos, V. Moreno-Juan, M. Valdeolmillos and G. Lopez-Bendito (2021). "Spontaneous activity in developing thalamic and cortical sensory networks." Neuron **109**(16): 2519-2534.
- Martini, F. J., T. Guillamón-Vivancos, V. Moreno-Juan, M. Valdeolmillos and G. López-Bendito (2021). "Spontaneous activity in developing thalamic and cortical sensory networks." Neuron **109**(16): 2519-2534.
- Mennerick, S. and C. F. Zorumski (2000). "Neural activity and survival in the developing nervous system." Mol Neurobiol **22**(1-3): 41-54.
- Meyer, H. S., D. Schwarz, V. C. Wimmer, A. C. Schmitt, J. N. Kerr, B. Sakmann and M. Helmstaedter (2011). "Inhibitory interneurons in a cortical column form hot zones of inhibition in layers 2 and 5A." Proc Natl Acad Sci U S A **108**(40): 16807-16812.
- Milner, L. D. and L. T. Landmesser (1999). "Cholinergic and GABAergic inputs drive patterned spontaneous motoneuron activity before target contact." Journal of Neuroscience **19**(8): 3007-3022.
- Miyoshi, G., S. J. Butt, H. Takebayashi and G. Fishell (2007). "Physiologically distinct temporal cohorts of cortical interneurons arise from telencephalic Olig2-expressing precursors." Journal of Neuroscience **27**(29): 7786-7798.
- Miyoshi, G. and G. Fishell (2011). "GABAergic interneuron lineages selectively sort into specific cortical layers during early postnatal development." Cerebral Cortex **21**(4): 845-852.
- Miyoshi, G., J. Hjerling-Leffler, T. Karayannis, V. H. Sousa, S. J. Butt, J. Battiste, J. E. Johnson, R. P. Machold and G. Fishell (2010). "Genetic fate mapping reveals that the caudal ganglionic eminence produces a large and diverse population of superficial cortical interneurons." Journal of Neuroscience **30**(5): 1582-1594.
- Mohler, H. (2006). "GABAA receptors in central nervous system disease: anxiety, epilepsy, and

- insomnia." J Recept Signal Transduct Res **26**(5-6): 731-740.
- Mueller, A. L., J. S. Taube and P. A. Schwartzkroin (1984). "Development of hyperpolarizing inhibitory postsynaptic potentials and hyperpolarizing response to gamma-aminobutyric acid in rabbit hippocampus studied in vitro." Journal of Neuroscience **4**(3): 860-867.
- Muramoto, K., M. Ichikawa, M. Kawahara, K. Kobayashi and Y. Kuroda (1993). "Frequency of synchronous oscillations of neuronal activity increases during development and is correlated to the number of synapses in cultured cortical neuron networks." Neuroscience letters **163**(2): 163-165.
- Nadarajah, B., P. Alifragis, R. O. Wong and J. G. Parnavelas (2002). "Ventricle-directed migration in the developing cerebral cortex." Nat Neurosci **5**(3): 218-224.
- Nery, S., G. Fishell and J. G. Corbin (2002). "The caudal ganglionic eminence is a source of distinct cortical and subcortical cell populations." Nat Neurosci **5**(12): 1279-1287.
- Nery, S., G. Fishell and J. G. Corbin (2002). "The caudal ganglionic eminence is a source of distinct cortical and subcortical cell populations." Nature neuroscience **5**(12): 1279-1287.
- O'Donovan, M. J. (1999). "The origin of spontaneous activity in developing networks of the vertebrate nervous system." Curr Opin Neurobiol **9**(1): 94-104.
- Obata, K., M. Oide and H. Tanaka (1978). "Excitatory and inhibitory actions of GABA and glycine on embryonic chick spinal neurons in culture." Brain Res **144**(1): 179-184.
- Oenarto, J., B. Görg, M. Moos, H.-J. Bidmon and D. Häussinger (2014). "Expression of organic osmolyte transporters in cultured rat astrocytes and rat and human cerebral cortex." Archives of biochemistry and biophysics **560**: 59-72.
- Opitz, T., A. D. De Lima and T. Voigt (2002). "Spontaneous development of synchronous oscillatory activity during maturation of cortical networks in vitro." Journal of neurophysiology **88**(5): 2196-2206.
- Owens, D. F., X. Liu and A. R. Kriegstein (1999). "Changing properties of GABA(A) receptor-mediated signaling during early neocortical development." J Neurophysiol **82**(2): 570-583.
- Parnavelas, J. G. (2002). "The origin of cortical neurons." Braz J Med Biol Res **35**(12): 1423-1429.
- Patz, S., J. Grabert, T. Gorba, M. J. Wirth and P. Wahle (2004). "Parvalbumin expression in visual cortical interneurons depends on neuronal activity and TrkB ligands during an Early period of postnatal development." Cerebral cortex **14**(3): 342-351.
- Petilla Interneuron Nomenclature, G., G. A. Ascoli, L. Alonso-Nanclares, S. A. Anderson, G.

- Barrionuevo, R. Benavides-Piccione, A. Burkhalter, G. Buzsaki, B. Cauli, J. Defelipe, A. Fairen, D. Feldmeyer, G. Fishell, Y. Fregnac, T. F. Freund, D. Gardner, E. P. Gardner, J. H. Goldberg, M. Helmstaedter, S. Hestrin, F. Karube, Z. F. Kisvarday, B. Lambolez, D. A. Lewis, O. Marin, H. Markram, A. Munoz, A. Packer, C. C. Petersen, K. S. Rockland, J. Rossier, B. Rudy, P. Somogyi, J. F. Staiger, G. Tamas, A. M. Thomson, M. Toledo-Rodriguez, Y. Wang, D. C. West and R. Yuste (2008). "Petilla terminology: nomenclature of features of GABAergic interneurons of the cerebral cortex." Nat Rev Neurosci **9**(7): 557-568.
- Polleux, F., K. L. Whitford, P. A. Dijkhuizen, T. Vitalis and A. Ghosh (2002). "Control of cortical interneuron migration by neurotrophins and PI3-kinase signaling." Development **129**(13): 3147-3160.
- Powell, E. M., D. B. Campbell, G. D. Stanwood, C. Davis, J. L. Noebels and P. Levitt (2003). "Genetic disruption of cortical interneuron development causes region- and GABA cell type-specific deficits, epilepsy, and behavioral dysfunction." J Neurosci **23**(2): 622-631.
- Priya, R., M. F. Paredes, T. Karayannis, N. Yusuf, X. Liu, X. Jaglin, I. Graef, A. Alvarez-Buylla and G. Fishell (2018). "Activity regulates cell death within cortical interneurons through a calcineurin-dependent mechanism." Cell reports **22**(7): 1695-1709.
- Rakic, P. (1974). "Neurons in rhesus monkey visual cortex: systematic relation between time of origin and eventual disposition." Science **183**(4123): 425-427.
- Redmond, L., A. H. Kashani and A. Ghosh (2002). "Calcium regulation of dendritic growth via CaM kinase IV and CREB-mediated transcription." Neuron **34**(6): 999-1010.
- Redolfi, N. and C. Lodovichi (2021). "Spontaneous Afferent Activity Carves Olfactory Circuits." Front Cell Neurosci **15**: 637536.
- Riedemann, T. (2019). "Diversity and Function of Somatostatin-Expressing Interneurons in the Cerebral Cortex." Int J Mol Sci **20**(12).
- Russell, J. M. (2000). "Sodium-potassium-chloride cotransport." Physiological reviews.
- Rymar, V. V. and A. F. Sadikot (2007). "Laminar fate of cortical GABAergic interneurons is dependent on both birthdate and phenotype." Journal of Comparative Neurology **501**(3): 369-380.
- Seeburg, D. P. and M. Sheng (2008). "Activity-induced Polo-like kinase 2 is required for homeostatic plasticity of hippocampal neurons during epileptiform activity." Journal of Neuroscience **28**(26): 6583-6591.

- Sin, W. C., K. Haas, E. S. Ruthazer and H. T. Cline (2002). "Dendrite growth increased by visual activity requires NMDA receptor and Rho GTPases." Nature **419**(6906): 475-480.
- Sivilotti, L. and A. Nistri (1991). "GABA receptor mechanisms in the central nervous system." Prog Neurobiol **36**(1): 35-92.
- Sloviter, R. S. (1996). "Hippocampal pathology and pathophysiology in temporal lobe epilepsy." Neurologia **11 Suppl 4**: 29-32.
- Somogyi, P. (1977). "A specific 'axo-axonal' interneuron in the visual cortex of the rat." Brain Res **136**(2): 345-350.
- Southwell, D. G., R. C. Froemke, A. Alvarez-Buylla, M. P. Stryker and S. P. Gandhi (2010). "Cortical plasticity induced by inhibitory neuron transplantation." Science **327**(5969): 1145-1148.
- Southwell, D. G., M. F. Paredes, R. P. Galvao, D. L. Jones, R. C. Froemke, J. Y. Sebe, C. Alfaro-Cervello, Y. Tang, J. M. Garcia-Verdugo, J. L. Rubenstein, S. C. Baraban and A. Alvarez-Buylla (2012). "Intrinsically determined cell death of developing cortical interneurons." Nature **491**(7422): 109-113.
- Spitzer, N. C. (2012). "Activity-dependent neurotransmitter respecification." Nat Rev Neurosci **13**(2): 94-106.
- Stambolic, V., A. Suzuki, J. L. de la Pompa, G. M. Brothers, C. Mirtsos, T. Sasaki, J. Ruland, J. M. Penninger, D. P. Siderovski and T. W. Mak (1998). "Negative regulation of PKB/Akt-dependent cell survival by the tumor suppressor PTEN." Cell **95**(1): 29-39.
- Sun, Y. J., G. K. Wu, B. H. Liu, P. Li, M. Zhou, Z. Xiao, H. W. Tao and L. I. Zhang (2010). "Fine-tuning of pre-balanced excitation and inhibition during auditory cortical development." Nature **465**(7300): 927-931.
- Szentagothai, J. and M. A. Arbib (1974). "Conceptual models of neural organization." Neurosciences Research Program Bulletin.
- Takahashi, T., T. Goto, S. Miyama, R. S. Nowakowski and V. S. Caviness, Jr. (1999). "Sequence of neuron origin and neocortical laminar fate: relation to cell cycle of origin in the developing murine cerebral wall." J Neurosci **19**(23): 10357-10371.
- Tamamaki, N., K. E. Fujimori and R. Takauji (1997). "Origin and route of tangentially migrating neurons in the developing neocortical intermediate zone." J Neurosci **17**(21): 8313-8323.
- Tamamaki, N. and R. Tomioka (2010). "Long-range GABAergic connections distributed throughout the neocortex and their possible function." Frontiers in neuroscience **4**: 202.

- Taniguchi, H., J. Lu and Z. J. Huang (2013). "The spatial and temporal origin of chandelier cells in mouse neocortex." Science **339**(6115): 70-74.
- Tatti, R., M. S. Haley, O. K. Swanson, T. Tselha and A. Maffei (2017). "Neurophysiology and regulation of the balance between excitation and inhibition in neocortical circuits." Biological psychiatry **81**(10): 821-831.
- Tomioka, R., K. Sakimura and Y. Yanagawa (2015). "Corticofugal GABAergic projection neurons in the mouse frontal cortex." Front Neuroanat **9**: 133.
- Traynelis, S. F., L. P. Wollmuth, C. J. McBain, F. S. Menniti, K. M. Vance, K. K. Ogden, K. B. Hansen, H. Yuan, S. J. Myers and R. Dingledine (2010). "Glutamate receptor ion channels: structure, regulation, and function." Pharmacol Rev **62**(3): 405-496.
- Tremblay, R., S. Lee and B. Rudy (2016). "GABAergic Interneurons in the Neocortex: From Cellular Properties to Circuits." Neuron **91**(2): 260-292.
- Tritsch, N. X., E. Yi, J. E. Gale, E. Glowatzki and D. E. Bergles (2007). "The origin of spontaneous activity in the developing auditory system." Nature **450**(7166): 50-55.
- Turrigiano, G. (2007). "Homeostatic signaling: the positive side of negative feedback." Curr Opin Neurobiol **17**(3): 318-324.
- Uematsu, M., Y. Hirai, F. Karube, S. Ebihara, M. Kato, K. Abe, K. Obata, S. Yoshida, M. Hirabayashi, Y. Yanagawa and Y. Kawaguchi (2008). "Quantitative chemical composition of cortical GABAergic neurons revealed in transgenic venus-expressing rats." Cereb Cortex **18**(2): 315-330.
- Uesaka, N., E. S. Ruthazer and N. Yamamoto (2006). "The role of neural activity in cortical axon branching." The Neuroscientist **12**(2): 102-106.
- Valcanis, H. and S. S. Tan (2003). "Layer specification of transplanted interneurons in developing mouse neocortex." J Neurosci **23**(12): 5113-5122.
- Verney, C., T. Takahashi, P. G. Bhide, R. S. Nowakowski and V. S. Caviness, Jr. (2000). "Independent controls for neocortical neuron production and histogenetic cell death." Dev Neurosci **22**(1-2): 125-138.
- Voigt, T., H. Baier and A. D. de Lima (1997). "Synchronization of neuronal activity promotes survival of individual rat neocortical neurons in early development." European Journal of Neuroscience **9**(5): 990-999.
- Voigt, T., T. Opitz and A. D. de Lima (2001). "Synchronous oscillatory activity in immature cortical network is driven by GABAergic preplate neurons." Journal of Neuroscience

- 21**(22): 8895-8905.
- Voigt, T., T. Opitz and A. D. de Lima (2005). "Activation of early silent synapses by spontaneous synchronous network activity limits the range of neocortical connections." Journal of Neuroscience **25**(18): 4605-4615.
- Voyvodic, J. T. (1996). "Cell death in cortical development: How much? Why? So what?" Neuron **16**(4): 693-696.
- Wagenaar, D. A., J. Pine and S. M. Potter (2006). "Searching for plasticity in dissociated cortical cultures on multi-electrode arrays." J Negat Results Biomed **5**: 16.
- Wagner-Golbs, A. and H. J. Luhmann (2012). "Activity-dependent survival of developing neocortical neurons depends on PI3K signalling." J Neurochem **120**(4): 495-501.
- Wang, Y., A. Gupta, M. Toledo-Rodriguez, C. Z. Wu and H. Markram (2002). "Anatomical, physiological, molecular and circuit properties of nest basket cells in the developing somatosensory cortex." Cereb Cortex **12**(4): 395-410.
- Watt, A. J., H. Cuntz, M. Mori, Z. Nusser, P. J. Sjöström and M. Häusser (2009). "Traveling waves in developing cerebellar cortex mediated by asymmetrical Purkinje cell connectivity." Nature neuroscience **12**(4): 463-473.
- Wichterle, H., J. M. Garcia-Verdugo, D. G. Herrera and A. Alvarez-Buylla (1999). "Young neurons from medial ganglionic eminence disperse in adult and embryonic brain." Nat Neurosci **2**(5): 461-466.
- Wichterle, H., D. H. Turnbull, S. Nery, G. Fishell and A. Alvarez-Buylla (2001). "In utero fate mapping reveals distinct migratory pathways and fates of neurons born in the mammalian basal forebrain." Development **128**(19): 3759-3771.
- Winkler, C., D. Kirik and A. Björklund (2005). "Cell transplantation in Parkinson's disease: how can we make it work?" Trends in neurosciences **28**(2): 86-92.
- Wonders, C. P. and S. A. Anderson (2006). "The origin and specification of cortical interneurons." Nat Rev Neurosci **7**(9): 687-696.
- Wong, F. K., K. Bercsenyi, V. Sreenivasan, A. Portales, M. Fernandez-Otero and O. Marin (2018). "Pyramidal cell regulation of interneuron survival sculpts cortical networks." Nature **557**(7707): 668-673.
- Wong, F. K. and O. Marin (2019). "Developmental Cell Death in the Cerebral Cortex." Annu Rev Cell Dev Biol **35**: 523-542.
- Wu, Q., M. Wada, A. Shimada, A. Yamamoto and T. Fujita (2006). "Functional characterization

- of Zn<sup>2+</sup>-sensitive GABA transporter expressed in primary cultures of astrocytes from rat cerebral cortex." Brain Res **1075**(1): 100-109.
- Xing, W., A. D. De Lima and T. Voigt (2021). "The structural E/I balance constrains the early development of cortical network activity." Frontiers in cellular neuroscience **15**.
- Xu, H., H. Y. Jeong, R. Tremblay and B. Rudy (2013). "Neocortical somatostatin-expressing GABAergic interneurons disinhibit the thalamorecipient layer 4." Neuron **77**(1): 155-167.
- Xu, Q., I. Cobos, E. De La Cruz, J. L. Rubenstein and S. A. Anderson (2004). "Origins of Cortical Interneuron Subtypes." The Journal of Neuroscience **24**(11): 2612-2622.
- Yanagida, M., R. Miyoshi, R. Toyokuni, Y. Zhu and F. Murakami (2012). "Dynamics of the leading process, nucleus, and Golgi apparatus of migrating cortical interneurons in living mouse embryos." Proc Natl Acad Sci U S A **109**(41): 16737-16742.
- Yizhar, O., L. E. Fenno, M. Prigge, F. Schneider, T. J. Davidson, D. J. O'Shea, V. S. Sohal, I. Goshen, J. Finkelstein, J. T. Paz, K. Stehfest, R. Fudim, C. Ramakrishnan, J. R. Huguenard, P. Hegemann and K. Deisseroth (2011). "Neocortical excitation/inhibition balance in information processing and social dysfunction." Nature **477**(7363): 171-178.
- Young, S. Z., M. M. Taylor, S. Wu, Y. Ikeda-Matsuo, C. Kubera and A. Bordey (2012). "NKCC1 knockdown decreases neuron production through GABAA-regulated neural progenitor proliferation and delays dendrite development." Journal of Neuroscience **32**(39): 13630-13638.
- Yozu, M., H. Tabata and K. Nakajima (2004). "Birth-date dependent alignment of GABAergic neurons occurs in a different pattern from that of non-GABAergic neurons in the developing mouse visual cortex." Neuroscience research **49**(4): 395-403.
- Zhang, L. I. and M. M. Poo (2001). "Electrical activity and development of neural circuits." Nat Neurosci **4 Suppl**: 1207-1214.
- Zhao, Y., P. Flandin, J. E. Long, M. D. Cuesta, H. Westphal and J. L. Rubenstein (2008). "Distinct molecular pathways for development of telencephalic interneuron subtypes revealed through analysis of Lhx6 mutants." Journal of Comparative Neurology **510**(1): 79-99.
- Zheng, J. Q. and M. M. Poo (2007). "Calcium signaling in neuronal motility." Annu Rev Cell Dev Biol **23**: 375-404.
- Zipancic, I., M. E. Calcagnotto, M. Piquer-Gil, L. E. Mello and M. Alvarez-Dolado (2010). "Transplant of GABAergic precursors restores hippocampal inhibitory function in a mouse

model of seizure susceptibility." Cell Transplant **19**(5): 549-564.

---

## 7. Declaration of Honour

“I hereby declare that I prepared this thesis without the impermissible help of third parties and that none other than the aids indicated have been used; all sources of information are clearly marked, including my own publications.

In particular I have not consciously:

- fabricated data or rejected undesirable results,
- misused statistical methods with the aim of drawing other conclusions than those warranted by the available data,
- plagiarized external data or publications,
- presented the results of other researchers in a distorted way.

I am aware that violations of copyright may lead to injunction and damage claims by the author and also to prosecution by the law enforcement authorities. I hereby agree that the thesis may be electronically reviewed with the aim of identifying plagiarism.

This work has not yet been submitted as a doctoral thesis in the same or a similar form in Germany, nor in any other country. It has not yet been published as a whole.”